SOME ELECTRICAL PROPERTIES

OF THIN FILMS OF POLYPROPYLENE

FORMED BY VACUUM EVAPORATION

A THESIS PRESENTED FOR THE

DEGREEE OF DOCTOR OF PHILOSOPHY

BY

TARIQ-IQBAL

Brunel University
Kingston Lane,
Uxbridge,
Middlesex,
England.

July 1980

To my wife Ghazala

and our parents

ACKNOWLEDGEMENTS

I wish to express my deep appreciation and gratitude to my supervisor, Professor C.A. Hogarth, for his encouragement, criticisms and guidance throughout this study.

I would like to thank my wife for her moral support and patience during my studies.

I also wish to thank Mr. Salman A-Y. Al-Ismail and Mr. S. Rahman for their very interesting discussions.

I would also like to thank Mr. D. Waterman for his help and valuable advice for setting up the apparatus.

I wish to thank Mr. R. Stevens for his invaluable services in the Stores.

I wish to thank all the technicians for their help, especially Mr. Stanley Woddisse, who tragically passed away on 12th April 1979.

I wish to thank Mr. T. Purser and Mr. L.E.L. Chandrasekera for electron microscope photographs and helpful discussions.

I wish to express my appreciation to Mrs. M.F. Limmer for typing this thesis.

I wish to thank the Metallurgy Department for providing facilities for the microphotometer.

Finally, I wish to express my appreciation and thanks to the Ministry of Education of Pakistan Government for their financial support without which this work could not have been accomplished.

ABSTRACT

The electrical properties of films of metal-polypropylene-metal structures with polypropylene thicknesses in the range 600 - 2600Å were studied for possible use as thin dielectric films and some standard and reproducible results of electrical measurements were obtained. As a consequence of using different electrode materials, systematic differences in the behaviour of these films were found, even though the voltage-current characteristics remained ohmic.

In these measurements there was evidence of electron trapping and the trap depth was estimated by using the thermally-stimulated current techniques, and was found equal to 0.33 eV.

Thin films of evaporated polypropylene having thicknesses less than 1000Å, showed electroforming effects and electron emission into vacuum under suitable conditions. The results were found to be consistent with a theory based on the generation of conducting filaments during the forming process. The increase in the a.c. conductivity of the sample after electroforming also indicated the presence of filaments in the formed device. Another useful application of the a.c. measurements was to identify the hopping conduction both at low and at room temperatures. A linear decrease in the capacitance of the device with increasing frequency was observed and was associated with the growing leakage current.

A vacuum heat treatment of the films at 110°C led to an increase in resistivity. The transmission electron diffraction patterns of several evaporated layers of polypropylene having thicknesses

between 150 to 1600Å certainly indicated the amorphous structure of these films. However, the examination by electron microscopy and by electron diffraction showed an aggregation of particulate material of more crystalline nature as a result of the heat treatment but the connecting chains were broken and dispersed as a result of the same treatment.

Some observations on the general character of evaporated polymers are made.

SOME ELECTRICAL PROPERTIES OF THIN FILMS OF POLYPROPYLENE FORMED BY VACUUM EVAPORATION

CHAPTER ONE

1. INTRODUCTION

1.1 PREVIOUS WORK ON EVAPORATED POLYMERS

1.1.1 General background

The electrical properties of polymeric materials have been the subject of extensive study[1-5]. Due to low production costs and to their excellent electrical and mechanical properties, polymers have many industrial applications. Thin polymeric films can be used for the investigation of electrical and optical properties and may be obtained by several means including thermal evaporation[4] and deposition by polymerization of monomers on surfaces bombarded with electrons or exposed to other radiations, e.g. a glow discharge[6] or ultra violet light. Radio-frequency sputtering[7] and dipping of a substrate into an appropriate solution can also produce thin layers of polymers[8]. When polymers are heated in vacuum, one result is the breaking of certain chemical bonds within the molecules, thus leading to the formation of active fragments which sublimate from the surface of the polymer material[9]. These fragments when incident onto a substrate react with one another to form a polymer coating on its surface[10-12]. Not all polymers release active fragments when heated in vacuum. Some of them such as the polyurethanes, epoxides and polyvinylchlorides decompose into gaseous fragments that are not capable of recombining on a substrate. Unlike vinyl polymers, halogen polymers such as polytetrafluorethylene (PTFE) and polychlortrifluorethylene release significant numbers of active fragments when they are heated in vacuum[13], and these fragments form polymer layers when they condense in vacuum.

The structure of the polymeric materials plays an important role in controlling their electrical properties. Most polymers of practical significance are composed of a fine mixture of small micrometre size crystalline regions, embedded in an amorphous matrix of similar molecular composition[14]. The polymeric chains are thought to be folded in an orderly arrangement within the crystalline regions and these regions have the form of small platelets having thicknesses of the order of a few nanometres. Since the amorphous regions have no structural order, it is therefore most likely that they contain most of the impurities present in the polymer. The available theories for the crystalline, polycrystalline and amorphous inorganic solids are usually used to describe the conduction process of organic materials. The charge carrier trap depth in certain polymeric materials has been investigated by using the technique of thermally-stimulated currents[15-17]. It has also been found that on exceeding a threshold applied voltage, thin films of polymeric materials sandwiched between metal electrodes may undergo an electroforming process[4,18]. We have examined the properties of evaporated polypropylene for possible use as a thin dielectric film and were able to produce standard and reproducible results of electrical measurements. The trap depth in the evaporated polypropylene was calculated from the measurements of thermally stimulated currents and was found to be 0.33 eV[15]. A vacuum heat treatment of the films at 110^{o}C leads to an increase in its resistivity. Examination by electron microscopy and by electron diffraction showed an aggregation of particulate

material of more crystalline nature as a result of the heat treatment. The a.c. conductivity measurements of polypropylene demonstrated the power law dependence of conductivity on frequency, which characterizes a process of hopping conduction[19].

1.1.2 Thermal decomposition

Two types of change take place when polymers are heated in vacuum or in an inert gas atmosphere, namely,(i) depolymerization and (ii) degradation. When thermal decomposition gives rise to the evaporation of volatile low molecular weight products mainly consisting of original monomers, the process is known as depolymerization, while in the case of degradation a considerable decrease in both the chain length and average molecular weight of the polymer are observed. Also, some volatile products may appear but these are normally present in negligible amount.

1.1.2.1 Degradation

During the degradation a considerable reduction in the molecular weight and in the chain length of the polymer are observed. Thermal degradation of a number of polymers, such as polystyrene, polyisoprene, polybutadiene and polyethylene was brought about in vacuum at 300 to 400^{o}C by Madorsky et al[20]. The resultant volatile products were composed of fragments varying in size from a monomer to material having a molecular weight of about 1000. Madorsky[21] evaporated the polyethylene(PE) under high vacuum conditions at 10^{-6} torr and the temperature range was from 380 to 475^{o}C. The average

molecular wieght of the resultant fragments was found equal to 700, which indicates that the chains were broken at random positions. Grassie[22] pointed out that when the temperature is raised the first sign of thermal degradation in polyethylene which occurs around 290°C is a decrease in the molecular weight. Two stage degradation in many polymers has been observed. Luff and White[23] found that the degradation of polyethylene (PE) starts at 300°C and the polyethylene undergoes a two-stage degradation process. Figure 1.1 shows the evaporation rate plotted against the reciprocal of temperature. According to Amelin et al[24], the low temperature range having an activation energy of ~ 1 eV characterizes the breaking of the weak bonds and removal of side chains from the main molecule. The second stage which reflects the rupturing of primary bonds has an activation energy of 3.04 eV. Luff and White[23] reported the activation process above 350°C as having an activation energy of 3.68 eV.

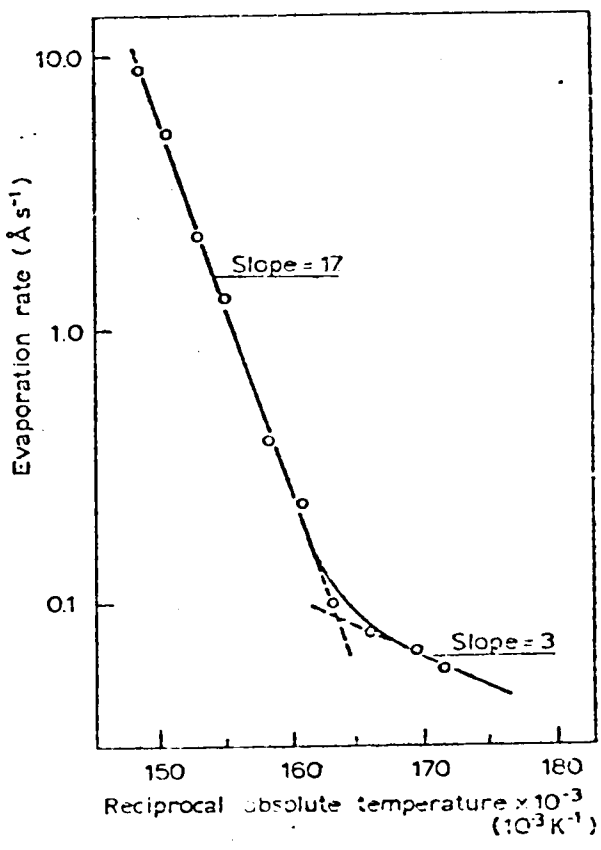

Figure 1.1 Evaporation rate vs reciprocal of absolute temperature (after Luff and White[23])

Two-stage degradation was also observed in polymethylmethacrylate and in polystyrene[24]. Polystyrene when heated in high vacuum at 325 to 375°C gives rise to the evaporation of the monomer and of some dimer, trimer, etc. This shows that the chains are broken largely at the ends. Madorsky[21] calculated the activation energy at various temperatures, on the basis of degradation, as 2.95 eV for polyethylene and 2.51 eV for polystyrene. Evaporation of PTFE was studied by Lane[25] under high vacuum at 400°C. It was found that PTFE degrades to leave a residue of carbon in the evaporation source, while on completion of a similar evaporation of PE, no residue of PE was found[26]. Thermal degradation of polyvinyl compounds was described by Grassie and Melville[27]. They put forwa the three possible extreme degradation mechanisms as random breaking, stepwise degradation and depolymerization. Recently Kinstle[28] observed the thermal decomposition of poly(oxycarbonylimino-1,4 phenylene) a polymer which undergoes a purely decomposition process.

When polypropylene is heated in vacuum, the decomposition rate at 412°C is 1000 times that at 320°C. The gas consists of 34-52% propylene, 2-6% butenes and 39-41% amylenes and pentenes. Also the non-volatile residue left in the evaporation source becomes amorphous[29]. The molecules weight of the polypropylene decreases to a value characteristic of normal polyethylene in the temperature range of 230-300°C[30]. Decomposition of polypropylene starts by the random breaking of C-C bonds which then leads to the breaking of terminals from macroradicals. Then the hydrogen atoms are removed from the neighbouring

molecules. Finally, the chains are broken as shown below.

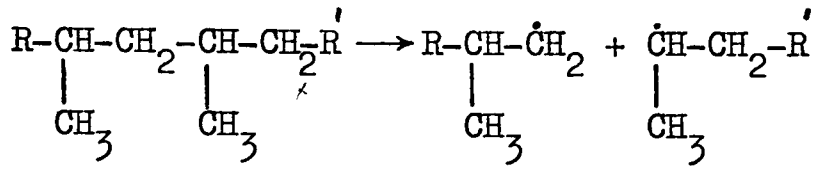

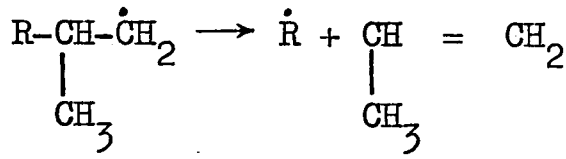

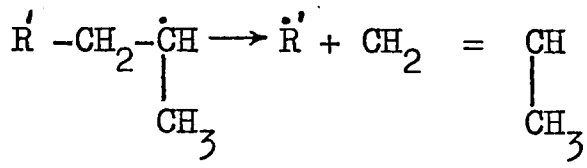

($\dot{R}$ and $\dot{R}'$ are macroradicals)

1.1.3 Electrical properties

The mechanism of electrical conduction in polymers is quite complicated and there is no satisfactory theory to explain the conduction mechanism in these organic disordered materials, so the available theories for the crystalline, polycrystalline and amorphous inorganic solids are usually used to describe the conductivity of these materials. The conduction mechanism in polymeric thin films may depend on the thickness and also on the method of producing them. As a consequence different workers have reported different conduction mechanisms for the same nominal material.

1.1.3.1 Ohmic conduction

Ohmic conduction in polymer thin films is not very common and most of the polymer films exhibit non-ohmic behaviour at high electric fields. Gregor[31] examined thin films of polydivinylbenzene having thicknesses between 100 - 1000 Å and produced

by the glow discharge method. He reported ohmic conduction in 1000 Å films up to the breakdown point which occurred above 10^6 V cm^{-1}. Hogarth and Iqbal[5] obtained their films of polypropylene (PP) by vacuum deposition having thicknesses between 1200 - 2400 Å . They found systematic differences in the electrical behaviour of these films as a consequence of using different electrode materials, even though the voltage-current characteristics remained ohmic. The voltage-current characteristics of Cu-PP-Cu and Al-PP-Cu samples with three different thicknesses of polypropylene are shown in Figure 1.2.

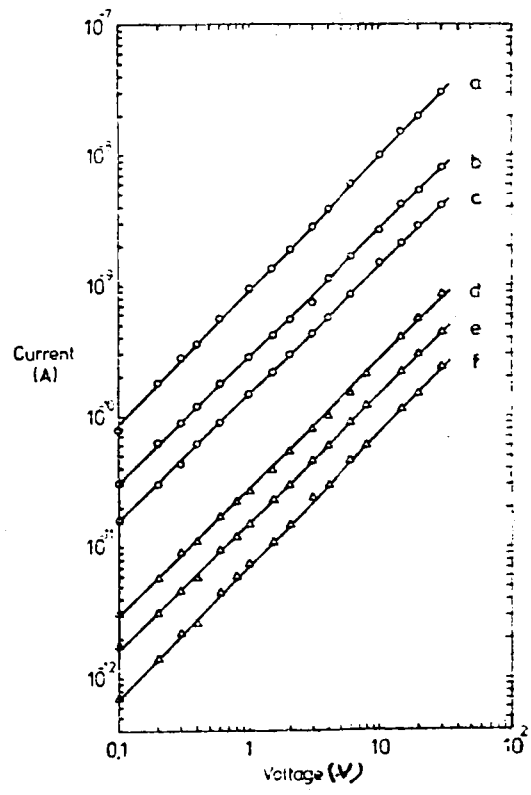

Figure 1.2 Voltage-current characteristics for some thin films of polypropylene (PP): curve a, Cu/PP(1200 Å)/Cu; curve b, Cu/PP (1800 Å)/Cu; curve c, Cu/PP (2400 Å)/Cu; curve d, Al/PP (1200 Å)/Cu; curve e, Al/PP (1800 Å)/Cu; curve f, Al/PP (2400 Å)/Cu. (after Hogarth and Iqbal[5])

It was found that the polypropylene films were highly resistive with resistivities of the order of 10^{14} ohm-cm. The breakdown of the films was not thoroughly investigated; nevertheless the films withstood an applied field of 2.48×10^{6} V cm^{-1}.

1.1.3.2 Super-ohmic and tunnelling characteristics

Super-ohmic and tunnelling effects have been reported as the dominant conduction mechanisms in many thin polymer films. Super-ohmic effects include the conduction by Schottky emission or by the Poole-Frenkel effects. In Schottky emission the electrons are emitted by thermal activation from metal electrodes into the conduction band of the insulator over a potential barrier at the metal/insulator interface. In the Poole-Frenkel effect, the electrons are thermally emitted from randomly-distributed trapping centres to the conduction band of the insulator by means of the lowering of the Coulombic potential barrier surrounding the trapped electrons by an external electric field. Thin polymer films prepared from silicone oil and having thicknesses between 50 and 2500 Å were investigated by Christy[2], Emtage[32] and Mann[33]. Christy[2] obtained these films by electron bombardment and they had thicknesses between 50 and 150 Å. He concluded that the conduction mechanism at 4K was due to tunnelling, while at room temperature no single mechanism was adequate to describe the conduction process, although the current showed a $\log I \sim V^{\frac{1}{2}}$ dependence on voltage characteristic of either a Schottky or Poole-Frenkel process. Emtage and Tantraporn

reported that Schottky emission was the main conduction mechanism in 100 Å films at 300 K formed in the say way as shown in Figure 1.3. For films in the thickness range from 500 - 2500 Å, sandwiched between aluminium electrodes, Mann found that in the temperature range from 4 - 300 K, the conductivity in the high electric fields was related to Schottky emission or tunnelling or to a mixture of both.

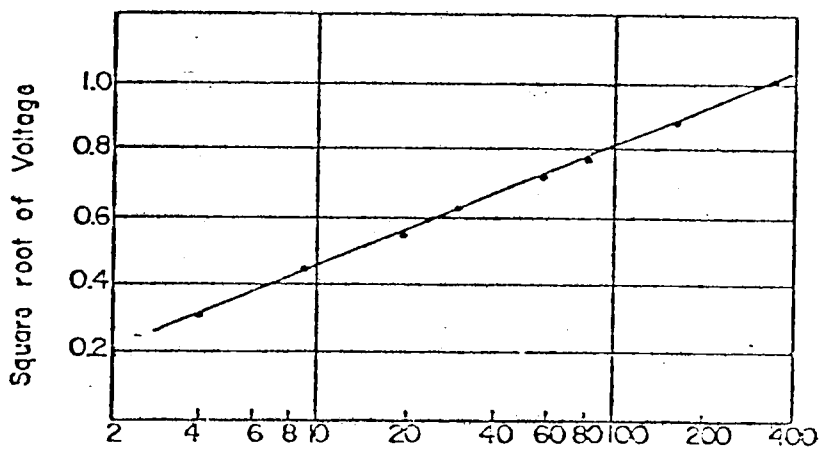

Figure 1.3 Voltage-current characteristics of a Au-Siliconoil (PSO)-Au system at 300 K. (after Emtage and Tantraporn[32]).

Gregor and Kaplan[34] who studied the thin films of epichlorohydrin (100 Å thick), produced by electron bombardment, came to the conclusion that the electrical characteristics could be related to a combination of tunnelling and either the Poole-Frenkel or Schottky emission, depending upon the temperature range and electric field strength. The electrical properties of thin films of polysilazane having thicknesses between 0.6 and 3.5μm formed by the glow discharge method were investigated by Trezkowski et al[35]. They suggested that electrode-limited (Schottky) conduction was the dominant conduction mechanism.

Gregor[31] examined thin films of polydivinylbenzene having thicknesses between 100 - 1000 Å, produced by the glow discharge method and concluded that Schottky emission was the dominant conduction mechanism in 100 - 500 Å thick films as shown in Figure 1.4. Lengyel[36] investigated films of polyethylene terephthalate (Mylar) and polyvinylformal, and reported the conduction mechanism as Schottky emission for fields between 20 and 200 K V^{-1}cm and temperatures from 298 to 373 K. Lilly and Modowell[37] worked on Mylar and Teflon (polytetrafluorethylene) films. They also interpreted their results using the theory of Schottky emission. According to Lilly and Lowitz[38]

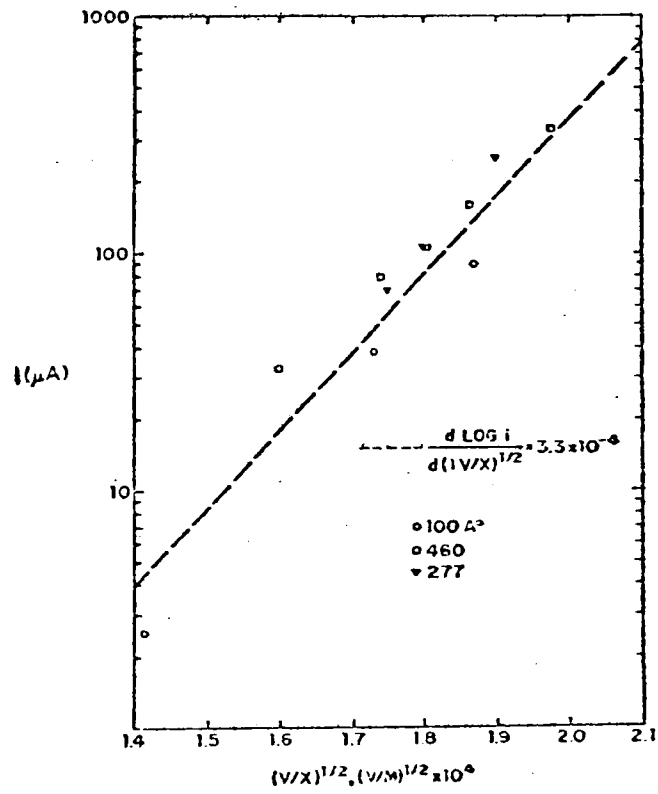

Figure 1.4 Logarithm of current vs square root of electric field for Pb- Polydivinylbenzene -Pb structure at 300 K (after Gregor[31]).

the conduction mechanism in 25 - 125μm thick Mylar films was governed by the O'Dwyer[39] theory of space-charge conduction. The space charge extended throughout the thickness of the sample

rather than being localised near the cathode. Kamisako et al[40] measured the steady-state conductivity of polystyrene films and the conduction mechanism was explained in terms of a space charge formed by the injection of electrons into the film over the Schottky barrier and was found diffusing towards the anode. They also made a rough estimate of the density of traps and its temperature dependence. The electrical conductivity of thin polycrystalline P-terphenyl films was investigated as a function of temperature, electric field and film thickness by Staryga and Swiatek[41]. They interpreted their data in terms of a hopping process between localized sites over potential barriers lowered by the electric field according to the Poole-Frenkel formula as shown in Figure 1.5.

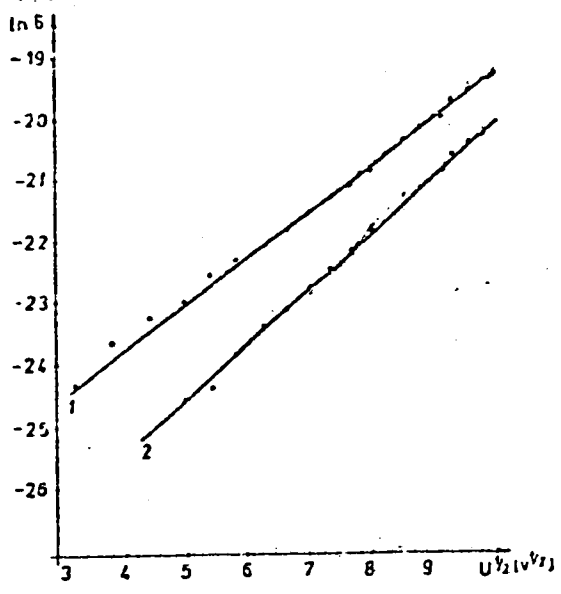

Figure 1.5 The $\ln\sigma$ vs $v^{\frac{1}{2}}$ characteristics for p-terphenyl layers.

curve 1, d = 2.6 μm, T = 298 K

curve 2, d = 3.5 μm, T = 298 K

(after Staryga and Swiatek[41])

Kryszewski and Swiatek[42] investigated the electrical properties of thin polystyrene (PS) and poly(N-vinyl carbazole) (PVK) films, obtained by the glow discharge method. The conductivity was described by both electrode-limited and bulk-limited conduction processes. At lower field strengths, $E \leq 10^5$ V cm^{-1}, the electrode-limited conduction mechanism was dominant, while at higher fields ($E \geq 10^5$ V cm^{-1}) the conductivity was related to the volume properties of the polymer, i.e. it was dominated by the Poole-Frenkel effect. Figure 1.6 and Figure 1.7 show the current-voltage characteristics of PS and PVK films at different temperatures respectively.

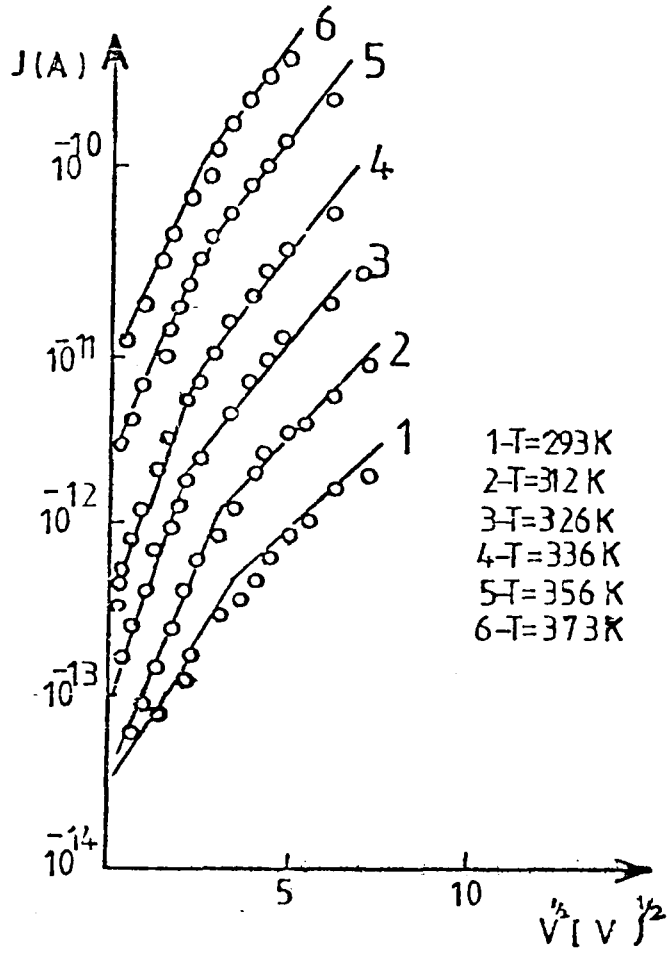

Figure 1.6 Schottky plot for polystrene film of thickness 314 Å (after Kryszewski and Swiatek[42]).

Electrical conduction through insulating layers of polyethylene has been investigated by many research workers during the last

few years. The current-voltage behaviour of thermally evaporated polyethylene films sandwiched between aluminium electrodes was

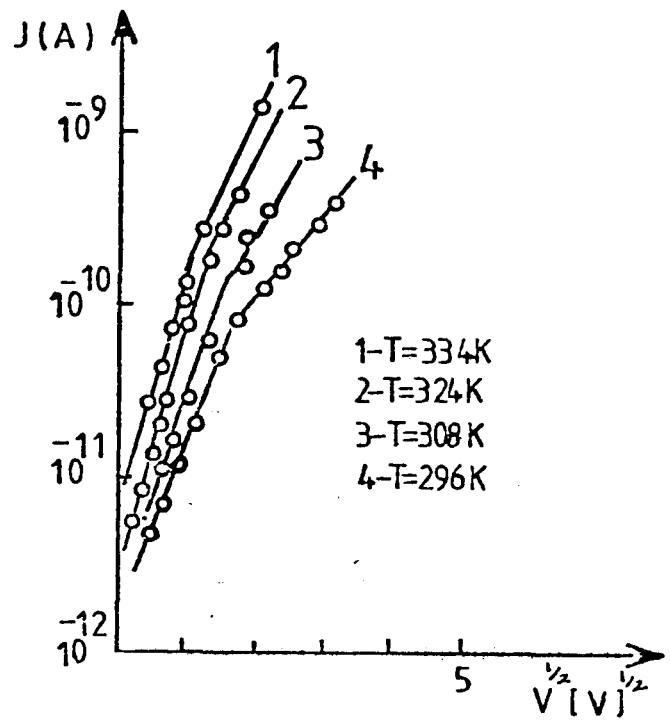

Figure 1.7 Current-voltage characteristics for Poly(N-Vinyl-carbazole)PVK) film of thickness 740 Å
(after Kryszewski and Swiatek[42])

explained in terms of the anomalous Poole-Frenkel effect by Zor[43]. Miyoshi and Chino[44] studied polyethylene films formed by vacuum deposition and also by dipping the substrate into solution. They discussed their results by using the simple theories of tunnelling (in 50 Å films) and Schottky emission (in 500 - 1200 Å films). Rogger[45] observed the current-voltage characteristics of 100 Å thick polyethylene films and found tunnelling as the conduction mechanism. Das Gupta and Barbarez investigated the conduction process in polyethylene films and concluded that the carriers were introduced into the conduction band of the polymer via defects or impurity levels and

the subsequent motion through the insulator was by means of hopping. Suzuki et al[47] obtained their films of polyacrylonitrile by vacuum deposition. After subjecting the films to heat treatment in nitrogen, they suggested that the conduction should be understood in terms of the hopping transport of charge carriers in the localized states present in the forbidden band due to the random networks of conjugate double bond systems of carbon-to-carbon and carbon-to-nitrogen.

1.1.3.3 Space-charge-limited conduction

If the electrode makes ohmic contacts to the insulator, the electrons travel from the metal into the conduction band of the insulator with a velocity determined by their mobility in the electric field, and form a space charge similar to that of a vacuum diode, then the conduction process is known as space-charge-limited.

Space-charge-limited currents provide the dominant conduction mechanism in some polymer thin films as has been reported by several workers. Shireesh et al[48] obtained their films of polyerocene sandwiched between Al electrodes and having thicknesses between 210 - 300 Å by a plasma polymerization method. They concluded that the conduction mechanism was governed by space-charge-limited currents as shown in Figure 1.8. An investigation was undertaken by Chutia and Barua[49] and the conduction mechanism in polymethyl-methacrylate (PMMA) films was found to be due to space-charge-limited currents. Zor[43] also found the space-sharge-limited currents as the dominant conduction mechanism in evaporated polyethylene films, having thicknesses in the range from 1200 -

- 4200 Å and sandwiched between Cu and Al electrodes. Some influence of space-charge-limited currents above 300 K, was found in the current-voltage characteristics of vacuum deposited polycrystalline P-terphenyl films by Staryga and Swiatek[41]. Some

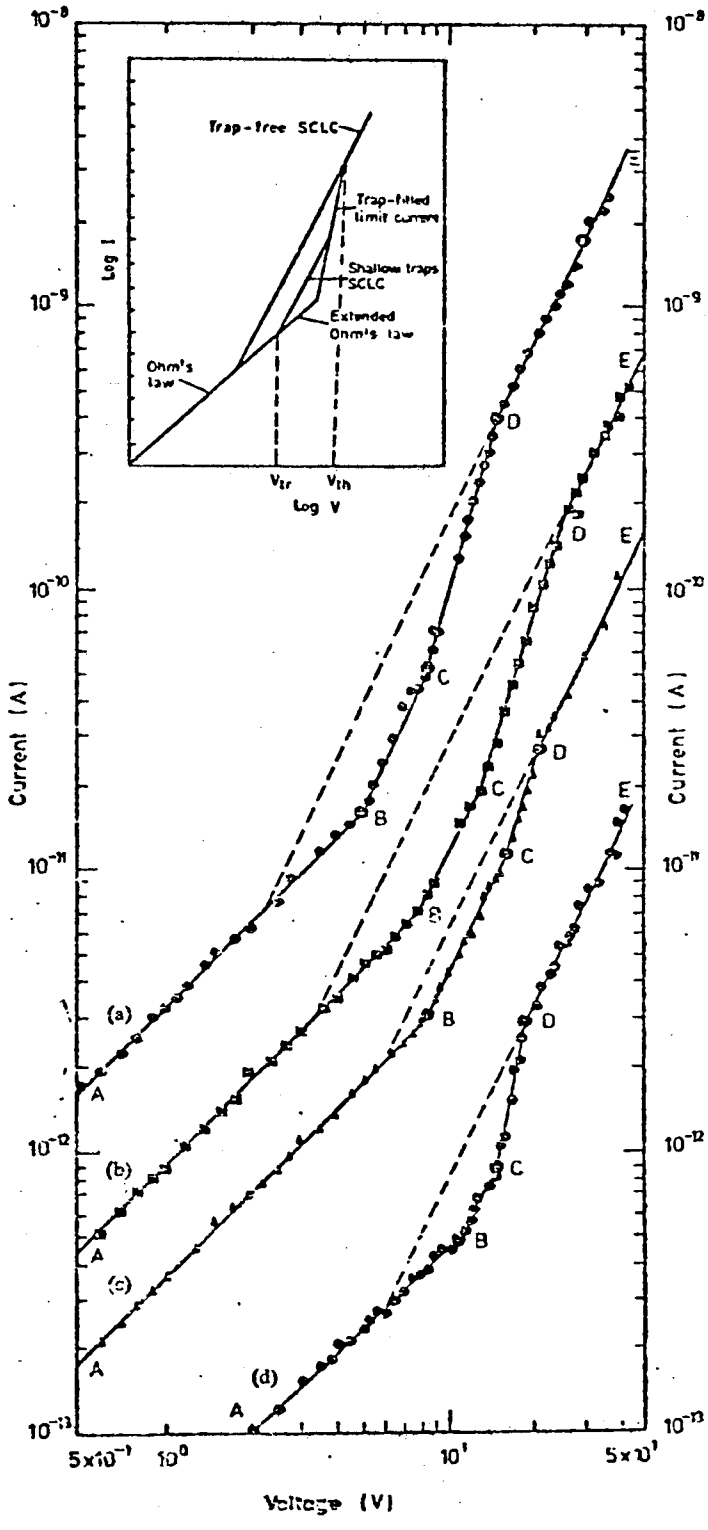

Figure 1.8 Voltage-current characteristics for some thin films of polyferrocene; curve a, Al/PF(210 Å)/Al, curve b, Al/PF(600Å)/Al; curve c, Al/PF(900 Å)/Al, curve d, Al/PF(3000 Å)/Al : (after Shireesh et al[48])

electrical properties of the polymers discussed above are presented in Table 1.

1.1.3.4 Electroforming

Electroforming, in which a large reduction in the apparent resistance of the material is observed when a threshold voltage is applied, may occur in the thin layers of many polymeric materials. Associated with the electroforming process are a voltage-controlled negative resistance (VCNR), electroluminescence, electron emission and a memory effect. A number of theories[50-57] have been proposed to explain electroforming and associated effects in insulators. Mann[33] worked on thin films of silicone oil prepared by the electron bombardment method and having thicknesses between 500 and 2500 Å sandwiched between Al electrodes and observed differential negative resistance similar to that reported by Hickmott[50] in some of his samples. The current rose exponentially to its maximum value at about 5 V and was found independent of the film thickness. While applying a decreasing voltage a similar negative resistance effect was noticed but always with a smaller maximum current. The memory effect was also reported up to 3 volts and this was stable and independent of temperature. For voltages greater than 6 volts and up to 50 volts, tunnelling was observed in these devices as shown in Figure 1.9. Gundlach and Kadlech[58] investigated the monomolecular multi-layers of cadmium arachidate sandwiched between Al and Au electrodes. The monolayers were deposited onto previously evaporated aluminium electrodes, by dipping the substrate several times into an aqueous solution of cd ions and with monomolecular layers of arachidic acid spread

TABLE 1

SELECTED RESULTS ON EVAPORATED POLYMER FILMS

No.	Author	Polymer	Method of obtaining films	Thicknesses	Temperature K	Observed Conduction Mechanism	Ref.
1	Christy	Silicon Oil	Electron bombardment	(50-150) Å	4-300	Tunnelling at 4K, log I vs $V^{\frac{1}{2}}$ dependence at 300K. No single mechanism was dominant	2
2	Emtage and Tantraporn	Silicon Oil	Electron bombardment	100 Å	300	Schottky emission	32
3	Mann	Silicon Oil	Electron bombardment	(500-2500)Å	4-300	Schottky emission or tunnelling or a mixture of both.	33
4	Gregor and Kaplan	Poly-epichlorohydrin	Electron bombardment	100 Å	160-300	Tunnelling at low temperature (160K) and low voltages. Schottky emission or the Poole-	34

TABLE 1 (cont.)

No.	Author	Polymer	Method of obtaining films	Thicknesses	Temperature K	Observed Conduction mechanism	Ref.
5	Gregor	Polydivinyl-benzene	Glow discharge	(100-1000) Å	300	Schottky emission in 100 to 500 Å films, while Ohmic conduction in 1000Å films up to the breakdown point, which occurred at 10^6 V cm^{-1}	31
6	Lengyel	Polyethylene-terephthalate (Mylar)	Commercially supplied samples were used.	27.50 μm	298-383	Schottky emission for fields between 20-200 K V cm^{-1}.	36
		Polyvinyl-formal	Commercially supplied samples were used.	(50-55) μm	298-383	Schottky emission for fields between 20 - 200 K V cm^{-1}	36
7	Lilly and Mcdewell	Mylar and Teflon (Poly tetrafluorethylene)	Films were cut from the sheets of Maylar and	(25-250) μm	343-436	Schottky emission	37

TABLE 1 (cont.)

No.	Author	Polymer	Method of obtaining films	Thicknesses	Temperature K	Observed Conduction Mechanism	Ref.
8	Rogger	Polyethylene	--	100 Å	298	Tunnelling	45
9	Lilly and Lowitz	Mylar	--	(25-125) μm	300-425	O'Dwyer theory of space charge conduction	38
10	Dos Gupta & Barbarez	Polyethylene	Films were supplied by Mansanto Chemical Limited	(25-75) μm	313	Poole-Frenkel and hopping	46
11	Suzuki et al	Polyacrylonitrite	Vacuum deposition	1000 Å	160-500	Hopping through localized states in the forbidden gap.	47
12	Staryga and Swiatek	Polycrystalline P-terphenyl	Vacuum deposition	(1.7-3.5) μm	298	Poole-Frenkel and hopping. Also, space-charge limited conduction above 300 K.	41
13	Shireesh et al	Polyerocene	Plazma polymerization	(210-3000) Å	298	Space-charge limited currents.	48

TABLE 1 (cont.)

No.	Author	Polymer	Method of obtaining films	Thicknesses	Temperature K	Observed Conduction Mechanism	Ref.
14	Chutia and Barua	Polymethyl-methacrylate	Isothermal immersion	9646 Å	298-333	Space-charge limited currents	49
15	Hogarth and Iqbal	Polypropylene	Vacuum deposition	(1200-2400)Å	300	Ohmic	5
16	Kamisaka et al	Polystyrene	Styroflex(NSW Co) films were used	(33-40)μm	300-375	Schottky emission	40
17	Kryszewski and Swiatek	Polystyrene and poly(N-vinyl carbazole	Glow discharge (NSW Co)	200 to 800Å	293-373	For $E \leq 10^5$ V cm^{-1}, electrode limited	42
						$E \geq 10^5$ V cm^{-1}, Poole Frenkel	42
18	Tyezkowski et al.	Polysilazane	Glow discharge	(0.6-3.5)μm	298	Schottky emission	35

TABLE 1 (cont.)

No.	Author	Polymer	Method of obtaining films	Thicknesses	Temperature	Observed Conduction Mechanism	Ref.
19	Lane	PTFE	Vacuum deposition	(400 to 1650)Å	298	No single conduction mechanism	25
20	Miyoshi and Chino	Polyethylene	Vacuum deposition	(1000-2000) Å	298	Schottky emission in PE single crystal of 500 - 1200 Å	44
			Solution deposition	(50 -1000) Å	200-400	Tunnelling in 50 Å	
21	Zor	Polyethylene	Vacuum deposition	(1100-4200)Å	298	Space-charge limited currents with copper electrodes. Poole-Frenkel effect with aluminium electrodes.	43

on the surface of the water. Each mono-layer had a thickness of 26 Å. To complete the sandwich, top electrodes of gold or aluminium were evaporated. For the electrical measurements

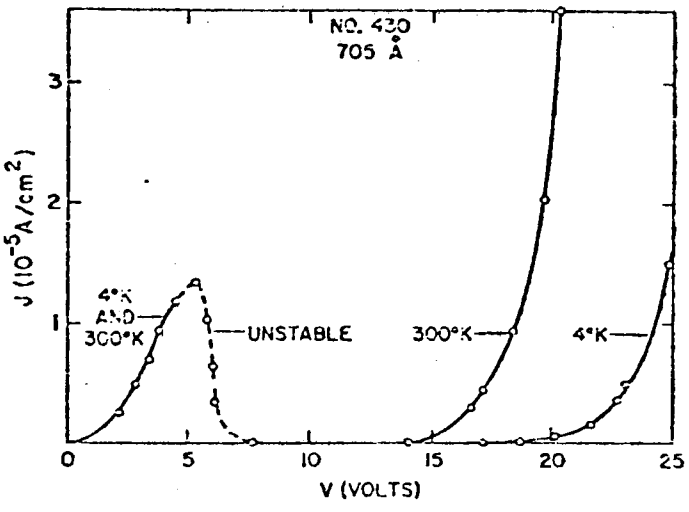

Figure 1.9 Differential negative resistance and tunnelling in M-DOW-Corning DC 704-M structures (after Mann[33]).

the sample was cooled down to 77 K and the top electrode was always positively biased. A sawtooth voltage with an increasing rate of 0.3 Vs^{-1} was used. The device was electroformed by applying a bias voltage of 5 to 6 volts or more. Now the sandwich was warmed at a rate of 5 deg min^{-1} and the first sign of the differential negative resistance (DNR) was observed at about 150 K. The DNR was most pronounced at about 190 K and it disappeared above 210 K. The current-voltage characteristics of an [Al-(Al oxide) -eleven monolayer-Al] sandwich with increasing temperature are shown in Figure 1.10. It was not possible to form the devices having thicknesses less than five monolayers. On decreasing the voltage within 0.025 the device was left in a memory state which was erased at a threshold voltage of between 2 to 3 volts. The electroforming of evaporated polyethylene has been reported by many research workers.

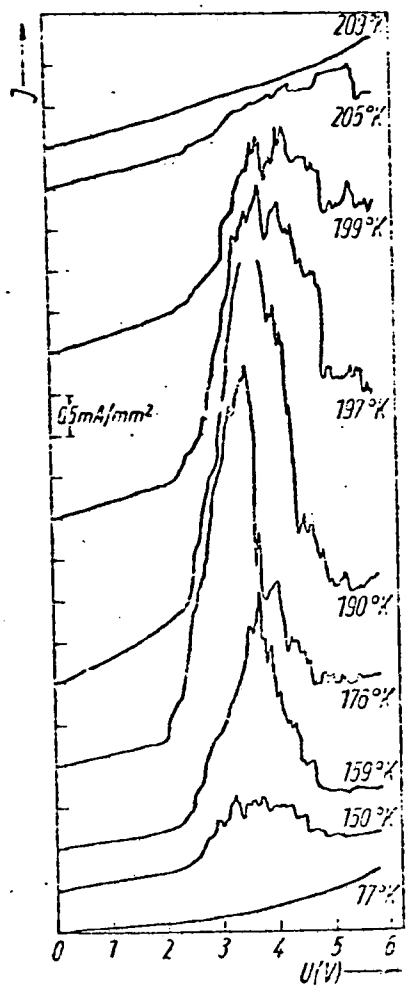

Figure 1.10 Current-voltage characteristics of an Al-(Aloxide)-eleven monolayer-Au sandwich for increasing temperature. The vertical scale is displaced for each curve for clarity (after Gundlach and Kadlec[58]).

Gazso[59] observed the DNR in the evaporated polyethylene films, having thicknesses in the range of 1000 - 2000 Å and sandwiched between aluminium and gold electrodes. The conductivity increased due to the in-diffusion of gold from the top electrode under the influence of the applied electric field. This was supported by the fact that the sandwiches prepared only with aluminium electrodes did not show any electroforming. Miyoshi and Chino[44] also observed the negative resistance similar to Hickmott[50] in their samples of evaporated polyethylene having same thicknesses as reported by

Gazso. Hogarth and Zor[4] evaporated polyethylene at 10^{-4} torr onto previously deposited aluminium electrodes. Their films were 1140 Å thick. In order to complete the M-I-M structure aluminium was evaporated as top electrodes. Unlike Gazso[59] in these films of polyethylene, sandwiched between Al electrodes, the electrical process was influenced by the injection of metal from the electrodes and irreversible forming and related effects were also observed. Figure 1.11 shows the effect of time when a

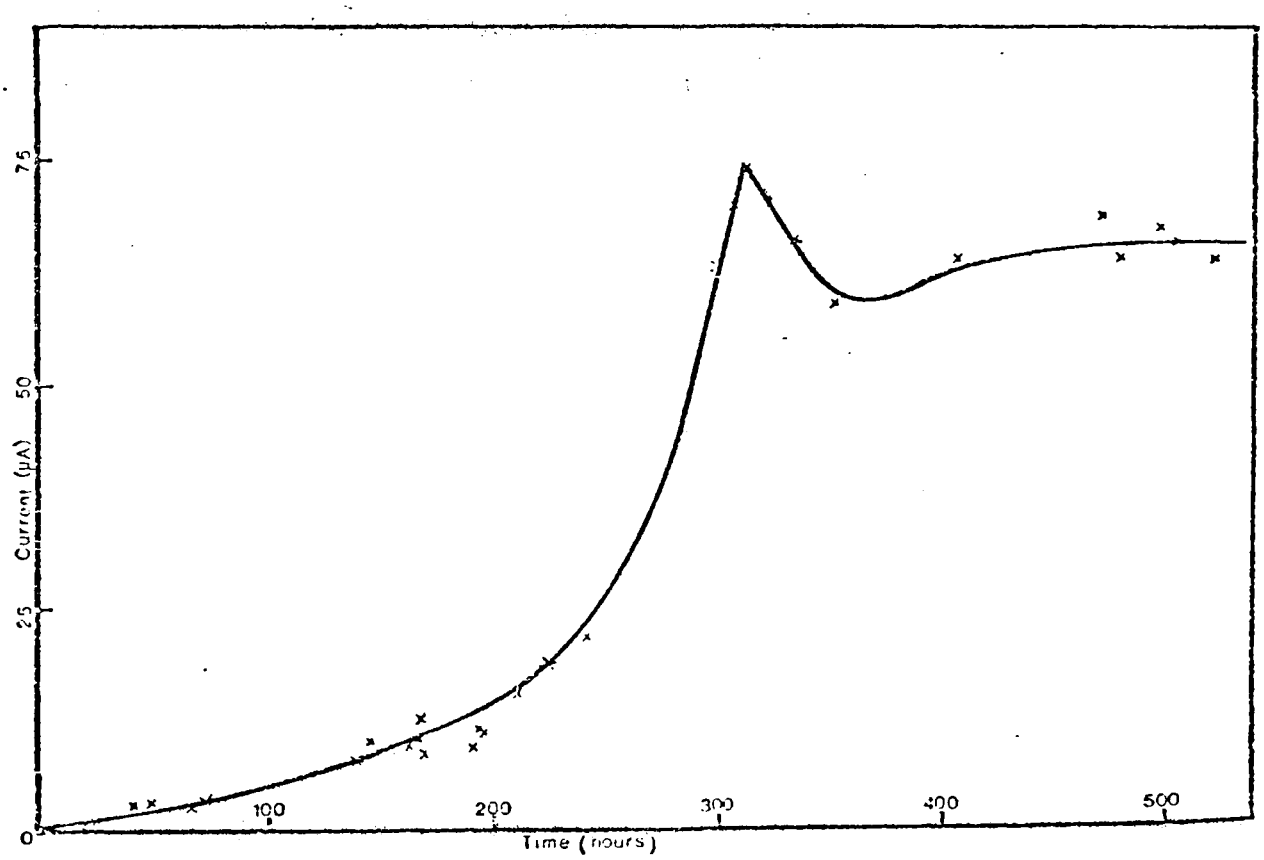

Figure 1.11 Current at constant supply voltage as a function of time for an Al-PE(1140 Å)-Al structure (after Hogarth and Zor[4]).

Al-PE(1140 Å)-Al sample was left under 16 volts (minimum forming voltage) for an extended period and significant forming was observed after 313 h. At the end of this time on increasing the applied voltage up to 25 volts, no further forming was observed. Thin layers of evaporated polypropylene sandwiched between metal

electrodes (aluminium or copper) having thickness ranging from 600 to 1000 Å showed electroforming effects followed by negative resistance and electron emission into a vacuum under suitable conditions as described by Hogarth and Iqbal[60]. In their measurements the forming voltage varied from 12 to 15 volts and the peak current in formed specimens occurred at between 5 and 7 V. The results were found consistent with a theory based on the generation of conducting filaments during the forming process. Figure 1.12 shows the voltage-current characteristic of a Cu-PP(600 Å)-Cu sample after electroforming at room temperature and under a pressure of $\sim 10^{-5}$ torr. The emission current as shown in Figure 1.12 was collected by a subsidiary anode biased to 100 V and positioned about 1.5 cm from the surface of the sample. Unlike the behaviour of many reported M-I-M samples, the rapid rise of emitted current occurred not at a voltage corresponding to a peak current but at a voltage corresponding closely to the initial forming voltage 14.6 V. The behaviour in polyethylene reported by Hogarth and Zor[4] was quite different.

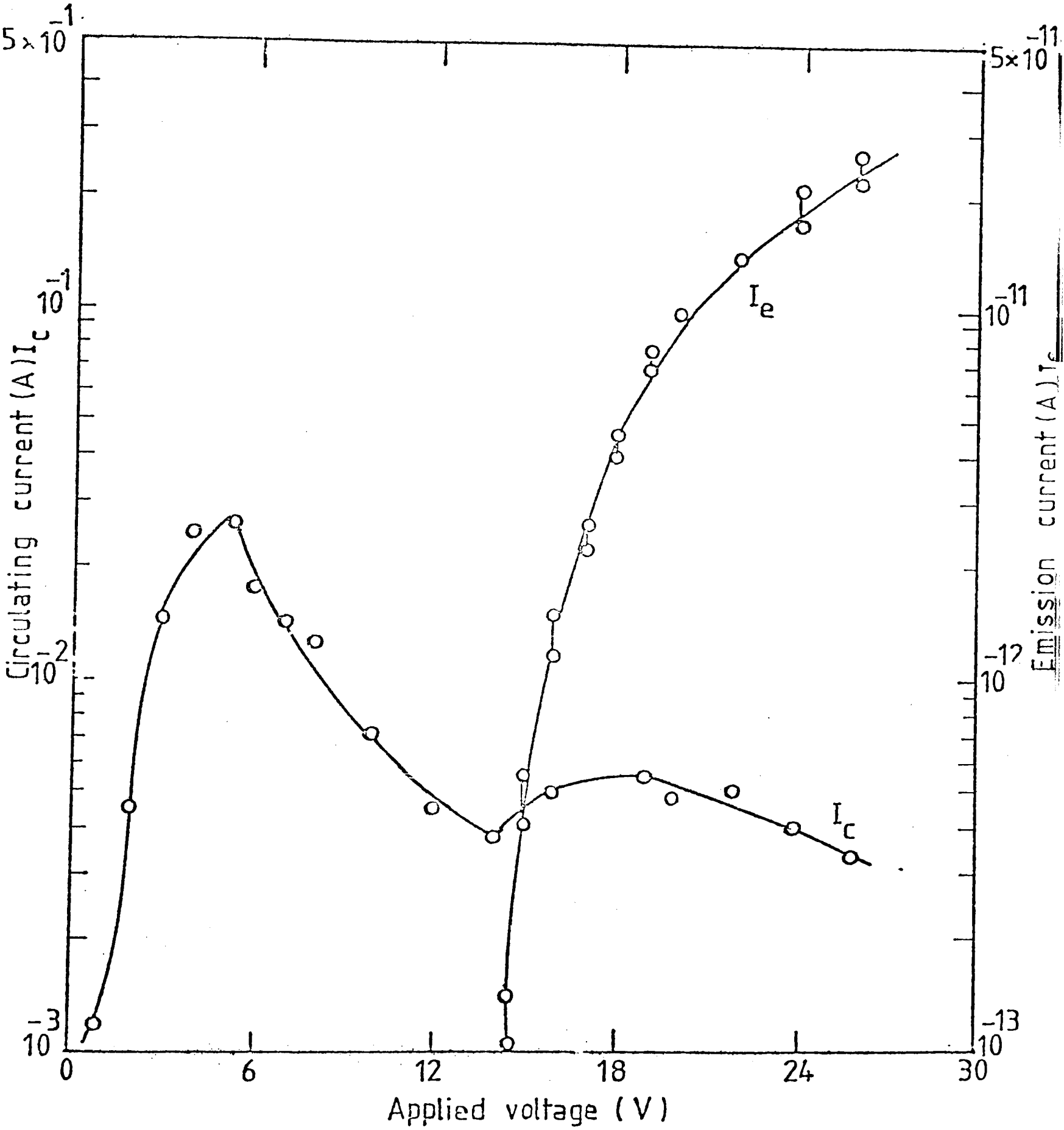

Figure 1.12 Circulating and emission current as function of applied voltage for a Cu-PP(600Å)-Cu sample. (Room temperature, ambient pressure 10^{-5} torr.) (after Hogarth and Iqbal[60]).

1.2 CONDUCTION IN DIELECTRICS

The details of the mechanism of electrical conduction in polymeric materials are not clear so far. Therefore the available theories for the crystalline, polycrystalline and amorphous inorganic solids are normally used in an attempt to describe the conduction mechanism in these organic materials. In this section we shall describe briefly the different conduction mechanisms observed in dielectric films, prior to electroforming, and these conduction mechanisms are also extended to explain the electrical properties of polymers.

1.2.1 Structure and electrical properties of polymers

The structure of the polymeric materials has an important role in governing their electrical properties. Most polymers of practical significance are composed of a fine mixture of micrometre size crystalline regions, embedded in an amorphous matrix of similar molecular composition[14]. The polymeric chains are thought to be folded in an orderly manner within crystalline regions and these regions have the form of small platelets having thicknesses of the order of a few nanometres. Since the amorphous regions have no structural order it is most likely that they contain most of the impurities present in the polymer. There is no comprehensive theory which could explain the conduction process in polymers and the picture concerning their electronic energy level is quite complicated. However, we may say that, all the polymers contain two types of bonds.[1] The strong covalent intra-molecular bonds have activation energies in the range of 3 - 8 eV. These bonds form a band of

bonding states, sometimes also known as the valence band. It is normally full in the absence of electron acceptor molecules[2]. The inter-molecular bonds are relatively weaker and are of the van der Waals types. The conduction band, or the band of antibonding states lies at an energy ΔW_i above the valence band and is usually empty. The width of both these bands is expected to be more than one electron-volt. The situation is schematically shown in Figure 1.13. The structural

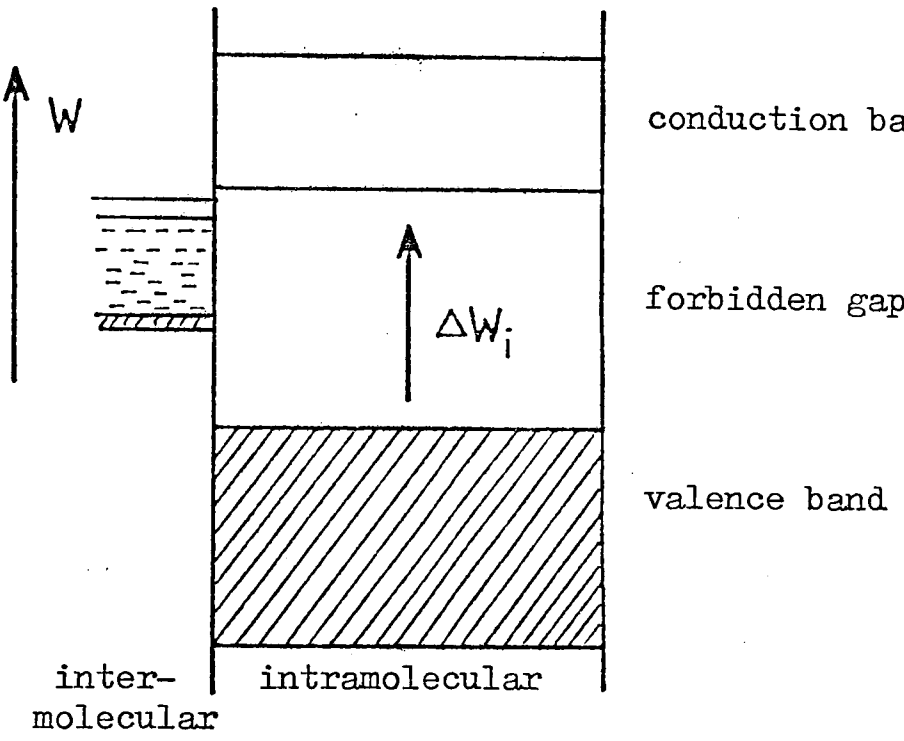

Figure 1.13 Schematic representation of the band structure of a typical polymer, showing valence band, forbidden energy gap ΔW_i, conduction band and localized levels due to disorder of intermolecular arrangements.

disorder resulting from the chain termination, chain folding and from the amorphous/crystalline interface will produce

localized levels, which are distributed in energy and space, as shown in Figure 1.13. These localized levels may be occupied by the electrons. The weaker intermolecular bonds result in narrow bands which along with localized levels are responsible for the very low electrical conductivity in the insulating polymers. The strong excitation by electron bombardment or by ultra-violet radiation may increase the conductivity of the polymers.

A carrier, electron or hole, is only free to move within the molecule in the main band and its transition into a neighbouring molecule may be possible by the thermal excitation over the potential barrier between them or by the tunnelling process of low probability. According to Mott and Davis[61] for the group of materials having a value of σ_o between 10^2 and 10^4 $\Omega^{-1}cm^{-1}$ conduction is due to the carriers excited into extended states. For the value of σ_o of the order of 10 $\Omega^{-1}cm^{-1}$, they suggested that the conduction is due to carriers excited into localized states at the band edges. A value of σ_o much less than this could correspond to conduction due to carriers hopping between localized states from one occupied state to an empty one nearby. Hopping between localized levels randomly distributed in space and energy is shown in Figure 1.14 (a). While Figure 1.14 (b) shows the hopping between a more regular array of molecular levels which are unable to form an extended band because of insufficient intermolecular overlap. In either case the transition probability $1/\tau_{ij}$ for hopping from site i to site j is

as defined below.

$$1/\tau_{ij} = \nu_o \exp\left(-\alpha R_{ij} - \Delta W_{ij}/kT\right)$$

Where ν_o is the characteristic frequency, α represents the tunnelling coefficient, R_{ij} is the spatial separation between the sites and ΔW_{ij} is the energy difference between them.

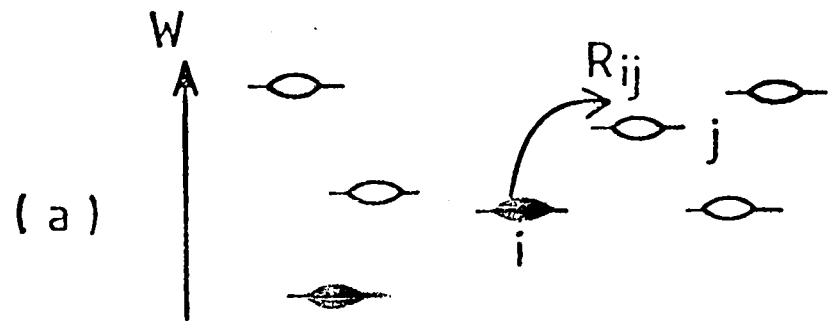

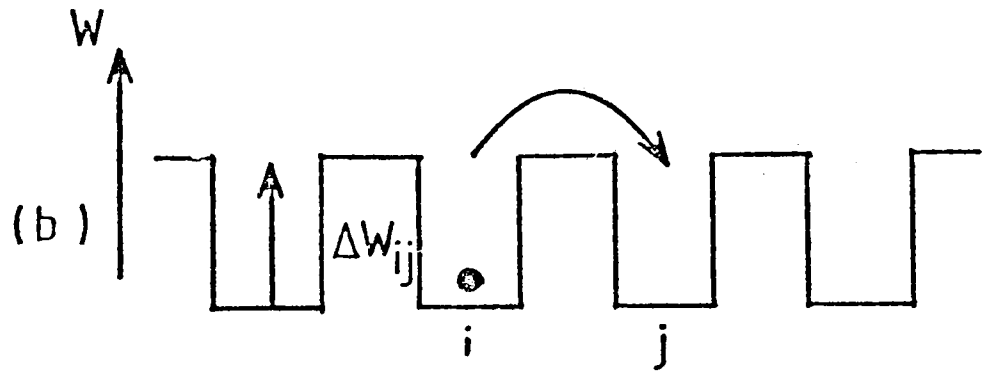

Figure 1.14 Two types of hopping motion in polymers.

(a) hopping between localized levels distributed randomly in space and in energy.

(b) hopping in a regular array of potential wells. The spatial distance of hop between site i and j is R_{ij}, while ΔW_{ij} represents the corresponding energy.

1.2.2 Space-charge-limited conduction

If the electrodes make ohmic contacts to the insulator, the electrons travel from the metal into the conduction band of the insulator, with a velocity determined by the mobility in the electric field and form a space-charge similar to that of a vacuum diode, then the conduction process is known as the space-charge limited.

Mott and Gurney[62] made the first theoretical study of SCL currents in insulators. They confined their studies to a trap-free insulator and for single carrier injection they obtained the following relationship

$$J = \frac{9\mu\varepsilon\varepsilon_o V^2}{8d^3} \qquad (1.1)$$

Here d is the thickness of the insulator, μ is the mobility and V is the applied voltage. The above equation predicts that SCL current is proportional to V^2 and inversely proportional to d^3. It also indicates that the current is temperature insensitive, which is contrary to the experimental observation.

The space-charge-limited currents in defect insulators (containing traps) were first investigated by Rose[63]. He pointed out that in such insulators a large fraction of the injected space charge condenses into the traps. In the trap-free insulator all the space charge contributes in the conduction process. So, the ratio θ, of a free-to-trapped charge in an insulator containing shallow traps is given by

$$\theta = \frac{N_c}{N_t} \exp\left(-\frac{E_t}{kT}\right) \qquad (1.2)$$

Where N_t is the density of the shallow traps, E_t is the trap depth below the bottom of the conduction band and N_c is the effective density of states in the conduction band.

For an insulator containing shallow traps, the Mott and Gurney equation can be modified by multiplying the R.H.S. with Θ So, equation (1.1) becomes

$$J = \frac{9\ \mu\ \varepsilon\ \varepsilon_o}{8\ d^3}\ \Theta\ V^2 \qquad (1.3)$$

Since Θ is temperature dependent, thus the inclusion of shallow traps in the insulator brings the theory into line with experimental observation. According to Lampert[64,65] when the injected free-carrier density n_i exceeds the volume generated free-carrier density n_o the space-charge effects will be observed, otherwise the ohmic conductivity will dominate. Lampert also calculated the voltage V_x at which the transition from ohmic to SCL conduction occurs, where V_x is equal to

$$V_x = \frac{e\ n_o d^2}{\Theta\ \epsilon\ \epsilon_o} \qquad (1.4)$$

It has been noted that if sufficient charge is injected into the insulator, the traps will be saturated. (Trap-filled limit, TFL). Now any additional injected charge into the insulator exists as free charge in the conduction band and the current rises by an amount Θ^{-1}. Beyond the TFL, the J.V characteristics follow the equation (1.1), rather than the equation (1.3). The voltage at which the TFL occurs is given by

$$V_{TFL} = \frac{e\ N_t\ d^2}{2\ \epsilon\ \epsilon_o} \qquad (1.5)$$

Figure (1.15) shows the schematic illustration of J-V characteristics for space-charge-limited conduction. Rose[63] has treated the case of an exponential trap distribution. The distribution of trap levels decreases exponentially in density with increasing energy below the conduction band, i.e.

$$N_t = A \exp\left(\frac{-E}{k T_c}\right) \tag{1.6}$$

where E is the energy measured from the bottom of the conduction band and T_c is a characteristic temperature greater than the temperature at which the currents are measured. The resultant current has been found to be[66]

$$I \sim \frac{V^{\frac{T_c}{T}+1}}{d^{\frac{T_c}{T}+1}} \tag{1.7}$$

which means that, since $T_c > T$, the current depends more strongly on V and d as compared with the trap-free or discrete level cases.

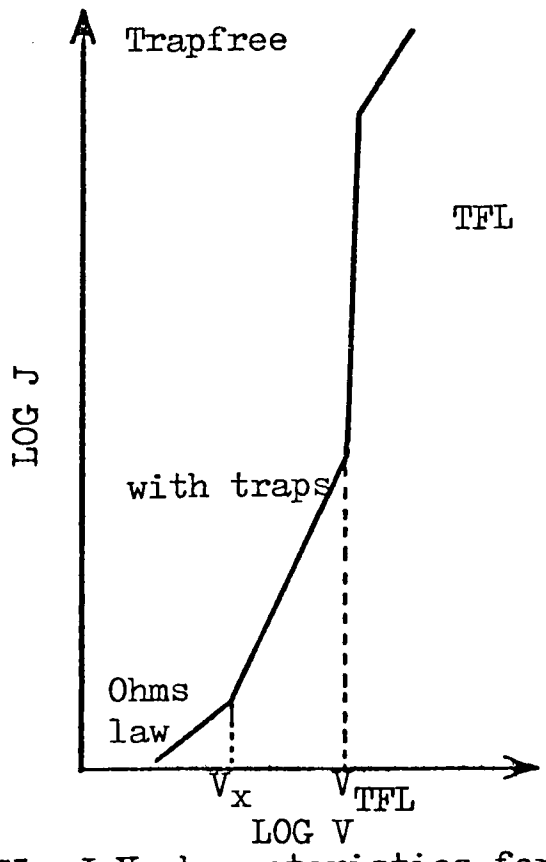

Figure 1.15 SCL, J-V characteristics for an insulator containing shallow traps.

Space-charge-limited currents of both signs of carrier can flow in an insulator if the cathode and anode are both ohmic to electrons and holes respectively. The current in the double-carrier injection case will be larger than those due to single-carrier injection under the same bias voltage. Also, in the case of double injection, the recombination between the two types of carriers makes the theory more complicated than the single-carrier theory. The details of the theory of double injection are given in the book by Lampert and Mark[67].

1.2.3 Schottky emission

In Schottky emission the electrons are emitted by thermal activation from the metal contact at negative potential, into the conduction band of the insulator over a potential barrier between the metal/insulator interface. Also, the applied electric field reduces the height of this barrier.

The following equation gives the current density for thermionic emission over a potential barrier ϕ_o.

$$J = AT^2 \exp\left(\frac{-\phi_o}{kT}\right) \qquad (1.8)$$

where A is the Richardson constant and is equal to 120 when J is expressed in amp cm^{-2}, k is Boltzmann's constant, T is absolute temperature and ϕ_o is the height of the potential barrier. The general shape of the potential barrier is shown in Figure 1.16.

The potential energy of the electron due to the image force is

$$\phi_{1m} = \frac{-e^2}{16\pi\epsilon\epsilon_o x} \qquad (1.9)$$

where ϵ and ϵ_o are the dielectric constant of the material and of free space respectively. Taking into account the effect of the image force, the height of the potential barrier as a function of the distance x from the interface is given by

$$\phi(x) = \phi_o + \phi_{im} = \phi_o - \frac{e^2}{16\pi\varepsilon\varepsilon_o x} \qquad (1.10)$$

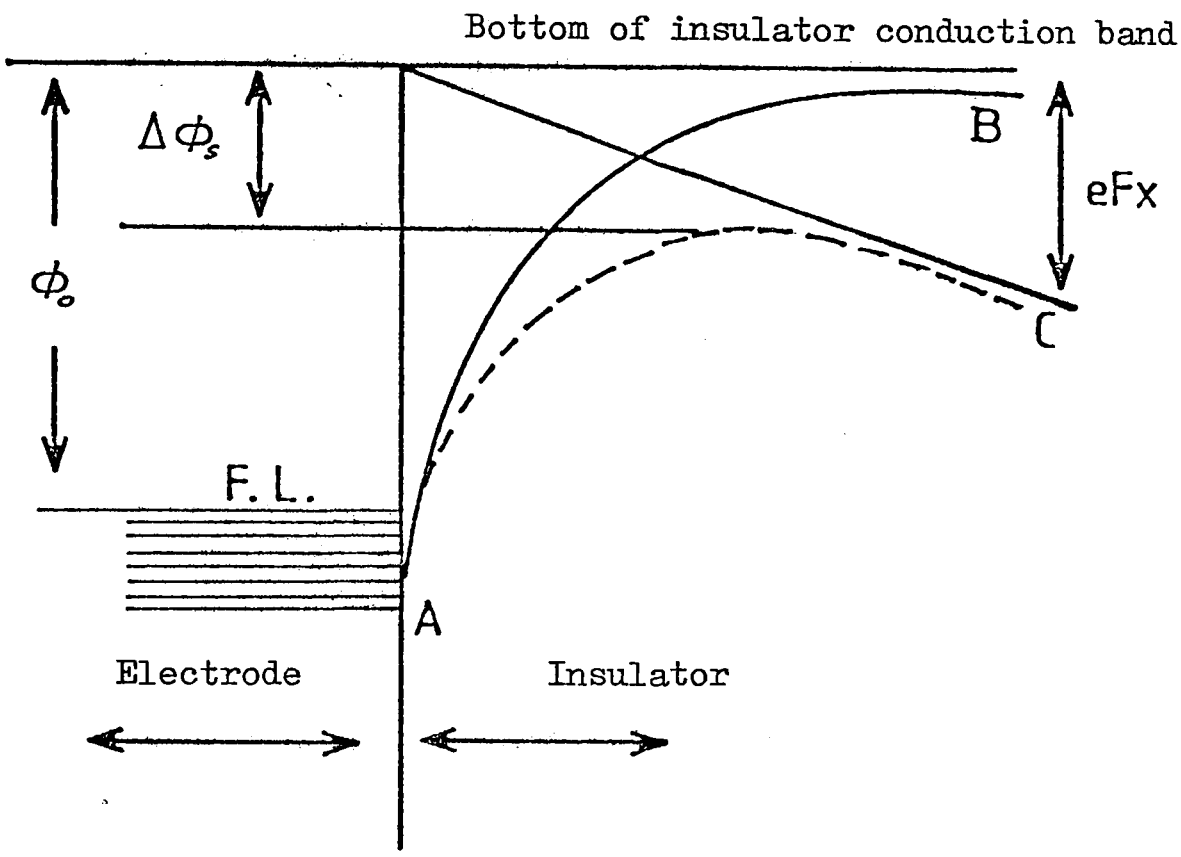

Figure 1.16 Schottky effect at a metal electrode.

In the presence of the uniform electric field at the surface of the cathode $\phi(x)$ is given by

$$\phi(x) = \phi_o - \frac{e^2}{16\pi\varepsilon\varepsilon_o x} - eFx \qquad (1.11)$$

$\phi(x)$ attains its maximum value at $x = x_m$ where

$$x_m = \left(\frac{e}{16\pi\varepsilon\varepsilon_o F}\right)^{\frac{1}{2}} \qquad (1.12)$$

The value of $\phi(x)$ at x_m becomes

$$\phi(x_m) = \phi_o - \left(\frac{e^3}{4\pi\varepsilon\varepsilon_o} \right)^{\frac{1}{2}} F^{\frac{1}{2}} \qquad (1.13)$$

The attenuation of the barrier height due to the interaction of the applied field with the image potential will be

$$\Delta\phi_s = \phi_o - \phi(x_m) \qquad (1.14)$$

which represents the Schottky effect.

Euqations (1.14) and (1.13) give

$$\Delta\phi_s = \left(\frac{e^3}{4\pi\varepsilon\varepsilon_o} \right)^{\frac{1}{2}} F^{\frac{1}{2}} = \beta_s F^{\frac{1}{2}} \qquad (1.15)$$

where

$$\beta_s = \left(\frac{e^3}{4\pi\varepsilon\varepsilon_o} \right)^{\frac{1}{2}}$$

Substituting $\phi(x_m) = \phi_o - \Delta\phi_s$ for ϕ in equation(1.8) we get

$$J = AT^2 \exp\left(\frac{\phi_o - \beta_s F^{\frac{1}{2}}}{kT} \right) \qquad (1.16)$$

[68]

This is the Richardson-Schottky equation for the neutral contact.

In this equation A is a constant and is given by

$$A = \frac{4\pi m e k^2}{h^3} \qquad (1.17)$$

where m is the electron mass and h is the Planck constant.

In a sandwich structure if we take into account the thermionic current in both directions, equation (1.8) will be modified as

$$J = AT^2 \left(e^{-\frac{\phi_1}{kT}} - e^{-\frac{\phi_2}{kT}} \right) \qquad (1.18)$$

where ϕ_1 and ϕ_2 are the maximum barrier heights above the Fermi-level of the negatively and positvely biased electrodes respectively. In this case the Richardson-Schottky formula

becomes[69]

$$J = AT^2 \exp\left[-\frac{\phi_o - (14.4\ eV/Ed)^{\frac{1}{2}}}{kT}\right] \qquad (1.19)$$

where V is the potential difference across the two electrodes and d is the thickness of the insulator.

1.2.4 The Poole-Frenkel effect

This effect involves a mechanism which is based on the same lowering of a potential barrier by an applied electric field as the Schottky effect. However, in this case the barrier in question is that for thermal excitation of trapped electrons into the conduction band of the insulator[70] as shown in Figure 1.17.

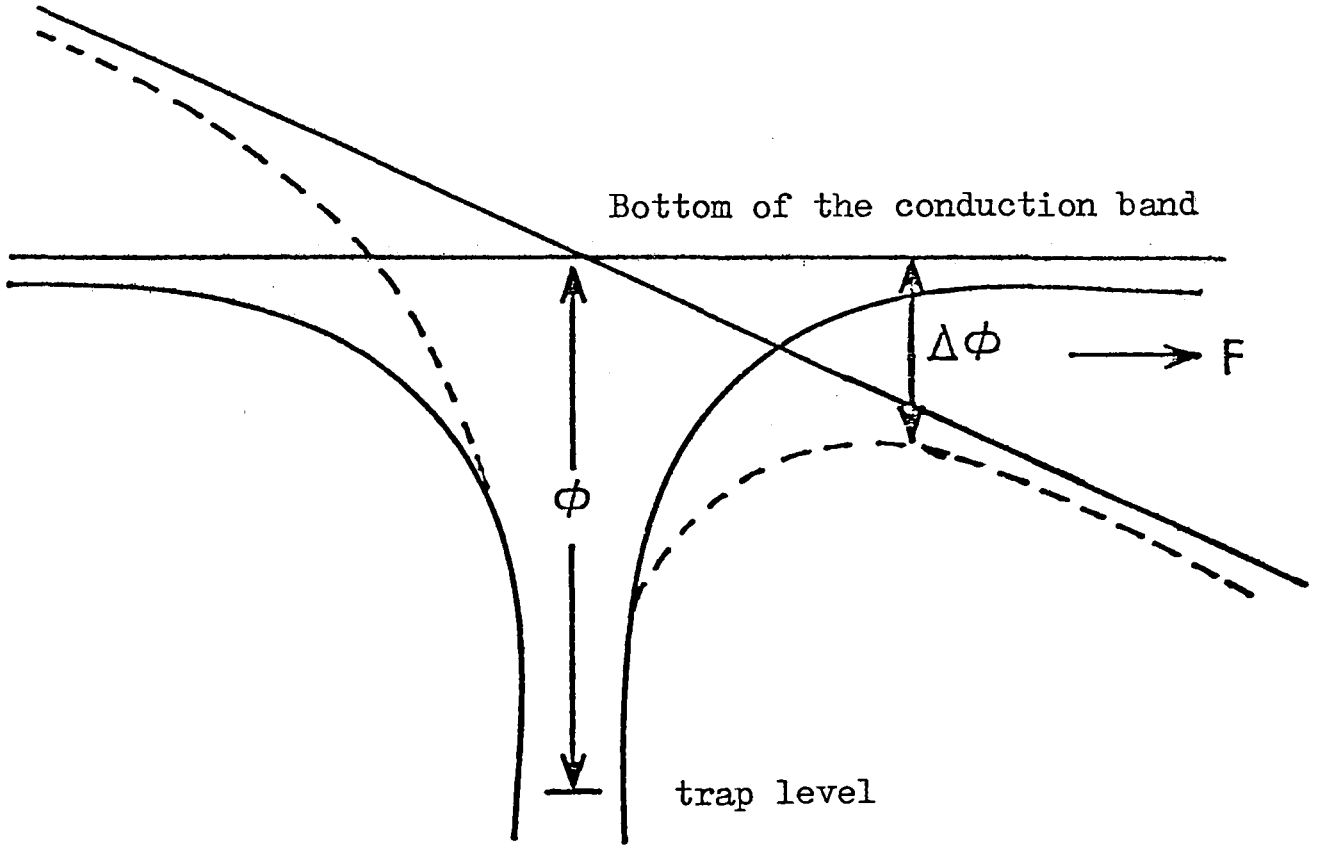

Figure 1.17 The varying of a potential barrier by an external electric field.

The potential energy of the electron in the coulombic field is

$$\phi(x) = \frac{-e^2}{4\pi\epsilon\epsilon_o x} \qquad (1.20)$$

comparing equation (1.20) with the equation (1.9) we see that the potential energy of the electron in a coulombic field is four times that due to the image force effects. Therefore ϕ_{PF}, the Poole-Frenkel attenuation of the coulombic barrier in a uniform electric field is given as

$$\Delta\phi_{PF} = \left(\frac{e^3}{\pi\epsilon\epsilon_o}\right)^{\frac{1}{2}} F^{\frac{1}{2}} = \beta_{PF} F^{\frac{1}{2}} \qquad (1.21)$$

Euqation (1.21) shows that

$$\beta_{PF} = 2\beta_s \qquad (1.22)$$

The field-dependent conductivity is given as

$$J = J_o \exp\left(\frac{\beta_{PF} F^{\frac{1}{2}}}{2kT}\right) \qquad (1.23)$$

where $J_o = \sigma_o F$ and σ_o is the low field conductivity. According to Mead[71] the current density in thin film insulator containing shallow traps is given as

$$J = J_o \exp\left(\frac{\beta_{PF} F^{\frac{1}{2}}}{kT}\right) \qquad (1.24)$$

Equation 1.24 is usually used as the Poole-Frenkel equation for thin film insulators instead of equation (1.23). The classical model of the Poole-Frenkel effect has been modified by Simmons[72,73] who showed that Poole's effect may be observed not only for charged traps but also for low-lying donor sites and neutral traps (see Figure 1.18). By introducing donor centres of different concentration in addition to occupied trapping centres

he could discuss the position of the Fermi level and arrived at the following equation for conductivity

$$J = J_o \exp\left(\frac{\beta_{PF} F^{\frac{1}{2}}}{2kT}\right) \qquad (1.25)$$

where $J_o = e \mu N_c \left(\frac{N_d}{N_t}\right)^{\frac{1}{2}} F \exp\left(-\frac{E_d + E_t}{2kT}\right)$ (1.26).

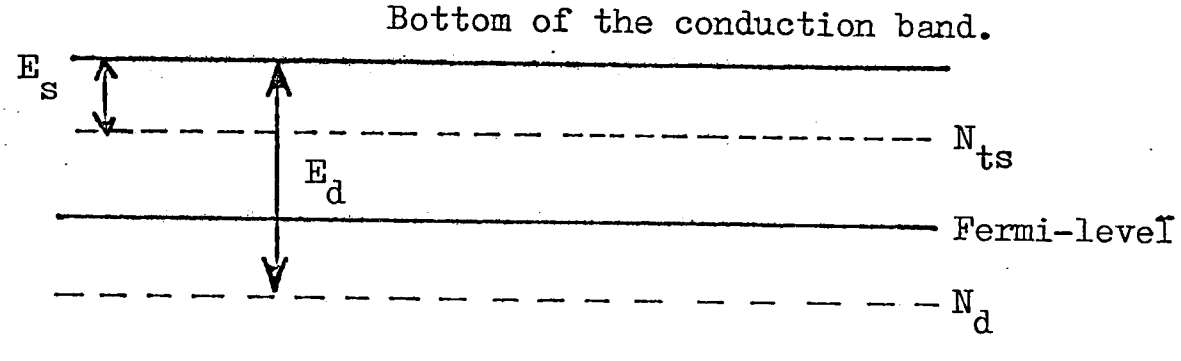

Figure 1.18 Energy diagram used to develop Equation (1.26) (after Simmons[71]).

Here e is the electronic charge, N_c is the effective density of states, μ is the mobility, $\frac{N_d}{N_t}$ is the ratio of the donor centres to the trap centres, E_d and E_t are the energy levels of the donor and trap centres from the bottom of the conduction band respectively.

1.2.5 Ionic conduction

The concept of ionic conduction due to lattice defects has been known for sometime[74-76]. The actual mechanism involves the migration of ions (or vacancies) by hopping over a potential barrier ϕ, from one defect site to the next in an applied

electric field F. Due to the presence of large numbers of defects in amorphous films this mechanism might be important in these materials. Higher activation energy, large transit time, transport of material from one electrode to the other and the polarization effects in a constant d.c. field are the main features of the ionic conduction[77,78]. These may also be used to distinguish it from the electronic conduction.

For an applied electric field F, there are three different cases for the ionic conduction.

(i) For low electric field, $F \ll \frac{kT}{qr}$, the current density J, is given by

$$J = AT^2 F \exp\left(\frac{-\phi}{kT}\right) \qquad (1.27)$$

where q is the charge of the ion, r is distance between two sites, A is a constant, k is Boltzmann's constant and T is the absolute temperature.

(ii) For $F \approx \frac{kT}{qr}$ the current density has the form

$$J = J_o \exp\left[-\left(\frac{\phi}{kT} - \frac{Fqr}{kT}\right)\right] \qquad (1.28)$$

where J_o is a constant.

(iii) For $F \gg \frac{kT}{qr}$, the current density is equal to

$$J = J_o \exp\left[-\frac{(\phi' - Fqr)}{2kT}\right] \qquad (1.29)$$

In equation (1.29) ϕ' is the sum of the zero field activation energy, ϕ, and the height of the first potential barrier[79].

1.2.6 Tunnelling

If the two electrodes are separated by a sufficiently thin

layer of the insulating material, current can pass between the electrodes by the quantum mechanical process called tunnelling. The current density due to electron tunnelling through such a barrier is given by the product of the number of the electrons arriving at the barrier per unit area per second and their probability of penetrating the barrier. For electrons tunnelling from electrode 1 to electrode 2, (assuming the barrier is in the x-direction) the current density is given by

$$J_1 = \int_0^{Vm} V_x \, n(V_x) \, P(\varepsilon_x) \, dV_x \qquad (1.30)$$

$$J_1 = \frac{1}{m} \int_0^{\varepsilon_m} n(V_x) \, P(\varepsilon_x) \, d\varepsilon_x \qquad (1.31)$$

where $n(V_x)\, dV_x$ is the number of electrons per unit volume having velocity between V_x and $V_x + dV_x$, $P(\varepsilon_x)$ is the probability that an electron with energy ε_x can penetrate the barrier and ε_m is the maximum energy of the electrons in the conducting regions. If we define J_2, as the current density for electrons tunnelling from region 2 to region 1, then the net current density will be

$$J = J_1 - J_2$$

The value of J is given as[80]

$$J = \frac{4\pi n^2}{h^3} \int_0^{\infty} \{ f_1(\varepsilon) - f_2(\varepsilon) \} \, dt \int_0^{\varepsilon_m} p(\varepsilon_x) \, d\varepsilon_x \qquad (1.32)$$

where $f_1(\varepsilon)$ and $f_2(\varepsilon)$ are the Fermi-Darac distribution function in region 1 and 2 respectively.

Fowler and Nordheim[81] were the first to calculate the current

flowing through thin metal-insulator-metal structures. Since then a number of papers have been published on this subject[82-85].

1.3 EFFECTS OF ELECTRODES

It is necessary to connect electrodes to the surface of an insulator to measure its conductivity. Talking in terms of the energy-band diagram, the insu-lator erects a potential barrier between the electrodes, extending from the electrode Fermi level to the bottom of the insulator conduction band, as shown in Figure 1.19. After the contact, in thermal equilibrium, the vacuum and Fermi levels of the electrodes and insulator must be continuous across the interface. Actually, now we do not distinguish the electrode and insulator Fermi level. The vacuum level is defined as the energy of an electron at rest just outside the surface of the material, while the energy difference between the vacuum and Fermi levels is known as the work function of the material. Three types of contact exist at the metal-insulator interface, namely (i) ohmic, (ii) neutral and (iii) blocking contacts.

1.3.1 Ohmic contact

The contact at a metal-insulator interface is known as ohmic if the electrode work function ψ_m is smaller than the insulator work function ψ_i. In order to satisfy the thermal equilibrium conditions electrons are injected from the electrode into the conduction band of the insulator. An ohmic contact acts as a reservoir of charge and is capable of supplying electrons to the insulator as required by the bias conditions. Thus, with

a contact of this type the conduction depends upon the rate of flow of electrons through the bulk of the insulator and the current-voltage characteristics of the sample will be determined by the bulk properties of the insulator, so we can say that the conduction mechanism is bulk-limited. Figure 1.19 explains the energy diagram of metal and the insulator before and after the formation of an ohmic contact.

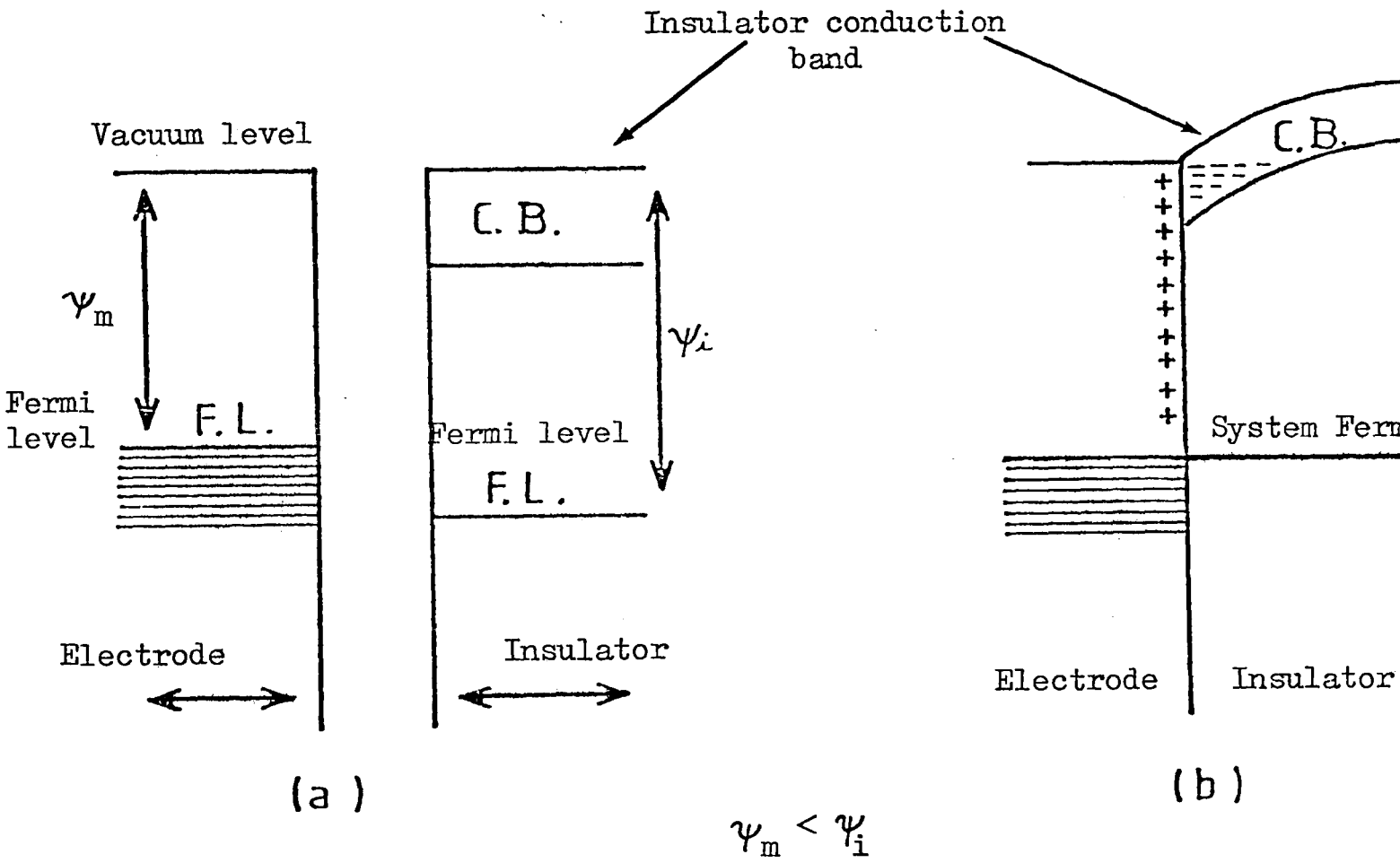

Figure 1.19 Energy band diagram of metal and insulator (a) before contact (b) after contact (ohmic contact)

1.3.2 Neutral contact

When the electrode work function ψ_m, is equal to the metal work function ψ_i, and there is

no charge transfer between the electrode and insulator at the interface, the contact is called the neutral contact. Also, in the absence of any space-charge within the insulator, the conduction band is flat right up to the interface, i.e. no band bending is present as shown in Figure 1.20. This contact is a transitional stage between an ohmic and blocking contact.

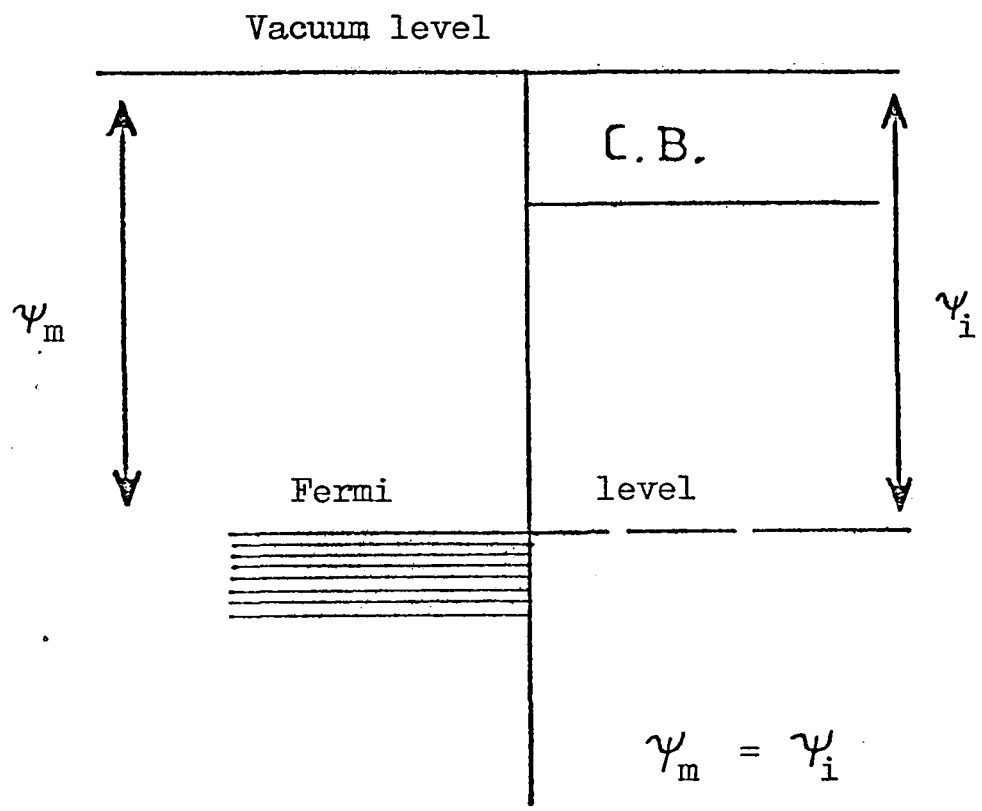

Figure 1.20 Energy band diagram of a neutral contact.

1.3.3 Blocking contact

When an electrode having a work function ψ_m makes a contact with an insulator whose work function is ψ_i, such that $\psi_m > \psi_i$, the contact is known as blocking. In order to satisfy the thermal equilibrium condition the

electrons flow from the insulator into the metal. As a result of this, a positive space-charge is created inside the insulator while an equal negative charge resides on the metal electrode. Therefore a local field exists within the surface of the insulator due to the electrostatic interaction of these oppositely charged regions. The net effect of this field is to bend the bottom of the insulator conduction band within the bulk of the insulator in the downwards direction until it lies at an energy $(\Psi_i - \chi)$ above the system Fermi level. However the flow of electrons through the system is determined by the rate at which they flow over the interfacial barrier, hence the conduction process is electrode-limited. A blocking contact is shown in Figure 1.21.

The interfacial barrier in the case of a blocking contact is equal to $\Psi_m - \chi$, where Ψ_m is the electrode work function and χ is the electron affinity of the insulator. This value of the barrier height has been chosen for the real surfaces. In some cases the potential barrier is often found to be independent of the electrode work function.

Bardeen[86] suggested that this discrepancy is due to the presence of surface states and these states produce a potential barrier at the semiconductor surface. The sudden displacement of the surface atoms from their lattice position, the absorbed gas and the water vapours are the main reasons

for the existence of these surface states.

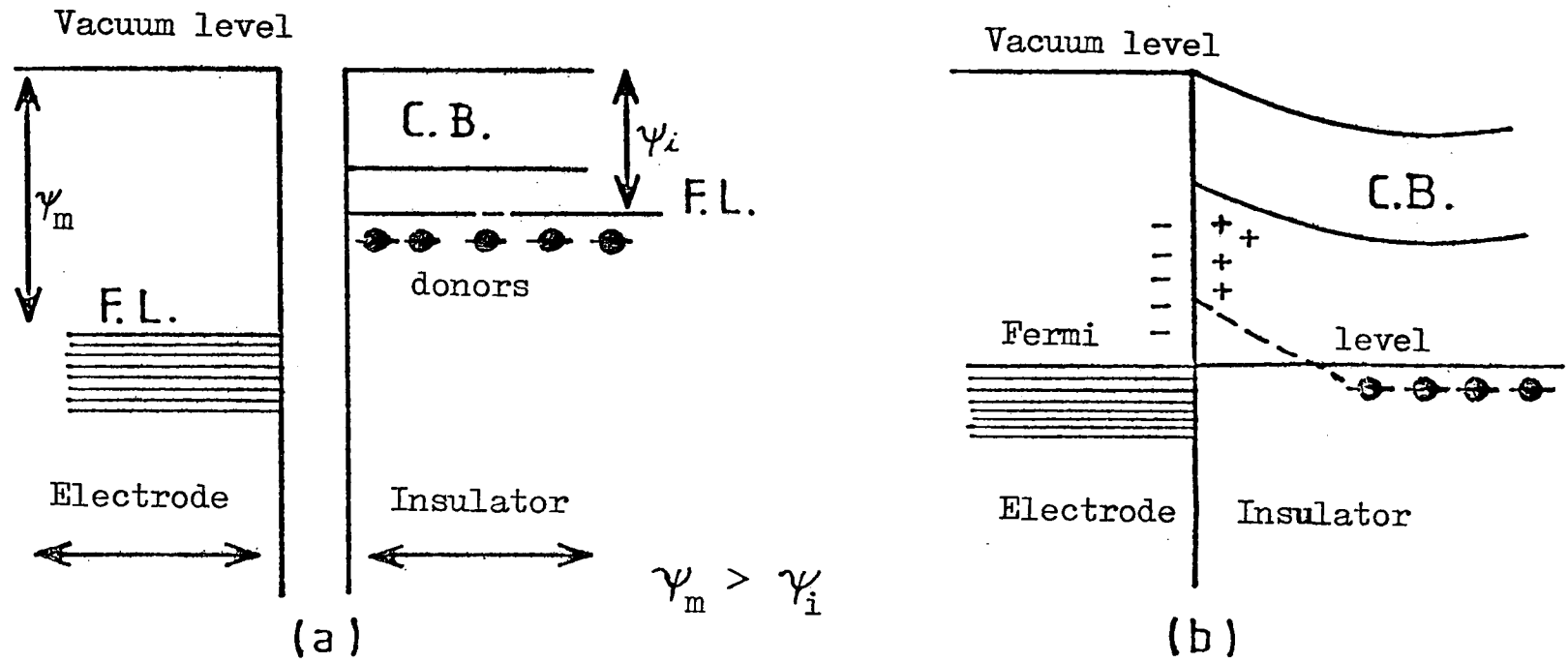

Figure 1.21 Energy band diagram (a) before contact (b) after contact (blocking contact)

1.4 THERMALLY-STIMULATED CURRENTS

The measurements of thermally-stimulated currents (TSC) have been widely used to determine the properties of traps, i.e. the density and energy distribution of charge carrier trapping centres in solids.

1.4.1 Experimental technique

In this technique the samples are kept overnight under

vacuum in a dark chamber with their electrodes short circuited as described by Slowick[16]. The samples are then cooled rapidly to liquid nitrogen temperature while still in the dark and are illuminated through the top electrode with light of the appropriate wave length to fill the trapping centres. Now a constant external field is applied and the samples are heated in the dark at a constant heating rate. The current flowing in the external circuit is recorded as a function of temperature. The emptying of traps when a particular temperature is reached leads to an increase in the current in the form of a peak over and above the normal background current. For the fixed heating rate, Pai[87] reported that the peak temperature shifts to lower values, as the applied field is increased. But, when the field is fixed and the heating rate is varied, the peak shifts to higher temperature as the heating rate increases.

1.4.2 Theory (TSC)

Haine and Carley-Read[88] have given a method for analysing the thermally-stimulated conductivity curves. The different symbols used in their analysis are defined below.

n_t is the density of electrons in the trapping level, θ is the trapping factor, τ_t is the electron trapping time, τ is the recombination life time, N_C is the equivalent density of states

at the bottom of the conduction band, N_t is the density of trapping centres for the particular level, E_t is the trap depth, S_t is the capture cross-section of the trapping level, V is the thermal velocity of electrons in the conduction band, T is the absolute temperature, k is the Boltzmann constant, n_{c_1} refers to the carrier density at heating rate $\dot{T}_1$ and similarly for n_{c_2}, n'_{c_1} is $\frac{dn_{c_1}}{dT}$ and similarly for n'_{c_2}, A is the cross-sectional area, d is the thickness of the specimen and μ is the carrier mobility.

The rate of release of electrons from a particular trapping level is given by $\frac{n_t \theta}{\tau_t}$

where θ and τ_t are given as

$$\theta = \left(\frac{N_c}{N_t}\right) \exp\left(\frac{-E_t}{kT}\right) \qquad (1.33)$$

and

$$\tau_t = \frac{1}{N_t S_t V} \qquad (1.34)$$

The rate of retrapping of electrons for finite occupancy is given by

$$\frac{n_c (1 - {}^{n}t/N_t)}{\tau_t}$$

Also, the rate of recombination is $\frac{n_c}{\tau}$

For a single trapping and recombination level, these rates are related by the following equation.

$$\frac{dn_c}{dt} = \frac{n_t \theta}{\tau_t} - \frac{n_c}{\tau}\left(1 - \frac{n_t}{N_t}\right) - \frac{n_c}{\tau} \qquad (1.35)$$

Since the rate of change of n_c is very small as compared with the relaxation time of n_c, so we can neglect $\frac{dn_c}{dt}$

Now the equation becomes

$$\frac{n_t \theta}{\tau_t} - \frac{n_c}{\tau_t}\left(1 - \frac{n_t}{N_t}\right) - \frac{n_c}{\tau} = 0 \qquad (1.35)$$

Rearranging the above equation we get

$$n_c = \frac{n_t \theta}{\left(1 + \frac{\tau_t}{\tau} - \frac{n_t}{N_t}\right)} \tag{1.36}$$

Now differentiating equation (1.36) with respect to temperature using primed symbols to represent such differentiation.

$$\text{e.g.} \quad n_c' = \frac{dn_c}{dT}$$

Therefore,

$$n_c' = \frac{n_t \theta' + n_t' \theta}{\left(1 + \frac{\tau_t}{\tau} - \frac{n_t}{N_t}\right)} + \frac{n_t \theta\, n_t'}{N_t \left(1 + \frac{\tau_t}{\tau} - \frac{n_t}{N_t}\right)^2} \tag{1.37}$$

Now using equation (1.36) in (1.37) we obtain

$$n_c' = \frac{n_c \theta'}{\theta} + \frac{n_t\, n_c}{n_t} + \frac{n_t'\, n_c^2}{N_t\, n_t \theta} \tag{1.38}$$

Dotted symbols can be used to represent differentiation with respect to time.

Hence,

$$\dot{n}_t = \frac{dn_t}{dt} = -\frac{n_c}{\tau} \tag{1.39}$$

and

$$n_t' = \frac{dn_t}{dT} = \frac{-n_c}{\tau \dot{T}} \tag{1.40}$$

Rewriting equation (1.33)

$$\theta = \left(\frac{N_c}{N_t}\right) \exp \left(\frac{-E_t}{kT}\right)$$

$$\theta' = \frac{d\theta}{dT} = \frac{N_c}{N_t}\left(\frac{E_t}{kT^2}\right) \exp\left(\frac{-E_t}{kT}\right) + \frac{N_c'}{N_t} \exp\left(\frac{-E_t}{kT}\right)$$

or

$$\theta' = \theta\left(\frac{E_t}{kT^2} + \frac{N_c'}{N_c}\right)$$

Since $N_c \alpha T^{3/2}$, $N_c' = \frac{3}{2}\frac{Nc}{T}$, using this in the above equation.

$$\theta' = \frac{\theta}{T}\left(\frac{E_t}{kT} + \frac{3}{2}\right) \tag{1.41}$$

The temperature dependence of N_c can be neglected if $E_t >> kT$. Using this approximation and substituting equations (1.40) and (1.41) in equation (1.38), also using (1.36) to eliminate n_t we obtain

$$n_c' = \frac{n_c}{\tau + \tau_t}\left[\frac{E_t\,(\tau + \tau_t)}{kT^2} - \frac{(n_c + N_t\theta)^2}{\dot{T}\,N_t^2\theta}\right] \tag{1.42}$$

Putting the value of θ from equation (1.33) into equation (1.42) gives the following result.

$$\frac{n_c'}{n_c} = \frac{E_t}{kT^2} - \frac{\left\{n_c + N_c \exp\left(-E_t/kT\right)\right\}^2}{\dot{T}\,N_t\,(\tau + \tau_t)\,N_c \exp\left(-E_t/kT\right)} \tag{1.43}$$

Rearrangement of the above equation yields

$$N_t\,(\tau + \tau_t) = \frac{\left\{n_c + N_c \exp\left(-E_t/kT\right)\right\}^2}{\dot{T} N_c\left\{E_t/kT^2 - n_c'/n_c\right\}\exp\left(-E_t/kT\right)} \tag{1.44}$$

At the current maximum of the TSC curve, $n_c' = 0$,

therefore equation (1.44) becomes

$$N_t(\tau + \tau_t) = \frac{kT^2\,N_c}{E_t\,\dot{T}} \exp\left(-\frac{E_t}{kT}\right)\left[1 + \frac{n_c}{N_c}\exp\left(\frac{E_t}{kT}\right)\right]^2 \tag{1.45}$$

n_c is given as

$$n_c = \frac{Id}{\mu eVA} \tag{1.46}$$

where I is the current flowing through the sample and V is the applied voltage.

Equation (1.44) contains two implicit unknown parameters, $N_t\,(\tau + \tau_t)$ and E_t, therefore two values of $\dot{T}$ are used, i.e. the samples are heated at two different rates but under the same applied field, and two points on the two peak curves corresponding to the same temperature are taken. Now two expressions are obtained from equation (1.44) and hence $N_t\,(\tau + \tau_t)$ can be eliminated to give the following expression.

$$\frac{\left\{ n_{c_1} + N_c \exp\left(-E_t/kT\right) \right\}^2}{\dot{T}_1 \left(E_t/kT^2 - n'_{c_1}/n_{c_1} \right)} = \frac{\left\{ n_{c_2} + N_c \exp\left(-E_t/kT\right) \right\}^2}{\dot{T}_2 \left\{ E_t/kT^2 - \left(n'_{c_2}/n_{c_2} \right) \right\}} \quad (1.47)$$

Rearranging equation (1.47) we get

$$\exp -\left(\frac{E_t}{kT}\right) = \frac{n_{c_2}X - n_{c_1}}{N_c\left(1 - X\right)} \quad (1.48)$$

where X^2 is defined as

$$X^2 = \frac{\dot{T}_1 \left(1 - n'_{c_1} kT^2/n_{c_1} E_t\right)}{\dot{T}_2 \left(1 - n'_{c_2} kT^2/n_{c_2} E_t\right)} \quad (1.49)$$

If we choose the current maximum value temperature for $\dot{T}_1$, then $n'_{c_1} = 0$, and equation (1.49) is further simplified as

$$X^2 = \frac{\dot{T}_1}{\dot{T}_2 \left(1 - n'_{c_2} kT^2/n_{c_2} E_t\right)} \quad (1.50)$$

We can see that equation (1.48) gives the single value of E_t and by substituting this into equation (1.44), a single value of $N_t(\tau + \tau_t)$ is obtained.

τ, can be calculated from the photocurrent using the following equation

$$\tau = \frac{I_L d^2}{fe\mu V} \quad (1.51)$$

where I_L is the photocurrent and f is the number of photons per second absorbed by the sample.

The area under the TSC curve is proportional to the concentration of charge carriers released from traps and is related as under

$$n_{to} = \frac{\alpha d}{\tau \mu V e A} \quad (1.51)$$

where n_{to} is the density of electrons in the trapping level at the start of the emptying period and α is the complete area under the TSC peak.

It can be assumed that the initial trap occupancy is the thermal equilibrium value at a lower temperature corresponding to the value of n_c (n_{co}) at equilibrium state in the presence

of the exciting radiation and the trap occupancy is given by

$$\frac{n_{to}}{N_t} = \left\{1 + \frac{N_c}{n_{co}} \exp\left(\frac{E_t}{kT}\right)\right\}^{-1} \qquad (1.52)$$

The value of τ is known from equation (1.51), therefore $n_{to}\tau$ can be calculated. If $n_{to}\tau$ is found equal to $N_t(\tau + \tau_t)$ it means that $\tau_t \ll \tau$ and the initial occupancy is 100%. Hence N_t can be found. Finally, we can say that if $\tau_t \ll \tau$ the value of N_t can be calculated without any assumptions, but τ_t and S_t cannot be found. But, on the other hand, if τ_t is comparable or larger than, τ , N_t and τ_t can only be obtained, provided it is assumed that the initial occupancy is determined by thermal equilibrium conditions.

Bube[89] calculated the trap depth E_t from the curves of the thermally-stimulated current by using the conductivity and the peak temperature (T_m). His calculation was based on the assumption that the Fermi level is located at the level corresponding to the traps, when the conductivity attains its maximum value and his expression of E_t includes re-trapping as well. So, according to Bube, the mean trap depth is given as

$$E_t = kT_m \ln \frac{N_c e \mu}{\sigma_m} \qquad (1.53)$$

where σ_m is the peak conductivity.

1.5 ELECTROFORMING IN M-I-M STRUCTURES

Thin films of MIM samples under certain conditions undergo an electroforming procession exceeding a threshold applied

voltage across the dielectric. The forming process is distinguished by a pronounced voltage-controlled negative resistance which appears in the I-V characteristics of the formed sample. Also, associated with the electroforming process are electron emission, electroluminescence and a memory effect. These phenomena have been reported for many insulators, including oxides[50-52, 90,91], halides[54], sulphides[92] and certain polymeric materials[93,58]. Recently Hogarth and Iqbal[60] have shown that thermally evaporated polypropylene undergoes a similar electroforming process. The electroforming is affected by the applied voltage, polarity of the bias voltage, thickness of the insulator, electrode material, temperature and pressure. Forming takes place in thin layers of insulator when a potential difference equal to or greater than the forming voltage V_F, is applied across the sample[50]. Also, a sinusoidal voltage of amplitude greater than V_F can induce[50,94] forming effects. The degree of forming is related to the maximum current flowing through the sample. The current-voltage characteristics almost follow the same path as long as the applied voltage does not exceed[53] the V_F limit. However, any attempt to break this limit will increase the degree of forming, provided the applied voltage remains within the breakdown point, which varies from material to material. The reverse polarity across the formed device will decrease the degree of forming, if the potential difference exceeds V_F. The reverse bias does not completely deform the device and forming could be achieved again by positively biasing the top electrode to V_F[53]. The degree of forming is also affected by

the thickness of the insulator and the peak current is inversely proportional to the cube of the thickness, i.e. $I_p \alpha d^{-3}$.

Electroforming has been reported in different oxides including Al_2O_3, SiO_x, Ta_2O_5, ZrO_2, TiO_2, MgO and Al_2O_3 having thicknesses between 100 to 20,000 Å [50,51,95-101]. The voltage V_m, for the maximum current was found to be independent of the thickness of the oxide[102], while V_F, the forming voltage, increases slowly for increasing insulator thickness. In the presence of impurities forming can be achieved easily. However, if the impurity concentration is too low, dielectric breakdown occurs before forming is induced[102]. Differential negative resistance has been observed in polymer layers varying in thicknesses from 150 to 2500 Å . The degree of forming in the case of halides and oxides is higher than for polymers, also the polymers are difficult to form as compared with other insulators[43]. Several metal electrodes have been used in MIM structures. These electrodes include Ag, Al, Au, Cu, Si, Sn, Pb, In, Bi, Fe, W and Ni, i.e. most common metals except Mg[101,103,54]. Verderber[53] et al studied the effect of electrode material on forming and found the same forming voltage for the Ag , Au and Cu electrodes when they were biased positively in a Al-SiO-metal system. Where the term metal refers to the material under investigation. They could not achieve electroforming with Al electrodes. Generally it is not possible to get electroforming at atmospheric pressure. However, it has been reported that fluorides[104] can be electro-formed in air at atmospheric pressure. In most cases it is

established at a low pressure of less than 10^{-2} torr or in inert gas at atmospheric pressure[53].

So far we have discussed the factors affecting the electroforming process. In the following section we shall outline some properties of the formed devices.

1.5.1 Differential negative resistance

As mentioned before, to achieve electroforming it is necessary to apply a voltage greater than or equal to the forming voltage V_F. Once the forming has been achieved, a differential negative resistance appears in the I-V characteristics of the device. A typical shape of the differential negative resistance characteristic is shown in Figure 1.22. Such a negative resistance is known as a voltage-controlled negative resistance, or VCNR.

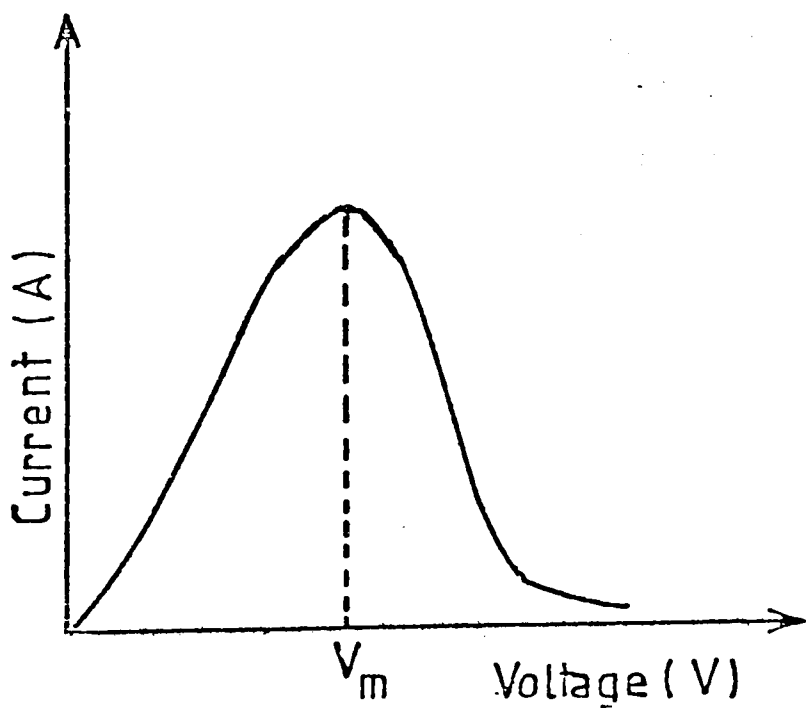

Figure 1.22 General shape of the voltage-controlled negative resistance.

After electroforming the device resistivity decreases and the current increases by several orders of magnitude[53]. The change in conductivity is permanent and the I-V characteristics show VCNR for both increasing and decreasing voltages. V_m corresponds to the maximum current flowing through the sample and was found independent of the insulator thickness, but its value varies slightly (3 to 5 V) with insulator and electrode material. However, the peak current depends upon the nature and the thickness of the insulator.

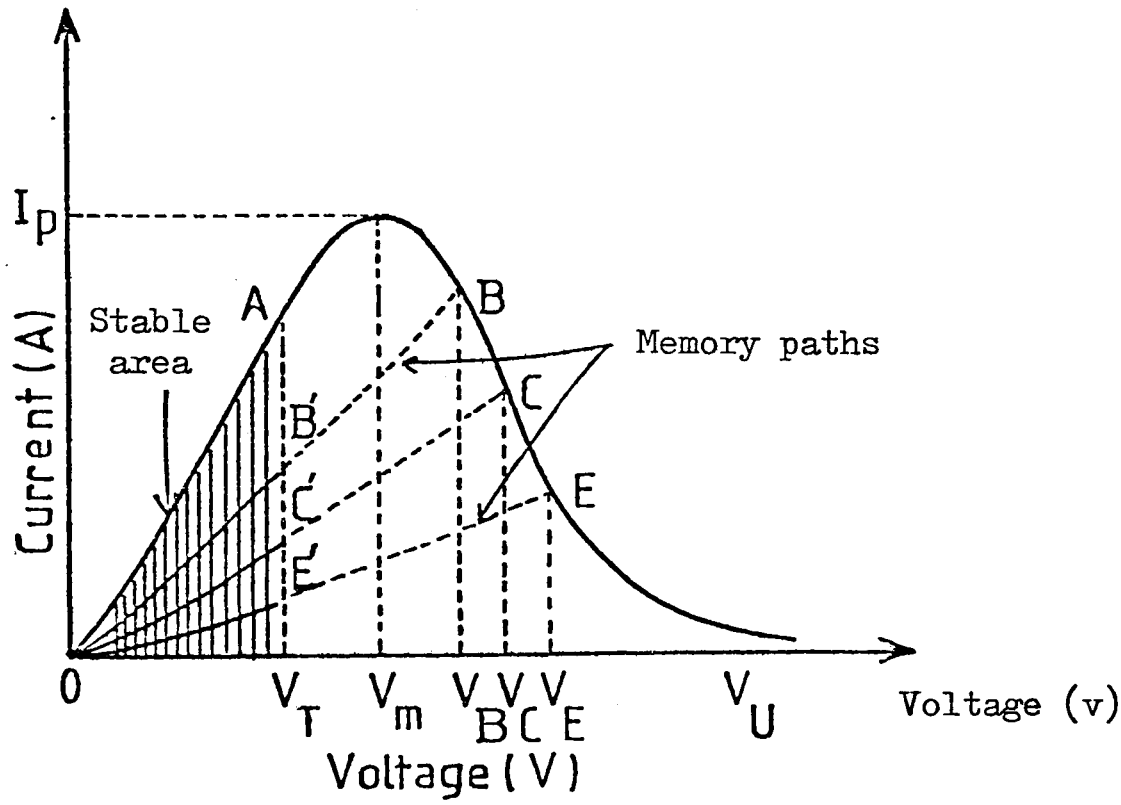

Figure 1.23 The I-V characteristics of a formed MIM sample, showing several high frequency characteristics OB, OC and OE and memory states as OB', OC' and OE'.

Let us consider Figure 1.23 where we notice that up to the threshold voltage V_T, the current is independent of the frequency i.e. the a.c. and the d.c. characteristics in a

formed sample are given by the same curve OA. Also the peak-current I_p decreases with frequency. Only the d.c. or low frequency measurements demonstrate a negative resistance[53]. For applied a.c. voltage $V > V_T$, a new set of I-V characteristics appears as shown by the dotted lines. In the range $V_T < V \ll V_u$ the overall impedance of the characteristics increases with increasing voltage amplitude. For instance, if the voltage amplitude is raised up to V_B, then decreasing the voltage involves following the curve BB' O, instead of BAO. Similarly we can explain the curves CC' O and EE' O. These characteristics do not exhibit negative resistance, although the locus of their end - points coincides with the d.c. characteristics.

1.5.2 Memory characteristics

When the applied voltage across the formed sample is taken beyond V_m and then switched off quickly, (less than 10^{-3} sec) a memory state is induced on the sample[52]. (See Figure 1.23). It follows that if the voltage corresponding to any operating point on the negative-resistance region (say to the point B) is reduced to zero in 0.1 ms, then on reapplication of voltage a high-impedance state OB' will prevail, rather than the low-impedance characteristics OA, provided the applied voltage does not exceed V_T. Similarly any voltage pulse corresponding to the points C and E, with trailing edge faster than 0.1 ms will generate respectively the new impedance states O C' and O E'. Switching from a low-to-high-impedance state is accomplished by a voltage pulse of duration about 2 to 3 ns. These memory states can be erased to get the previous low-

impedance state OA, by applying a voltage pulse slightly greater than V_T in height and about 100 ns wide. It takes almost 100 ns to complete a cycle of switching from high to the low-impedance state and back again. A period of time which varies between 10^{-6} to 10^{-1} seconds must elapse before the switching cycle is repeated. It is known as the dead time and depends upon the temperature and the sample fabrication[54]. Any operating point lying within the electrically stable area, enclosed by the perimeters OAB$'$ C$'$ E$'$ O is retraceable and stable but only the points on the curve ABCE are stable within the area enclosed by the perimeter E$'$ C$'$ B$'$ ABCEE$'$.

1.5.3 Thermal characteristics (Thermal-voltage memory)

At liquid nitrogen temperature, the application of a voltage across the formed sample will produce a negative resistance region similar to the low-impedance curve OABCE in Figure 1.23. If the voltage corresponding to any point between V_T and V_E on the curve ABCE is reduced to zero, irrespective of being fast or slow, the I-V characteristics follow the new high impedance path. For example when the voltage corresponding to the point C is reduced to zero, the OC$'$C$'$ state will be followed. The device will remain in this new high-impedance state, even if the applied voltage exceeds V_T, as long as it is kept below a certain critical temperature.

If the device temperature is raised to 300 K, any voltage $V > V_T$ will cause it to switch back into its initial low-impedance state OA. In fact, the sample will switch back to the low-impedance state, even if it is first heated up to

room temperature, followed by cooling it to 77 K and then applying any voltage greater than V_T. Thus the sample remembers the heating process and possesses a thermal-voltage memory in addition to the voltage memory.

1.5.4 Electron emission

Electron emission from the formed MIM samples into vacuum develops at the same time as VCNR. These electrons can be collected by a subsidiary anode biased to + 100V and positioned about 2 cm from the upper surface of the sample[105]. Electron emission into vacuum has been observed at a voltage just beyond V_m (where V_m corresponds to the maximum current flowing through the sample) and it rises steeply with increasing voltage. During emission some energetic electrons with energies extending up to the full applied potential difference across the sample are emitted. Small centres over the surface of the film are the source of emission and the intensity of emission varies with time at each point[106]. Hickmott[107] studied Al-Al_2O_3-Au diodes and pointed out that at low voltages emission occurs through the pin holes, which are uniformly distributed over the area of the diode. At higher voltages the emission becomes spotty and it is not possible to correlate electro-luminescent spots with regions of enhanced electron emission[108-110]. Electron emission has been observed in many MIM structures of oxides[102, 108, 109, 111] and in some polymers[60]. Also, the emission current is more temperature dependent than the circulating current[108].

1.5.5 Electroluminescence

Electroluminescence and electron emission appear simultaneously with the initial development of conductivity and negative resistance in the formed MIM sample. Electroluminescence occurs as a number of bright spots on the electrode surface[108]. These bright spots tend to be stable through several cycles of current-voltage characteristics, but sometimes they change their positions or disappear completely. Electroluminescence in Zns[112], Cds[113], ZnSe[86], Al_2O_3[51] and SiO_2[102] has been reported at low voltages. In some cases light with photon energy greater than the applied voltage has also been observed. According to Hickmott, electroluminescence and electron emission rise steeply above 1.5 V for Al-SiO-Au diode. Furthermore they are independent of the diode current and the thickness of the oxide. But, unlike electron emission the intensity of the electroluminescence does not depend upon the polarity of the applied voltage[108,115].

1.5.6 Theories of electroforming

A number of theories have been proposed to explain the phenomena of electroforming and associated effects in insulators. The important points of these theories are explained in the following section.

(i) The model of Hickmott

According to Hickmott's[102] model, a large number of immobile neutral impurity centres of energy E_I, situated approximately at the centre of the band are responsible for the electro-forming. The number and nature of these impurity centres in

an insulator are influenced by its method of preparation, structural faults and also by the existence of foreign atoms in the lattice. The conduction process is dominated by a high-field region normally situated near the cathode but can exist in any region of the insulator. A necessary condition for electroforming is the location of impurity band in energy within a few tenths of a volt from the mid-band gap $\frac{E_o}{2}$, before forming.

As a result of the applied voltage across the diode, Schottky emission takes place from both the cathode and the impurity centres; the latter electrons will leave the ionized impurity centres in the insulator. When the applied potential difference reaches the forming voltage, the number of ionized impurity centres in the insulator becomes large enough to form an impurity band in the insulator. Also, the metal-insulator interface is modified in such a way that electrons can easily be injected from the electrode into the insulator without any thermal activation. The conduction is due to low mobility injected electrons which hop from one centre to the next as shown by (1) in Figure 1.24. The impurities contributing to conductivity are uniformly distributed throughout the insulator, but the conductivity is controlled by positive impurity centres.

The phenomena of negative resistance, electron emission and electroluminescence are explained by postulating an immobile hole level E_H, between the impurity band and the valence band. As the voltage across the diode is increased, the hole levels are filled by the electrons excited by impact ionization or tunnelling from the valence band (2). The hole left behind

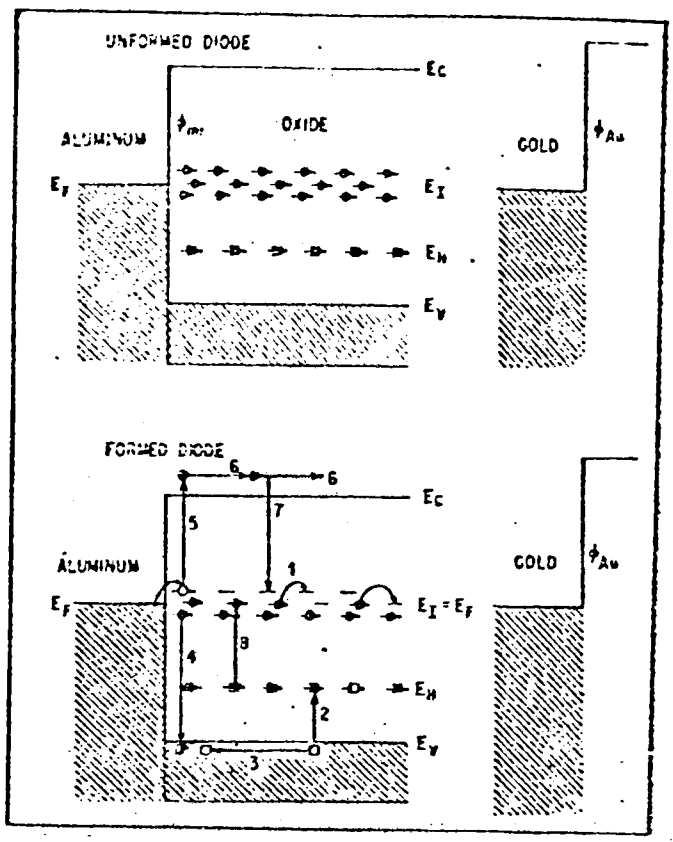

Figure 1.24 Schematic diagram of the unformed and formed sample and the establishment of conductivity in the high field region (after Hickmott[102]).

in the valence band moves towards the cathode under the influence of the high field (3). While moving towards the cathode the hole is neutralized by an electron from the impurity levels (4), or another electron trapped in an impurity centre is excited into the conduction band by its recombination energy (5). Now in the conduction band this electron is accelerated in the high field towards the anode (6). Electrons having energies greater than the electrode work-function can be emitted from the sample while others may be captured by the impurity band (7).

The ionized impurities in the impurity band, contributing to the circulating current are neutralized by the electrons tunnelling from the valence band or second impurity level, which results in

the appearance of the negative resistance region. Radiative transitions between E_I, E_H and E_V cause the electroluminescence (E_V is the energy of the top of the valence band).

(ii) The model of Verderber, Simmons and Eales.

The electroforming according to this model is explained in terms of the injection of positive ions into the insulator from the postively-biased electrode, when the applied voltage becomes equal to the forming voltage V_F[53]. These injected ions diffuse into the insulator under the influence of the forming field and the rate of diffusion is reflected by the time taken for a sample to form. For an unformed sample, the barrier height at the metal-insulator interface above the fermi level is given by

$$\phi_o = \psi_m - \chi_i \tag{1.54}$$

where ψ_m is the electrode work function and χ_i is the electron affinity of the insulator. The field at the metal-insulator interface is given by

$$F = \left(\frac{n_d \quad e^{\frac{1}{2}}}{2 \, \varepsilon \varepsilon_o} \right) \quad (\phi_o - \phi_b - V_d)^{\frac{1}{2}} \tag{1.55}$$

where ϕ_b is the bulk activation energy of the unformed insulator, V_d is the voltage drop across the depletion region, n_d is the donor density, ε is the dielectric constant, ε_o is the permittivity of the free space, e is the electronic charge and ϕ_o is the barrier height as defined above.

Figure 1.25 shows the energy-band diagram of the unformed MIM system for different bias voltages. When $V < V_F$, the energy diagram for the unformed system is shown in Figure 1.25(b)

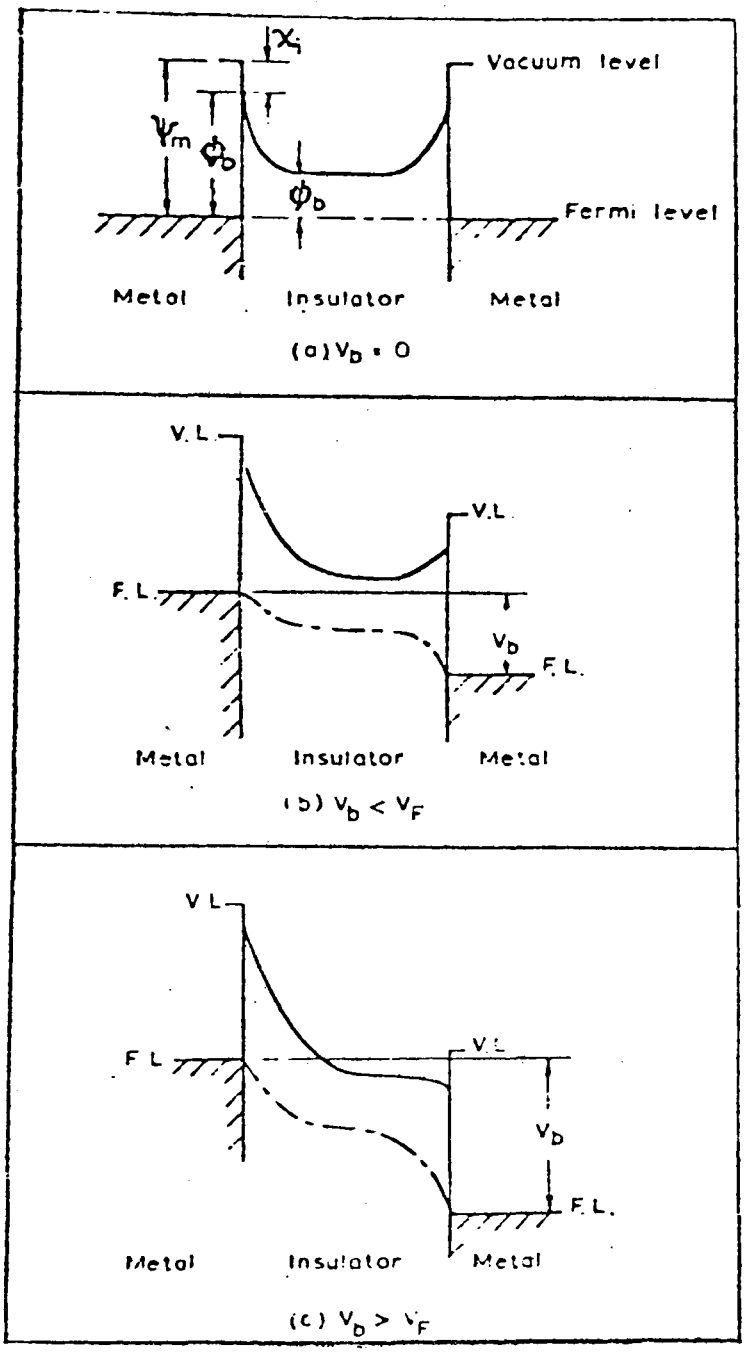

Figure 1.25 The energy band diagram of the unformed MIM system for different applied voltages.

(a) $V_b = o$ (b) $V_b < V_F$ (c) $V_b > V_F$

The effect of the voltage bias is to increase the width of the depletion region and the field at the negatively biased electrode and to decrease them at the positively biased electrode. The ionized charges in the depletion region give rise to a positive field at the anode which prevents any migration of ions from the anode into the insulator.
When the applied field attains the value V_F, the field at the interface becomes zero, as shown in Figure 1.25(c). So the

ions entering from the anode into the insulator are free to migrate throughout the insulator. The condition for F = 0, from equation (1.55) is

$$V_d = \Phi_o - \Phi_b \qquad (1.56)$$

If a similar voltage is dropped across the depletion region at the negatively-biased electrode, then the forming voltage will equal

$$V_F = 2V_d = 2 (\Phi_o - \Phi_b) \qquad (1.57)$$

The injected positive ions must drag into the insulator an equal number of electrons from the opposite electrode in order to satisfy the overall charge neutrality. It has been suggested that gold atoms act as donor centres and their polarity depends on their position with respect to the Fermi level of the insulator[52]. The gold "donors" would provid a discrete energy level in the forbidden band of an insulator having a crystalline structure. But in the case of an amorphouse insulator, the situation is different, mainly due to two reasons.

(i) The potential energy of the gold ion within the lattice is not well defined. This is because there is no consistency in nearest neighbour and next-nearest neighbour configurations so the ion does not have a uniquely defined environment.

(ii) An amorphous insulator contains a large number of traps; some of these situated below the Fermi level will be occupied, giving a negative charge. The net result of the above two effects is to produce a broad band of localized states within the forbidden energy gap of the insulator as shown in Figure 1.26(a) for the V = 0 condition. When the applied voltage V is less than Φ_i, an electron at the Fermi level can

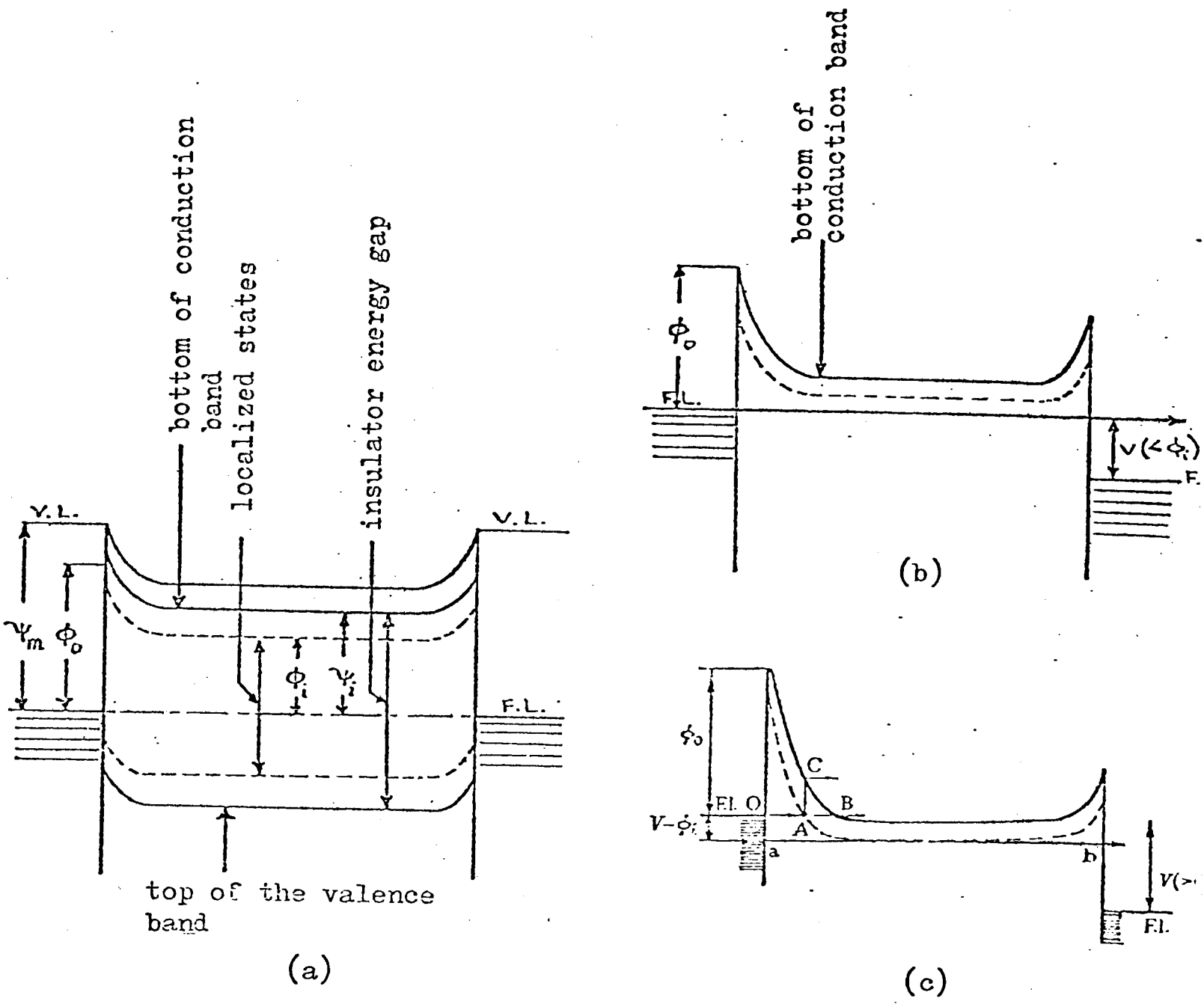

Figure 1.26 The energy-band diagram of the formed metal-insulator-metal sample for (a) no applied voltage (b) applied voltage less than ϕ_i. (c) for applied potential difference greater than ϕ_i. Where Ψ_m is the metal work-function, ϕ_o the metal-insulator barrier height and Ψ_i and ϕ_i respectively are the energies of the bottom of the condition band and top of the localized levels measured from the Fermi level.

pass through the band of adjacent sites, provided by the gold atom, to the other electrode by a tunnelling-hopping process as shown by the line a b in Figure 1.26(b). The differential negative resistance in this model is explained below. When the applied potential difference V, exceedsϕ_i, only the electrons having energies greater than V-ϕ_i below the Fermi level can contribute to the circulating current through the localized states as shown in Figure 1.26(c). Since the number of injected electrons contributing to the circulating current, falls off rapidly with the energy below the Fermi level, so the current passing through the sample decreases with increasing voltages.

Verderber and Simmons[109] explained the emission process as hot electrons emitted into the vacuum from the pinholes in the upper electrodes. Initially the electrons are excited into the conduction band by acquiring an energy E_i from the lattice. Those who do not suffer any losses in the insulator will enter the top electrode with an energy $eV + E_i$ above the Fermi level. These electrons can be emitted into vacuum if

$$eV + E_i > \psi_m$$

where ψ_m is the work function of the electrode.

(iii) The model of Green, Bush and Rawlings.

This model explains the evolution of gas, the importance of anode material and the dependence of the forming voltage on the insulator material during the electroforming process. However, the electroforming is the result of the high-field

solid-state electrolysis of the insulator in the localized regions. The anion vacancies are injected into the insulator provided a sufficient number of defects such as grain boundaries, dislocations and point defects are present in it[122].

For a hypothetical insulator MX, where M and X represent the electropositive (cations) and the electro-negative parts (anions) of the compound MX respectively, the reaction at the anode under a low-field condition, with inert electrodes in an inert atmosphere is given as

$$\overline{X} \longrightarrow \frac{1}{2} X_2 + \overline{e} \qquad (1.58)$$

and the reaction at the cathode is

$$M^+ + \overline{e} \longrightarrow M \qquad (1.59)$$

Under the high-field condition the reaction replaces the reaction (1.59) at the cathode.

$$\square_X + \overline{e} \longrightarrow \boxed{\overline{e}}_X \qquad (1.60)$$

As a result of the above reaction the electrons are injected into anion vacancies where

$\square_X \longrightarrow$ represents the anion vacancy.

$\boxed{\overline{e}}_X \longrightarrow$ represents the vacancy with trapped electron.

The evolution of fluorine from the fluoride and oxygen from the oxides can be explained by the reaction (1.58). The conduction occurs by the tunnelling of electrons through the localized conduction paths or chains of defect centres, caused by the diffusion of vacancies under the electric field. Such vacancies are generally formed at

the anode by the discharge of $\bar{X}$ ions.

In the presence of oxygen the following reaction takes place at the cathode.

$$\frac{1}{2} O_2 + 2\bar{e} \longrightarrow O^{2-} \qquad (1.61)$$

when the partial pressure of oxygen becomes sufficiently high, reaction (1.61) dominates and the reaction (1.60) which is the main source of conducting centres, vanishes. Therefore the chance of electroforming is eliminated. This model also explains the dependence of the degree of electroforming on the anode material. For a chemically reactive anode metal Ma, the following reaction replaced the reaction (1.58), which occurs at the inert electrode.

$$Ma \longrightarrow Ma^{n+} + n\bar{e} \qquad (1.62)$$

Reaction (1.62) results in the ionization of anode metal atoms, which then enter into the insulator. If the rate, by which the material enters into the insulator, is governed by the reactions (1.61) and (1.62) rather than by (1.58) and (1.59) the insulator thickens up and the high-field condition necessary for reaction (1.60) is diminished. Therefore the electroforming can only be achieved by using less reactive anode material and a lower oxygen content, this also reduces the possibility of reactions (1.61) and (1.62).

This model explains the memory and differential negative resistance in terms of trapped space-charge, which is formed when some of the electrons are excited by the electric field from the localised conducting paths into

the unformed dielectric. The energetic electrons capable of overcoming the work-function of the top electrode appear as emission current.

(iv) The model of Barriac, Pinard and Davoine

According to this model[116,55] the electroforming is explained in terms of injection of ions from the anode and the conduction is ionic. When a voltage is applied across the unformed sample, the electric field varies within the insulator due to the existence of imperfect regions. At a critical value of the voltage, electrical arcing across the region takes place and releases heat and causes local melting of the insulator. The positive metal ions injected from the anode into the insulator under the action of the applied electric field migrate towards the cathode and create a positive space charge in the cathode region such that all the voltage is dropped across a narrow region of width much less than the thickness of the insulator. The region is named as the effective thickness, which varies with the amount of space-charge and the applied voltage. Tunnelling of electrons from the cathode begins when the effective thickness reaches a saturated value and it also becomes voltage-independent at a certain value of the space charge. The tunnelling electrons have low energy and cannot tunnel through the ionic barrier. The positive ionic charge carrier becomes electrically neutral when attacked by these electrons and give rise to the neutral pairs termed "pseudo-atoms". A drop in the ionic current explains the differential negative resistance.

However, some of these electrons gain enough energy from the electric field so that they are able to tunnel through the ionic barrier and by overcoming the metal work function they contribute to the emission current which mainly appears along with the negative resistance in the formed devices. The reaction at the cathode[55] in the absence of oxygen is given by

$$M^+ + \bar{e} \longrightarrow [\, M^+, \bar{e}\,]$$

ion + electron $\longrightarrow$ Neutral pair

While, in the presence of oxygen the following reaction is most probable.

$$2M^+ + 2\bar{e} + \frac{1}{2}\, O_2 \longrightarrow M_2^{++}\,,\ \bar{O}^-$$

ion + electron $\longrightarrow$ oxide

The above equation shows that the ions form a stable metallic oxide in preference to neutral pairs. Also, the space charge in the cathode region is permanently neutralized. Therefore the VCNR cannot be obtained with the sample in an oxygen environment.

(v) The model of Dearnaley, Morgan and Stoneham.

According to this model the conduction, memory effects and electron emission are confined in highly localized regions and the rest of the matrix plays almost no part in the observed phenomena. The electroforming is believed to be due to the creation of filamentary paths between the electrodes. When the applied potential difference reaches the forming voltage, the power dissipation causes the rupturing of the chains and the electron emission begins at

this point[117].

The conduction through these filamentary paths is ohmic with negligible activation energies. Hopping conduction, space-charge effects and tunnelling are ignored. Moreover these filaments are not uniformly distributed and their resistance is due to the existence of weak spots which become heated by the flow of the electrons. The conducting chains are ruptured because of the phonon scattering at the weak hot spots of the filaments. The rupturing of the filaments explains the existence of negative resistance and memory properties of the formed layers.

Joule heating occurs during the electronic conduction through the filaments and the filaments have the temperature T, the same as that of the lattice.

If the temperature T, exceeds T_m, the rupturing of the filaments will start where T_m is the maximum temperature of the lattice, which the filaments could sustain, before they start rupturing. The temperature T, is either changed by Joule heating or by the loss of heat to the insulator. The rate of loss of heat to the insulator is proportional to the temperature difference between the filaments and its environment. Therefore the local temperature is given by

$$\frac{dT}{dt} = \alpha \frac{V^2(t)}{\rho} - \frac{1}{\tau_c}(T - T_o) \qquad (1.63)$$

where T_o is the temperature of the filaments' environment, ρ, is the resistance of the filament, τ_c and α are the cooling and heating times respectively. For the static

characteristics, it follows from the steady state solution of equation (1.63) that the value of the filament resistance should be greater than ρ_{min} to remain unfractured at the applied voltage V.

$$\rho_{min} = \frac{\tau_c \propto V^2}{(T_{max} - T_o)} \tag{1.64}$$

The total current through the filaments can be written as

$$I = \int_{\rho_{min}}^{\infty} \frac{V}{\rho} P(\rho)\, d\rho \tag{1.65}$$

Where $P(\rho)$ is the probability distribution of the various resistance and it is normalized as

$$\int_0^{\infty} d\rho\, P(\rho) = 1 \tag{1.66}$$

The probability distribution $P(\rho)$ also determines the shape of the characteristics and has two main features. Firstly there are very few filaments having resistances below the value ρ_T, which is

$$\rho_T = \frac{\tau_c \propto V_T^2}{(T_{max} - T_o)} \tag{1.67}$$

V_T corresponds to the threshold voltage. Secondly there are very few filaments with resistance greater than ρ_u, where

$$\rho_u = \frac{\tau_c \propto V_u^2}{T_{max} - T_o} \tag{1.68}$$

Here V_u stands for the voltage corresponding to the minimum current. The distribution of $P(\rho)$ is shown in the Figure 1.27. For small values of ρ, $P(\rho)$ is negative. This is due to the contribution of tunnelling at small voltages.

As described before, electronic conduction takes place under

the influence of the applied field which increases the phonon scattering and the electron temperature, particularly at the weak regions of the filaments, resulting in the electron scattering into the surrounding matrix of the insulator, where they are trapped and create highly polarized regions.

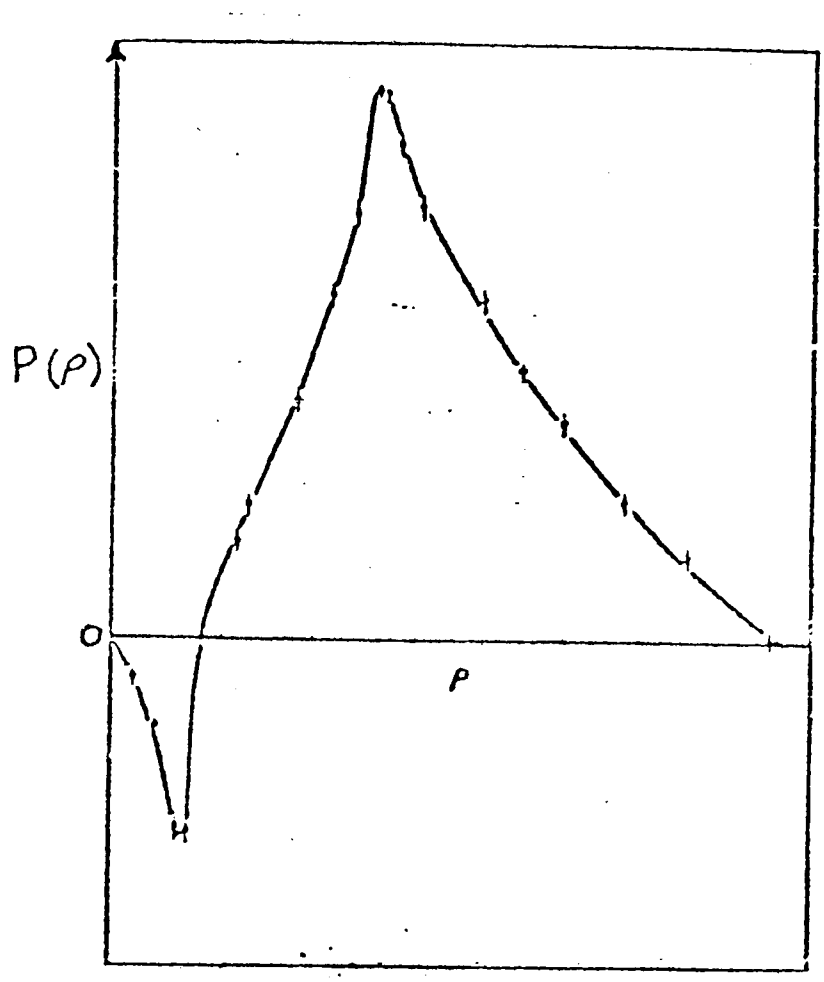

Figure 1.27 The probability distribution P(ρ) of filament resistances versus ρ (after Dearnaley et al).

These regions are released by the thermally-activated Poole-Frenkel emission of trapped charges. The time required for the completion of such emission is known as the relaxation time, which is higher at low temperatures, corresponding to the high-impedance memory state.

(vi) The model of Ralph and Woodcock

According to the model proposed by Ralph and Woodcock[57], the conduction through the formed insulating layers is due to the existence of filamentary paths, extending from one contact to the other, each associated with an impurity band. The density of impurity states and the effect of the local fluctuations in potential on these states control the properties of these impurity bands.

The impurity band and the Fermi level are assumed to be situated in the centre of the forbidden gap of the insulator for simplicity. These impurity centres may be charged or neutral and any other compensating charge existing on the unspecified centres would contribute to V_o where V_o is given by

$$\langle V^2 \rangle = V_o^2 \qquad (1.69$$

Here V is the random excess potential at each site.

The impurity band shows mobility edges at both the top and bottom of the band giving rise to the mobility bandwidth, which is less than the density of state bandwidth[119]. A large number of variations occur in the density of centres in the impurity band due to the non-uniformities in the initial layer before electroforming.

The local fluctuations in V_o and the non-uniformities in the initial layer result in the variation of mobility bandwidth and the density-of-states bandwidth. The regions consisting of narrow mobility bandwidth are referred to as constrictions. Figure 1.28 shows a constriction present in a filament which arises due to the asymmetrical increase in

the density-of-states bandwidth (E_I) and a corresponding decrease in the mobility bandwidth (E_M).

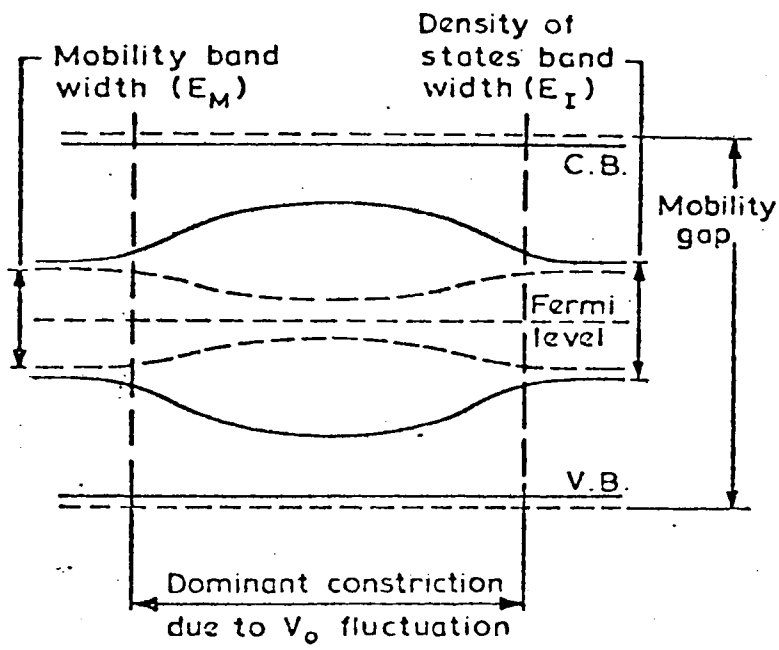

Figure 1.28 The proposed band picture of a formed amorphous insulator, showing the effect of fluctuating V_o, on a filamentary conducting region (after Ralph and Woodcock)[57].

The current flows in the filaments by iso-energetic tunnelling through the centre of the impurity band, when the applied voltage is small. As the potential difference across the filament is increased up to a certain point, some electrons become hot enough to leave the centre of the impurity band and enter the region of rapidly decreasing mobility in the constriction, as shown by (a) in Figure 1.29. The filament continues to conduct via the trapping states by combination (b) thermal degradation (c) and by field emission (d).
The filament stops conducting due to trapping and this causes the fall in the current in the negative resistance region. The traps can cause the current to cease in the

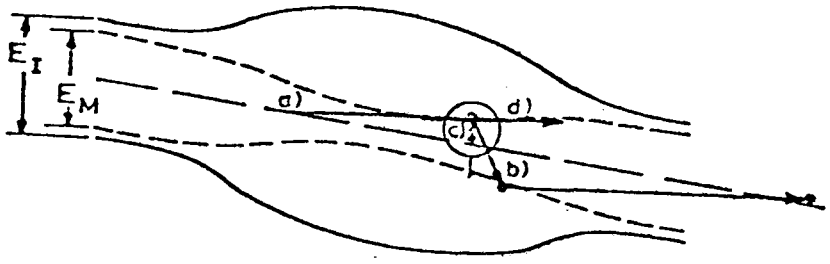

Figure 1.29 Different processes occurring in the constriction of a formed conducting filament:(a) iso-energetic tunnelling into the region of localised states. (b) radiative recombination:(c) thermal degradation: (d) field emission. (after Ralph and Woodcock.)[57].

following two ways. (i) If a positive charge is induced in the conducting part of the filament, due to a trapped negative space-charge in a region where the mobility band is narrow, the depletion of electron will lower the Fermi level into the region of localized states at the bottom of the conduction band and will stop the filament to conduct as shown in the Figure 1.30. (ii) The random potential V_o of the constriction is increased due to the trapping in its localised levels, thus changing the value of $V_o/_J$, where J is the bandwidth. The mobility bandwidth depends upon the value of $V_o/_J$. If it increases above a critical value the bandwidth disappears and all the states in this region become localised and prevent the filament conducting. This situation is shown in Figure 1.31.

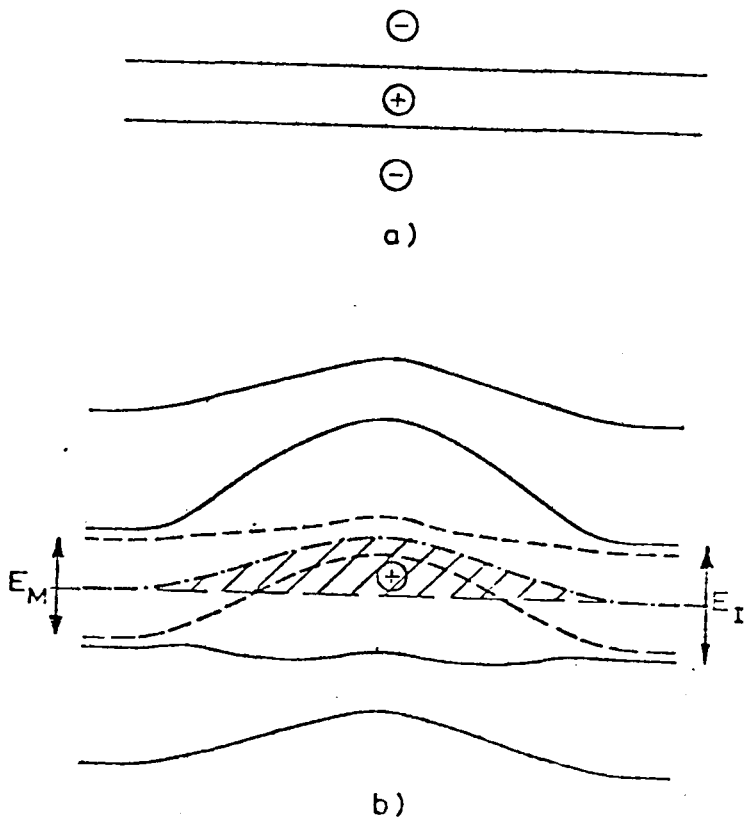

Figure 1.30 A non-conducting state of a filament caused by the trapped negative charge in the surrounding unformed material of the filament (a) geometrical representation, (b) the corresponding diagram for the filament. (after Ralph and Woodcock.)[57].

The memory state of the device arises from the fact that some of the filaments remain in the high resistance state by trapping sufficient charges, when the applied voltage is quickly reduced to zero. A constriction situated in the vicinity of the anode causes the electron emission. The emission also occurs from many small spots on the anode.

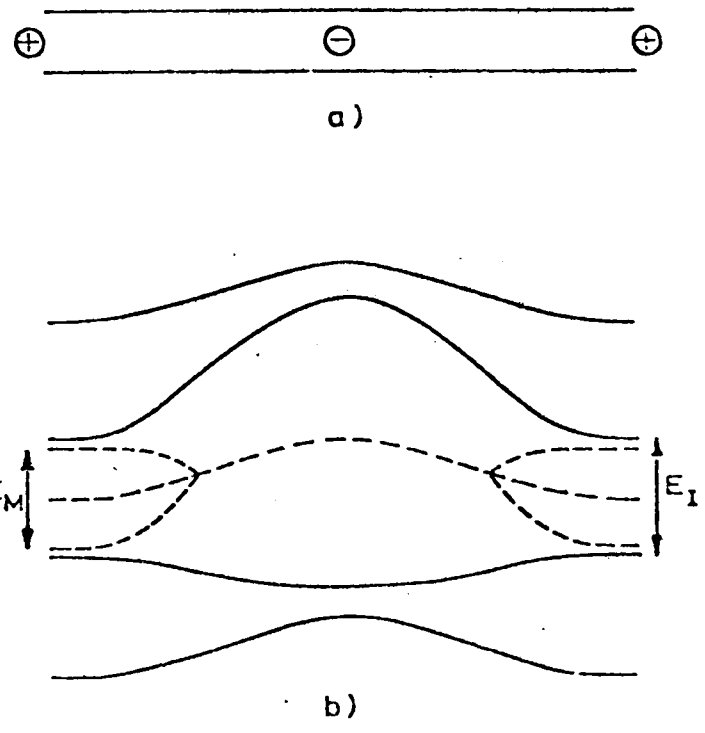

Figure 1.31 A non-conducting state of the filament caused by the trapped negative charge in the localised levels of a constriction (a) geometrical representation (b) corresponding band diagram for the filament. (after Ralph and Woodcock.)[57].

2. CHAPTER TWO

PREPARATION OF THIN FILM SAMPLES

2.1 Introduction

In the last chapter earlier work on polymer films has been reviewed and some of the conduction mechanisms before electroforming and the theories explaining forming effects were discussed.

Many attempts have been made to investigate the conduction mechanisms in dielectric polymer films. Zor[43] studied some electronic properties of thin films of polyethylene formed by vacuum evaporation and sandwiched between different metal electrodes. In order to perfect the technique, some (Cu-PE-Cu) samples were made and some of his results were reproduced.

Polypropylene is believed to be a better insulator than polyethylene, so it is of great interest to evaporate it under similar vacuum conditions as used for polyethylene in order to study its electrical properties.

In the following section the method of preparation of polypropylene films and details of the equipment used are given.

2.2 Cleaning of substrates

Corning 7059 borosilicate glass substrates (2.5 cm x 7.5 cm) were used throughout the experiments. Before any deposition the substrates were cleaned thoroughly in order to avoid any contamination. Four substrates were fixed in a glass stand (shown in Figure 2.1) and were cleaned every time according to the following procedure.

(i) Boil in a solution of Teepol in distilled water for 15 minutes.

(ii) Rinse in hot distilled water for 5 minutes.

(iii) Remove the traces of Teepol and grease by immersing in isopropyl alcohol.

(iv) Dry in a stream of air and use Selvyt cloth for dusting.

(v) Blow off any remaining dust particles by a stream of compressed air.

(vi) Finally clean by glow discharge during the pumpdown at a pressure between 0.1 and 0.05 torr.

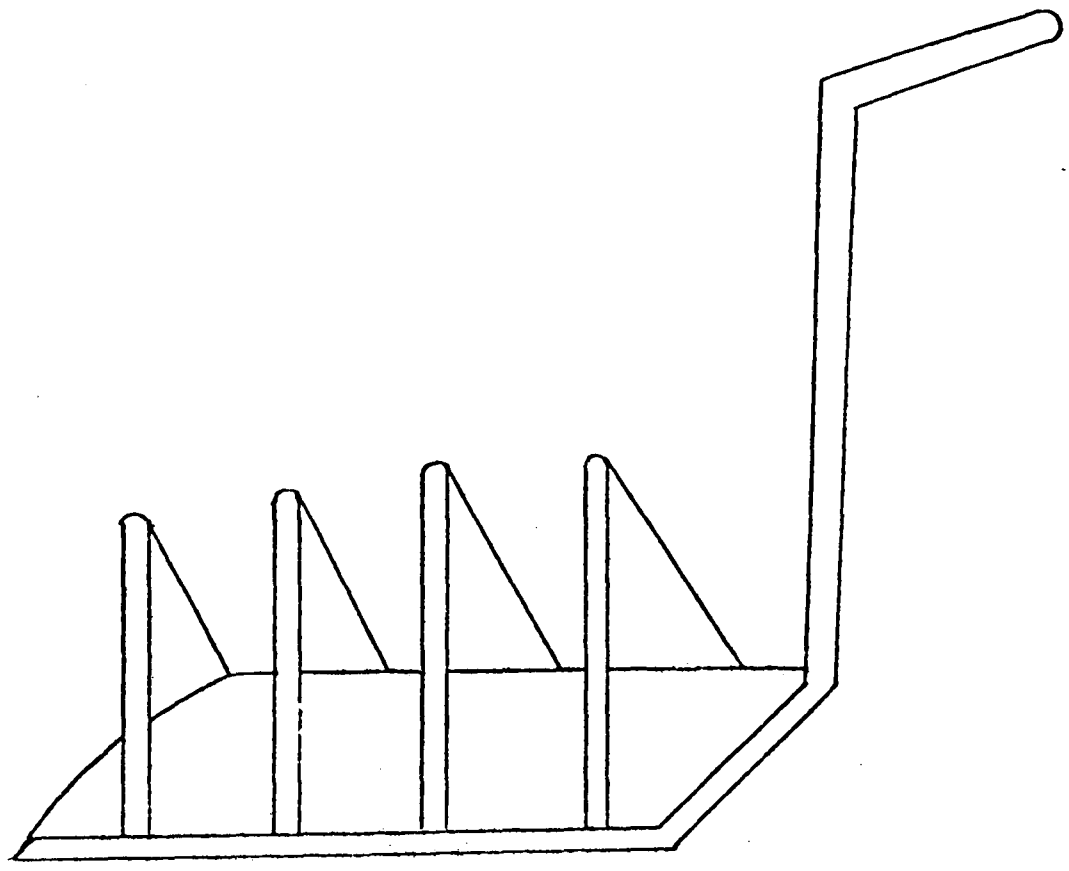

Figure 2.1 Glass stand for holding substrates.

2.3 Deposition of base electrodes

A Balzers BA510 coating unit was used for the evaporation of base electrodes. It was fitted with a DIFE1500 diffusion pump and a DU025 rotary pump and was capable of producing a

chamber pressure of 7×10^{-6} torr. The pressure inside the chamber was monitored with Pirani and Penning gauges. Facilities for producing a glow discharge and heating and cooling of the chamber were available. Evaporation sources were usually made in the form of boats. Cu, Ag and Au were evaporated from molybdenum boats, while the evaporation of Al was carried out using a tungsten filament (see Figure 2.2). The complete evaporation unit is shown in Figure 2.3.

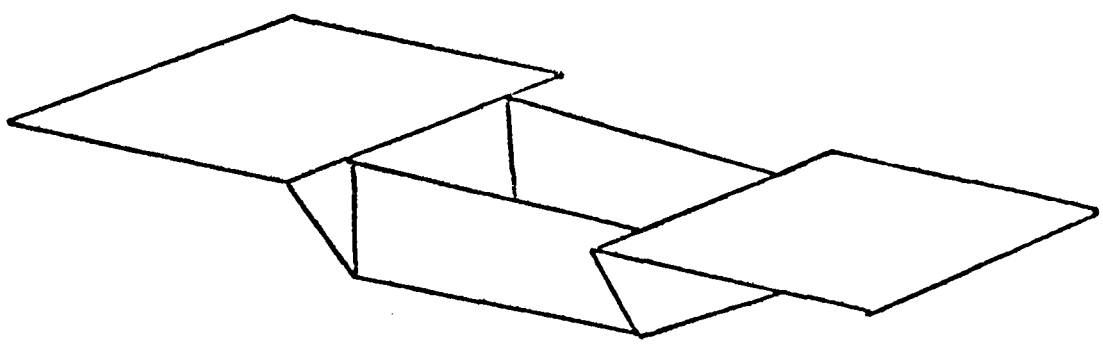

(a)

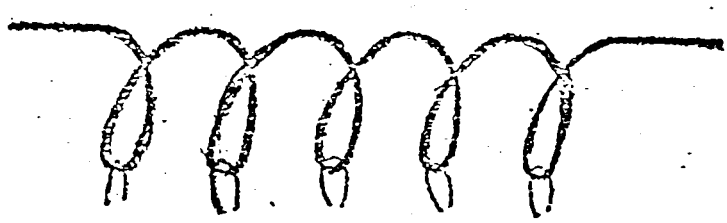

(b)

Figure 2.2 (a) Boat for evaporation of Cu, Ag and Au.
(b) Tungsten filament for evaporation of Al.

The current during the evaporation was controlled from outside the chamber by a rheostat. A quartz crystal monitor was used to measure the evaporation rate and the thickness of metal film and was mounted directly above the evaporation source. Three substrates were fixed in a holder which was mounted 25 cm above the boat. One of the substrates was

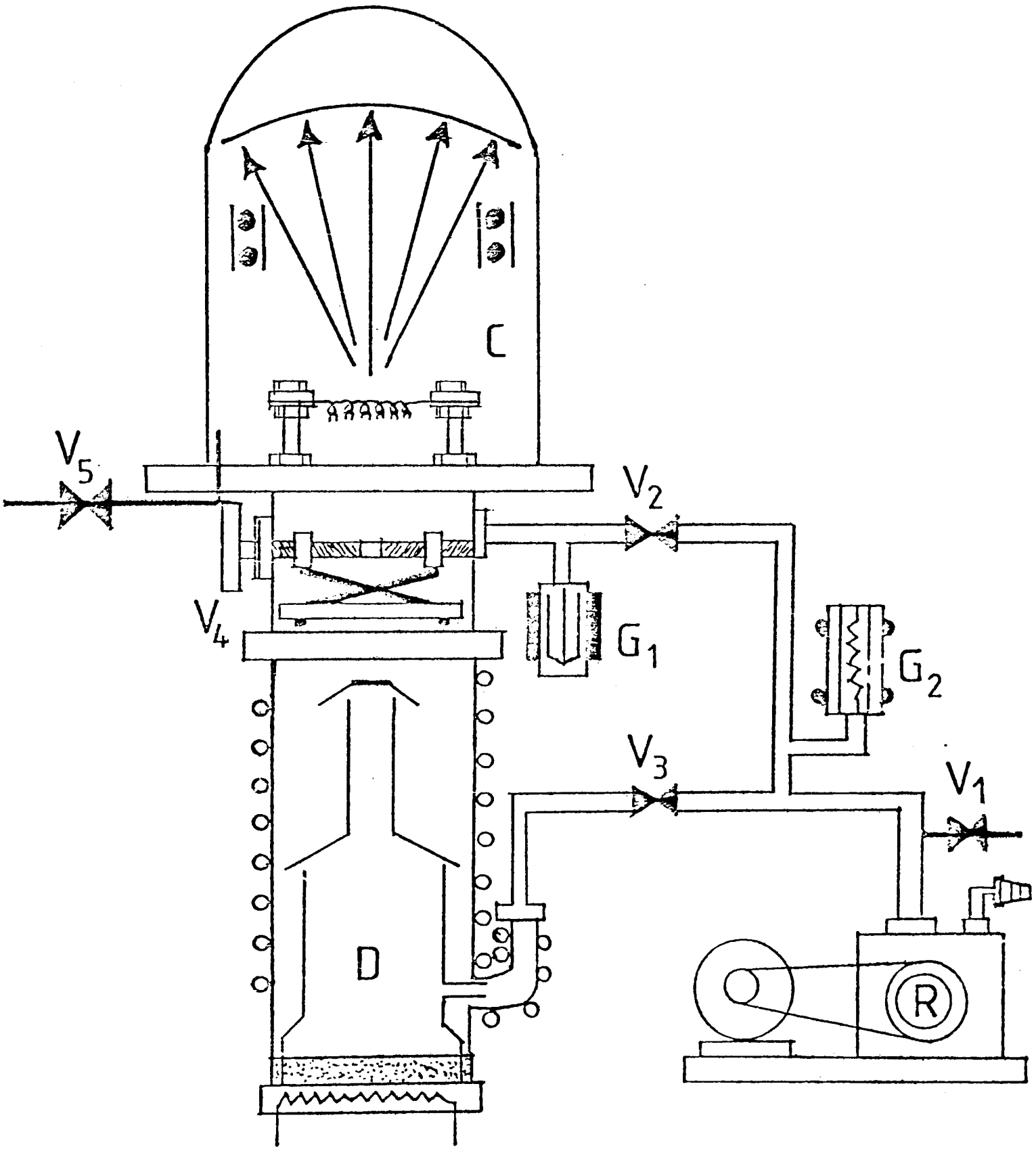

Figure 2.3 Complete vacuum system.

Where R is rotary pump, D is diffusion pump, C is vacuum chamber, V_1 is rotary pump air admittance value, V_2 is roughing bypass valve, V_3 is backing valve, V_4 is main valve, V_5 is chamber air admittance valve, G_1 is penning gauge and G_2 is Pirani gauge.

used for thickness measurements. A stainless steel mask of the required pattern was fixed just under the substrate holder and it was possible to change its position from outside the chamber without breaking the high vacuum. An aluminium shutter, having its control outside the chamber was used to cover the substrates while the initial evaporation conditions were established.

The evaporation was carried out at a chamber pressure of less than 10^{-5} torr, and at a substrate temperature of 100°C. Six isolated base electrodes were deposited on each slide, so twelve electrodes were deposited in one run. The substrates were allowed to cool down to room temperature while still under vacuum and were then transferred to another plant for the evaporation of the dieletric material.

2.4 Evaporation of polypropylene

The evaporation of the polymer was carried out in an Edwards coating unit 6E with an Edwards 1SP30 rotary pump backing the 102A oil diffusion pump and was able to attain a chamber pressure of 10^{-5} torr. It was possible to fix three substrates at a time on a stand inside the chamber. The middle one was always used to collect the material for thickness measurements. The source-to-substrate distance was 8 cm and the substrates were separated by a shutter. The pressure inside the chamber was kept steady by circulating cold water in the rubber pipes mounted around the chamber. Polypropylene was evaporated at 6×10^{-5} torr from a stainless steel boat (shown in Figure 2.4) covered with a lid having a number of holes of diameter 0.07 cm, onto the previously deposited base electrodes.

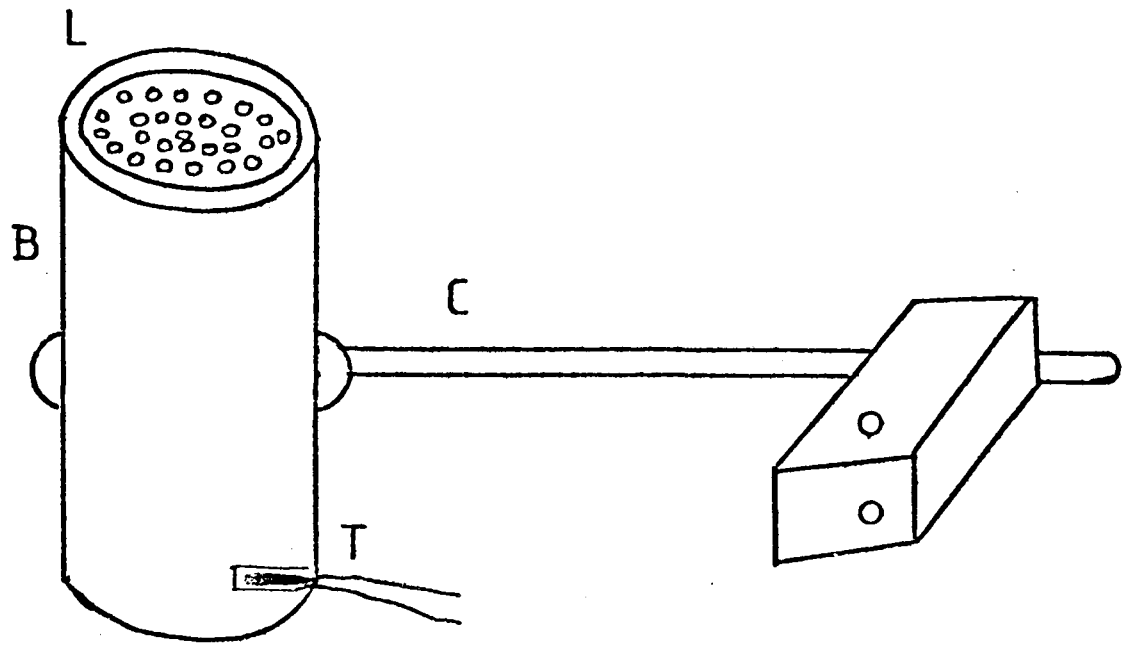

Figure 2.4 Schematic illustration of evaporation source for polypropylene. Where B is stainless steel boat, L is lid containing holes, T is thermocouple and C is clamp to fix the boat in the vacuum chamber.

The evaporation was carried out at a source temperature of $336 \pm 2^{o}C$ and the evaporation rate was 13.3 Å min^{-1}. This temperature was chosen to give a uniform deposition of polypropylene. The source temperature was measured with a chromel-alumel thermocouple connected to the base of the boat through a Comark 1602 electronic thermometer. A molybdenum heater was used to heat the boat and the current through the heater was controlled from outside using two rheostats, so that the source temperature could be controlled. The heater was electrically insulated from the boat by inserting mica layers. The shutter was kept close to the boat before any evaporation was started. An arrangement involving a moving shutter inside the chamber was made to

deposit three different thicknesses of polypropylene on the same substrate without breaking the high vacuum. The evaporation time was varied according to the required thickness of the polypropylene. Now the substrates were again transferred to the previous plant for the evaporation of top electrodes.

2.5 Deposition of top electrodes

Top electrodes were evaporated in the coating unit described in sec.2.3. Before evaporating the electrodes, the polypropylene layer was exposed to the glow discharge in order to initiate some cross-linking[43]. The glow discharge took place at a pressure between 0.05 and 0.1 torr. The current was 150 mA and the voltage was 120 volts. The substrates were not heated again before the evaporation, in order to avoid short circuiting between top and base electrodes. The evaporation was carried out at a chamber pressure of 10^{-5} torr. Twelve MIM specimens were prepared in every run. A substrate containing six complete samples is shown in Figure 2.5.

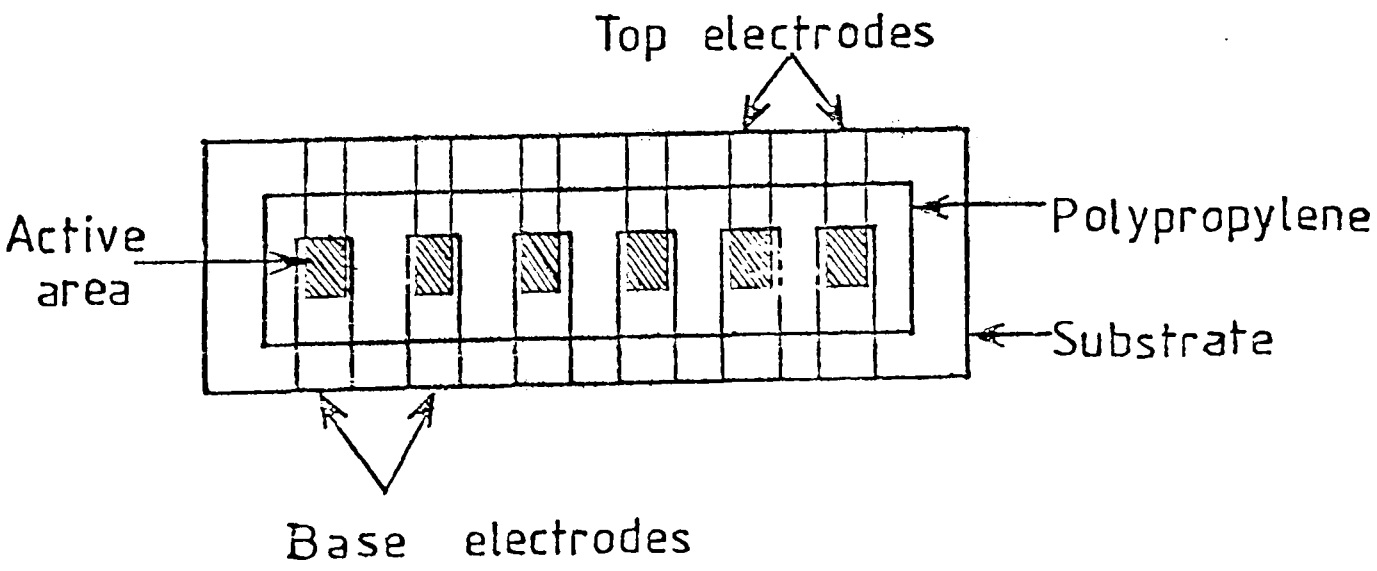

Figure 2.5 Substrate supporting samples.

Both base and top electrodes had thicknesses between 550Å to 850Å.

2.6 Thickness measurements

Edwards quartz film thickness monitors were used for monitoring the thickness of the evaporated metal electrodes. During the evaporation of metals and polypropylene, one of the substrates inside the vacuum chamber was always used to collect the material for the thickness measurements. Now a reflective coating of aluminium was evaporated over the whole substrate and the film thickness was measured by using the multibeam interferometry techniques. Typical observed interference fringes are shown in Figure 2.6. The thickness of the film was calculated by using the following formula

$$t = \frac{S}{d} \quad \frac{\lambda}{2} \qquad (2.1)$$

where t is the thickness of the film, S is the depth of step or well, d is the related distance between the fringes and λ is the wavelength of the light used.

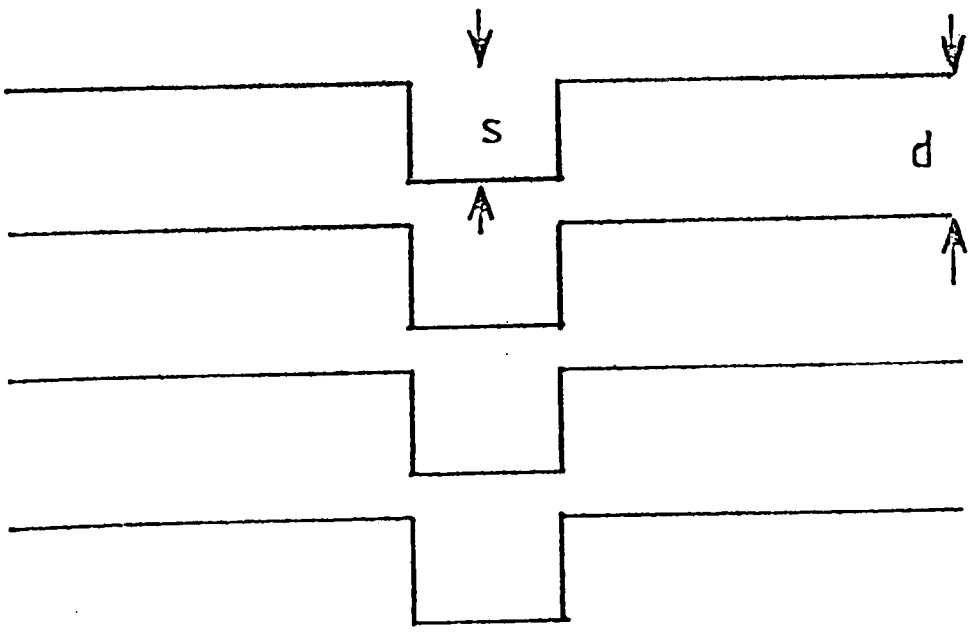

Figure 2.6 Interference fringes observed for thickness

3. CHAPTER THREE

ELECTRICAL CONDUCTIVITY

3.1 Measuring techniques

All electrical measurements were carried out in a vacuum chamber capable of maintaining the samples at a pressure below 10^{-5} torr. Arrangements inside the chamber were made for low and high temperature measurements. It was possible to cool the substrate to 100K, by mounting it on a copper plate with silver paste. The plate was fitted with a heater and most of its area was in good contact with a brass box, which could be filled with liquid nitrogen from outside. A perspex assembly was fixed around the substrate (containing the devices) so that the electrical connection could be made to the devices with copper strips and joined with silver paint. The temperature of the substrate was monitored by using a chromel-alumel thermocouple through a Comark electronic thermometer. Screened coaxial cables were used for the electrical connections. In order to eliminate any fluctuations during the measurements of low circulating and emission currents, an earthed aluminium cage was placed around the chamber, in which the samples were kept. The following two circuits (see Figure 3.1) were set up for the measurements of (a) $(I_c - T)_V$ and $(I_c - V)_T$ characteristics at constant voltage and temperature respectively,

(b) emission current.

Where I_c is the current passing through the sample, V is the applied voltage and T is the temperature $(I_c - T)_V$ and $(I_c - V)_T$ stand for the $I_c - T$ and $I_c - V$ characteristics at constant voltage and temperature respectively.

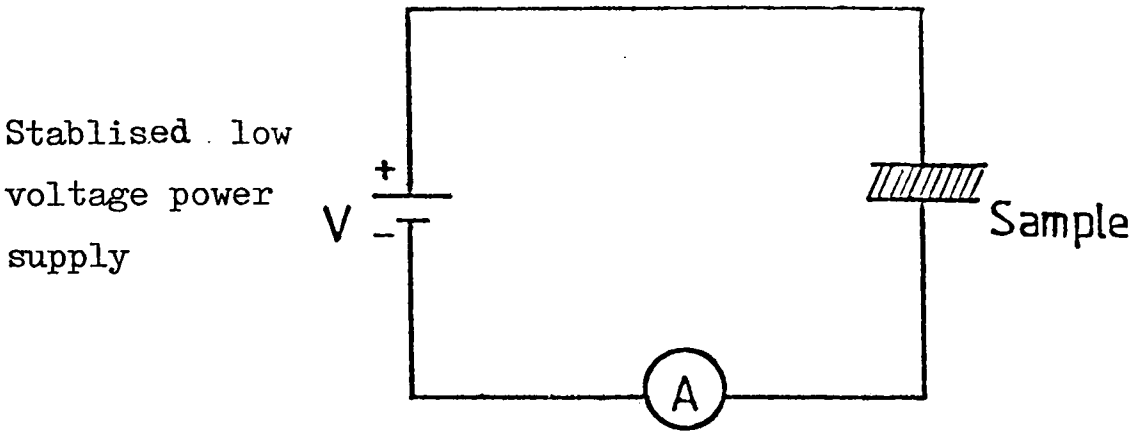

Figure 3.1(a) Circuit for measuring I_c - T and I_c - V characteristics at constant voltage and temperature respectively.

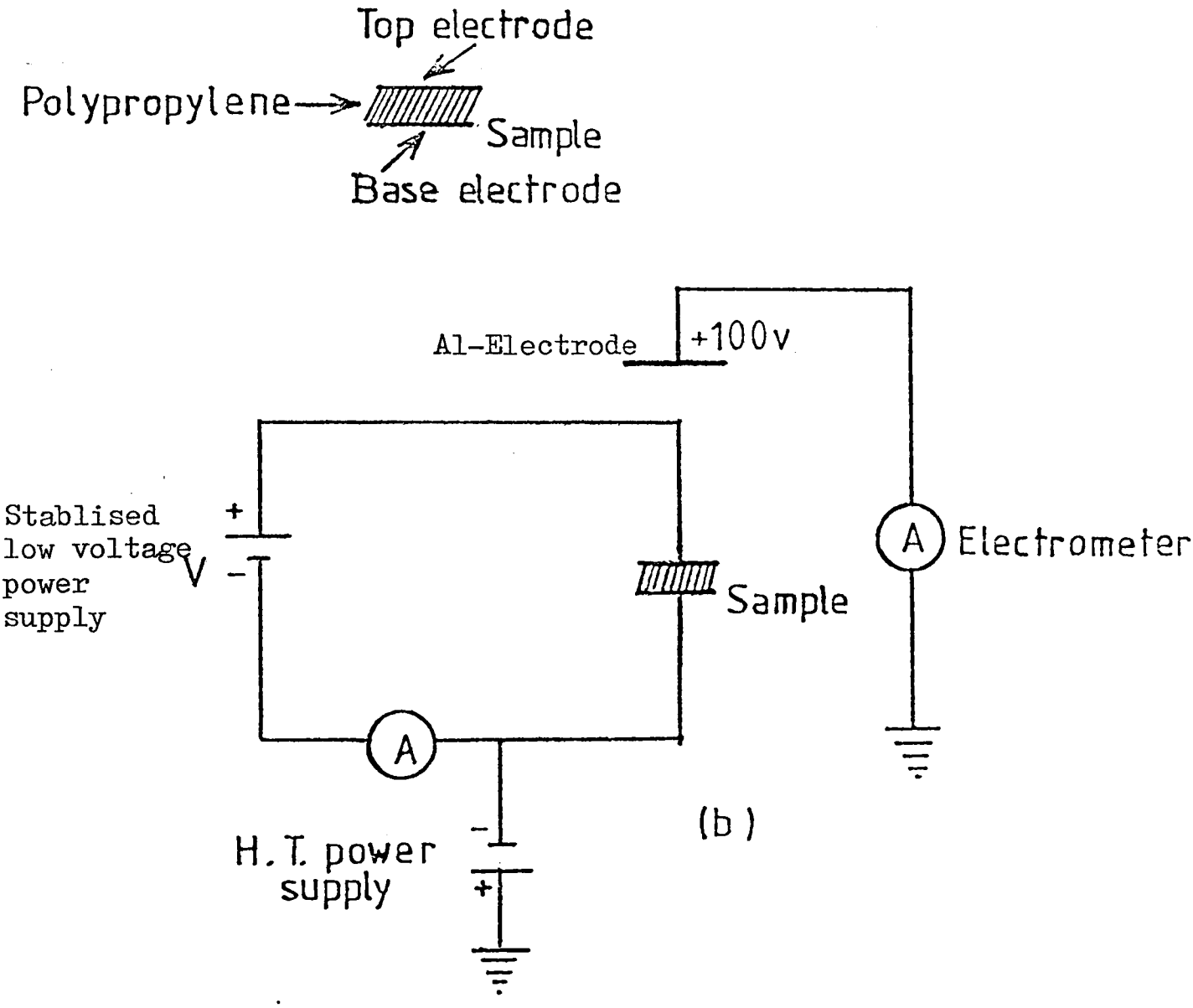

Figure 3.1(b) Circuit for measuring emission and circulating current for electroformed devices.

3.2 Electrode effects

I-V characteristics of evaporated polypropylene (PP), in the form of thin films sandwiched between different metal electrodes were studied. We used copper, aluminium, silver and gold as electrode materials. Electrodes were deposited by vacuum evaporation and the electrical measurements were carried out at a pressure of 10^{-5} torr as explained in Section 3.1.

3.2.1 Copper and aluminium electrodes

The voltage-current characteristics of Cu-PP-Cu and Al-PP-Cu samples with three different thicknesses of polypropylene (1200Å, 1800Å and 2400Å) are shown in the Figure 3.2. The maximum electric field at V = 30 volts in each case is given below.

$$E(1200\text{Å}) = 2.48 \times 10^{6} \text{ V cm}^{-1}$$
$$E(1800\text{Å}) = 1.66 \times 10^{6} \text{ V cm}^{-1}$$
$$E(2400\text{Å}) = 1.25 \times 10^{6} \text{ V cm}^{-1}$$

It was found that the polypropylene films were highly resistive with resistivities of the order of 10^{14} Ω-cm. The breakdown of the films was not thoroughly investigated; nevertheless the films withstood an applied field of 2.48×10^{6} V cm^{-1} and there was no sign of breakdown. The circulating current was thickness-dependent and its value was higher when copper was used for both base and top electrodes. These results were reproducible and the voltage-current characteristics remained ohmic. The field at any particular voltage could be calculated by using the relation

$$E = \frac{V}{d} \qquad (3.1)$$

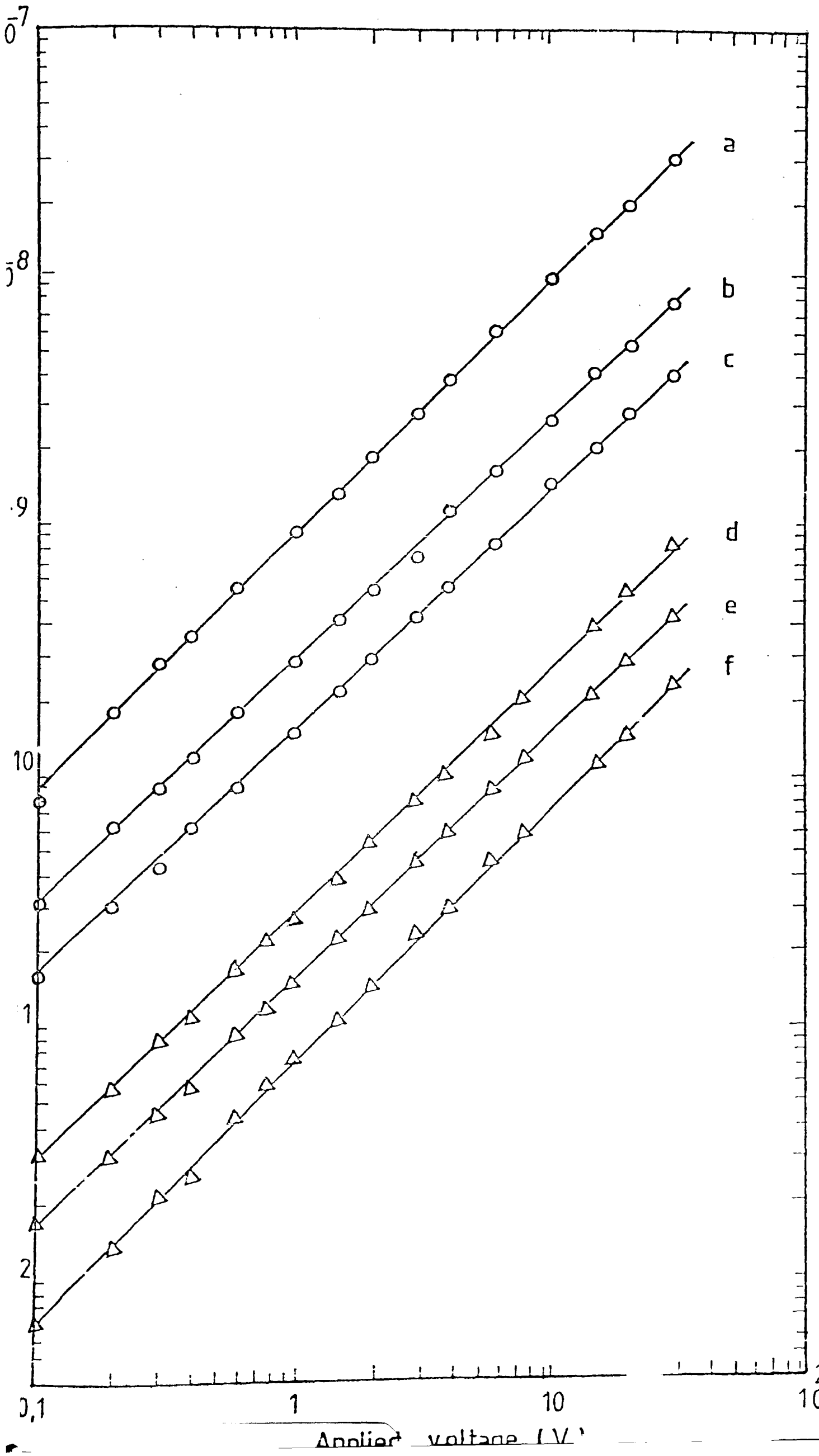

Figure 3.2 Voltage-curre characteristi for some thin films of poly- propylene (PP curve a, Cu/P (1200Å)/Cu; curve b, Cu/P (1800Å)/Cu; curve c, Cu/P (2400Å/Cu; curve d, Al/P (1200Å)/Al; curve e, Al/P (1800Å)/Cu; curve f, Al/P (2400Å)/Cu. (after Hogarth and Iqbal[5]).

where E is the field, V is the applied voltage across the sample and d is the thickness of the polypropylene film. The resistivity was obtained by using the following formula.

$$\rho = \frac{RA}{L} \qquad (3.2)$$

where ρ , is the resistivity, R is the resistance and L is the thickness of the film.

3.2.2 Aluminium electrodes

Figure 3.3 shows the I-V characteristics of a Al-PP(1200Å)-Al sample at room temperature and pressure less than 10^{-5} torr. The voltage was increased gradually up to 30 volts, but the voltage-current characteristics remained ohmic.

3.2.3 Silver electrodes

The thicknesses of the films sandwiched between silver electrodes were 750Å and 1090Å. The voltage was increased up to 30V and the current passing through the samples was noted. The results are shown in Figure 3.4. Again ohmic behaviour was noted.

3.2.4 Gold electrodes

I-V characteristics of two layers of polypropylene, sandwiched between gold electrodes are shown in the Figure 3.5. The applied voltage was increased up to 60 volts and the leakage current was recorded. The samples were fixed in a chamber at 10^{-5} torr and room temperature. The current was found to be thickness dependent and the dielectric remained ohmic.

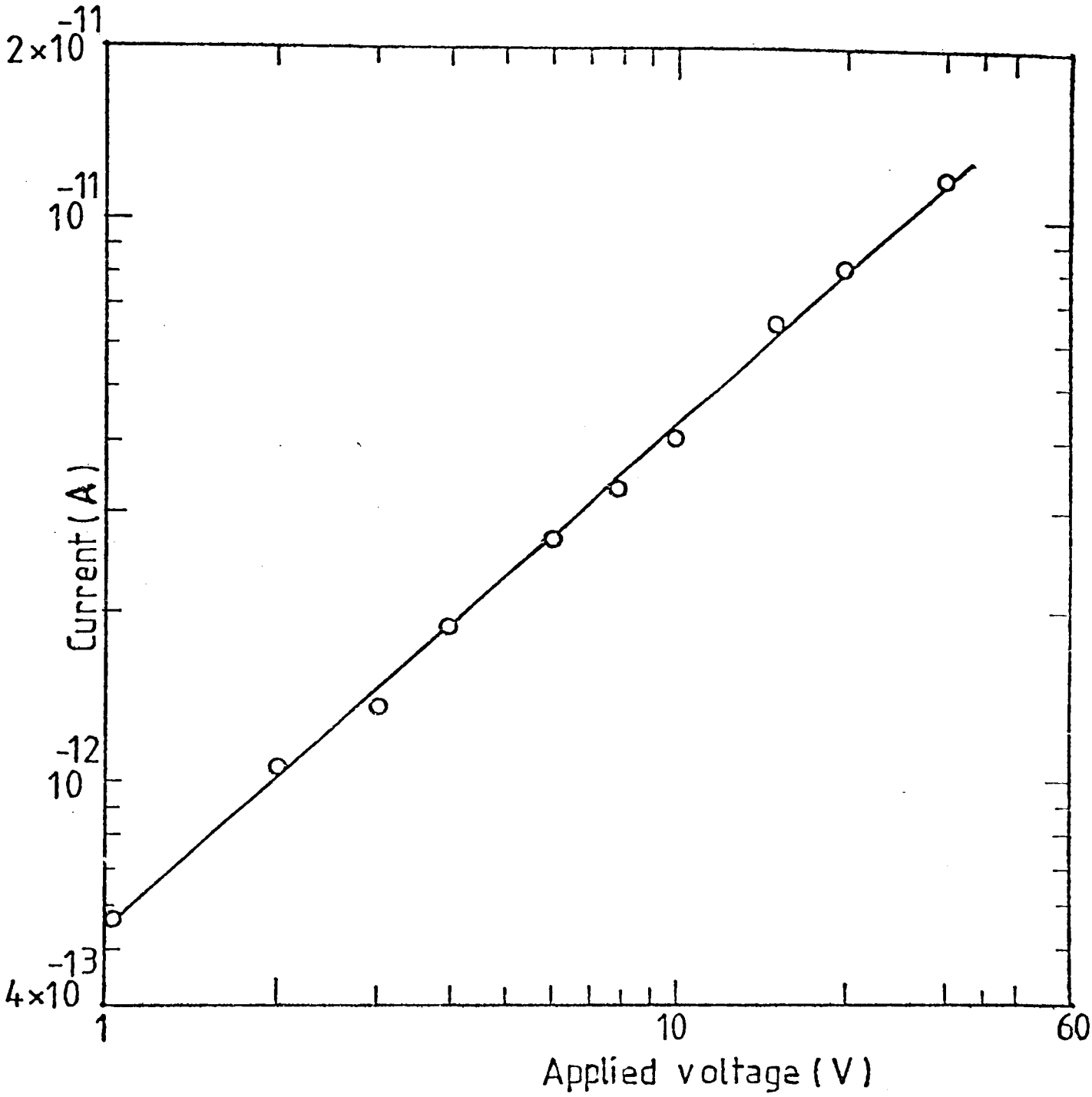

Figure 3.3 The I-V characteristics of Al/PP(1200Å)/Al samples.

3.3 Conclusion and discussion

The I-V characteristics of evaporated polypropylene having thicknesses between 750 and 2400Å, sandwiched between copper, aluminium, silver and gold electrodes are shown in the Figures 3.2, 3.3, 3.4 and 3.5 respectively. It is not possible to explain the conduction by the standard mechanisms, e.g. tunnelling, Schottky emission, Poole-Frenkel or the

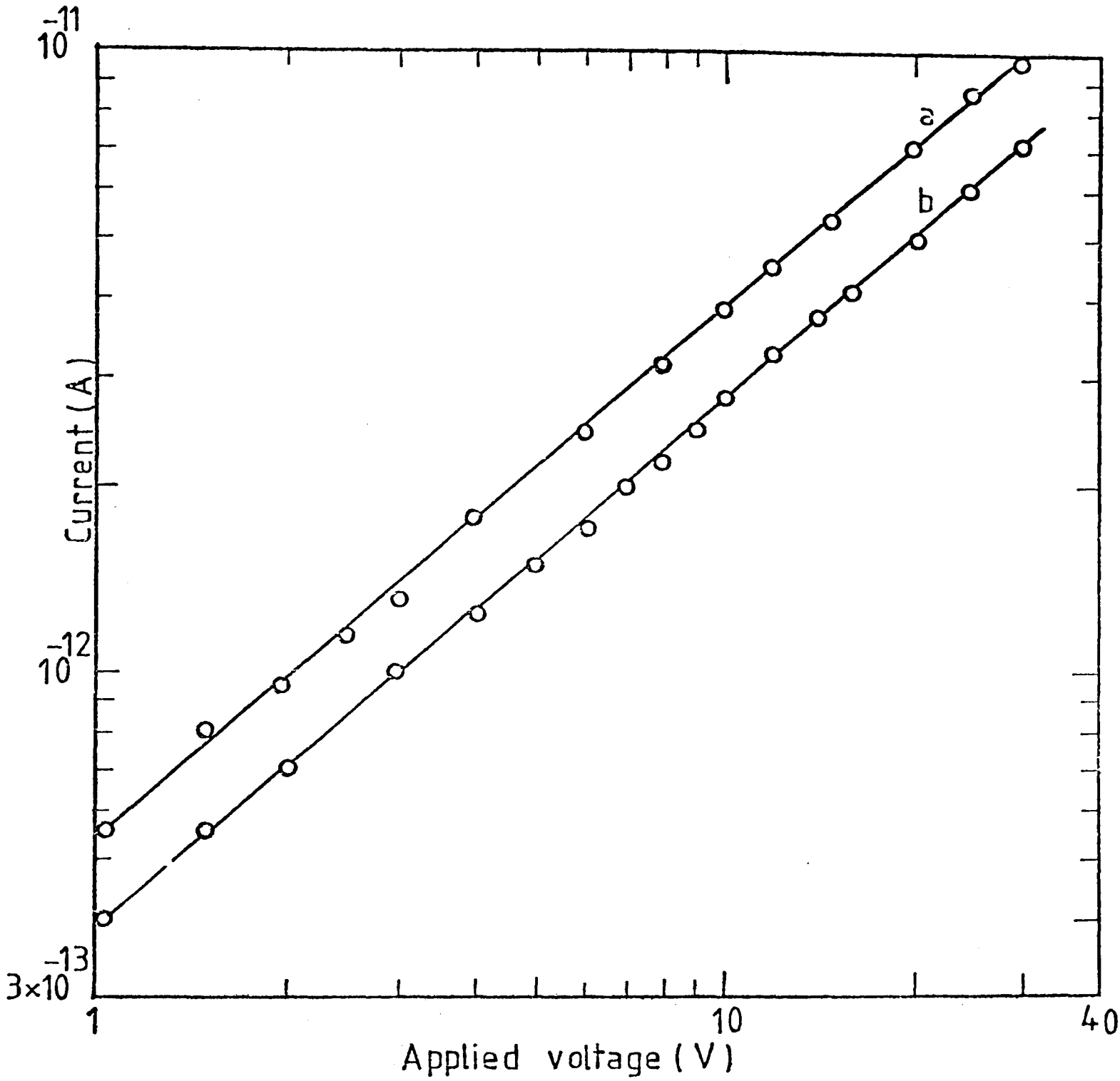

Figure 3.4 Voltage-current characteristics for some thin films of polypropylene (PP). Curve a, Ag/PP(750Å)/Ag, curve b, Ag/PP(1090Å)/Ag.

space-charge conduction due to the ohmic behaviour of the polypropylene films with all the electrodes. There seems to be no significant effect of the applied electric field

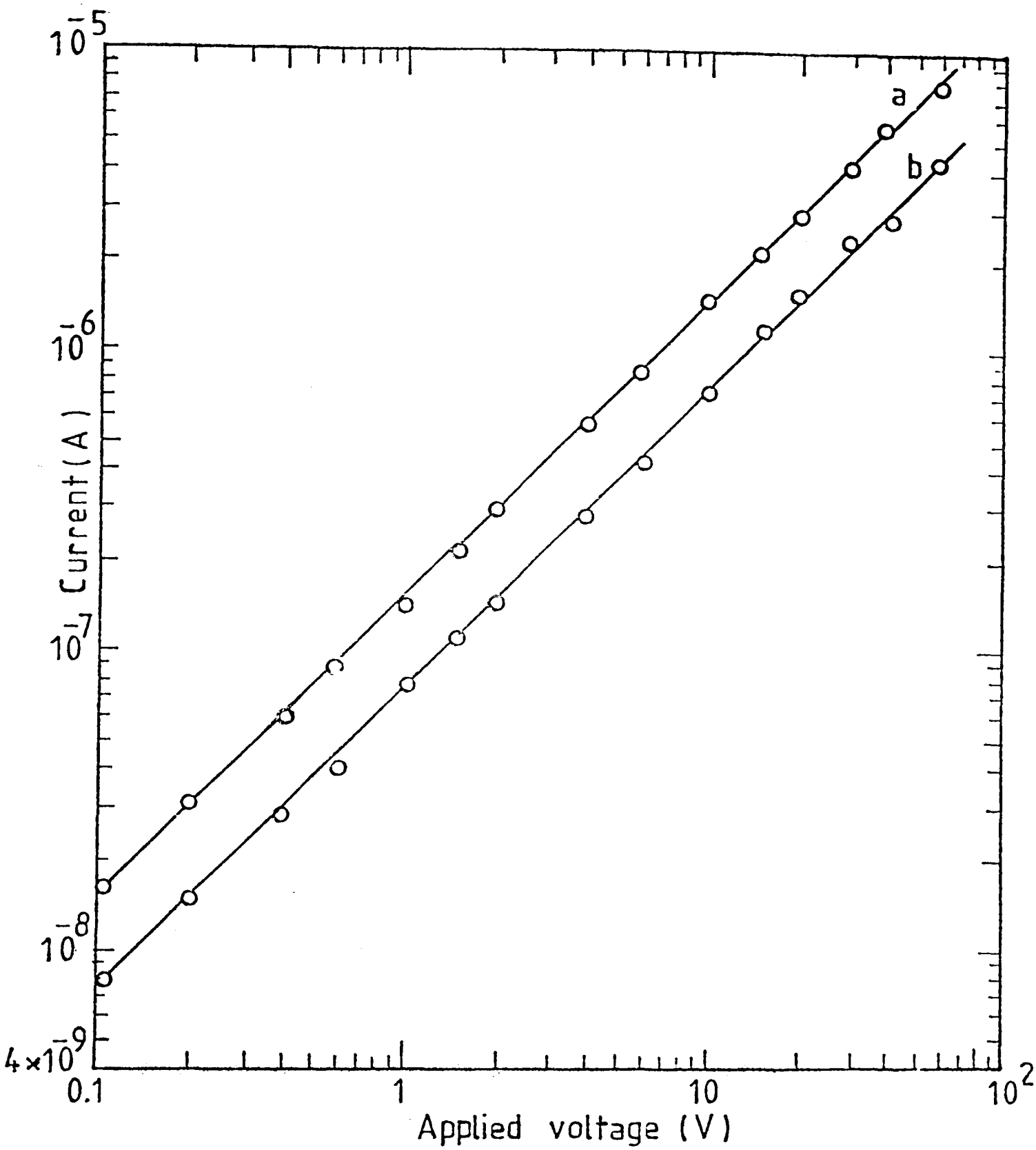

Figure 3.5 Voltage current characteristics for some thin films of polypropylene (PP). Curve a, Au/(1120Å)/Au and curve b, Au/(800Å)/Au.

because of the high resistivity of the film, which is of the order of 10^{14} Ω -cm. On the basis of these results, it could

be concluded that there is no evidence of the formation of rectifying barriers or channels and the dielectric remains ohmic[5]. This suggests that the impurities are distributed uniformly and the conduction may take place due to the hopping from one localized state to another. Stuke[123] showed that the electrical conductivity obeys the following relatuonship.

$$\sigma = \sigma_o \exp\left(\frac{-\epsilon}{kT}\right) = \sigma_o \exp\left(\frac{-E_{el}}{2kT}\right) \qquad (3.3)$$

Where ϵ , is the activation energy, E_{el} is the electrical energy gap and is defined as twice the activation energy ϵ for many amorphous semiconductors, k is Boltzmann's constant and T is the absolute temperature, σ_o is a constant and it is related to the effective densities of states. According to Mott and Davis[124] for the group of materials having the value of σ_o between 10^2 and 10^4 Ω^{-1} - cm^{-1} conductivity is due to the carriers excited into extended states. For σ_o of the order of 10 Ω^{-1} - cm^{-1} they suggest that the conduction is due to carriers excited into localized states at the band edges. Values much less than this for σ_o could correspond to conduction due to carriers hopping between localized states near the Fermi level. Figure 3.6 shows the plot of $\log\sigma$ vs $\frac{1}{T}$ for a Al-PP(1800Å)-Cu sample. The value of σ_o is of the order of 10^{-9} Ω^{-1} - cm^{-1}, so it could be concluded that the conduction in the evaporated polypropylene is due to the carriers hopping near the Fermi level.

Figure 3.2 indicates that the electrode material is introduced into the dielectric and the indiffusion of

copper under the influence of an electric field is more probable than the in-diffusion of aluminium[5]. (Here the diffusion should not be mixed with the fundamental diffusion resulting from the concentration gradient of the substance given by $J = -D \frac{\partial c}{\partial x}$, where D is the diffusion constant, C is the concentration of the substance and X is the distance). The in-diffusion of metal electrode material

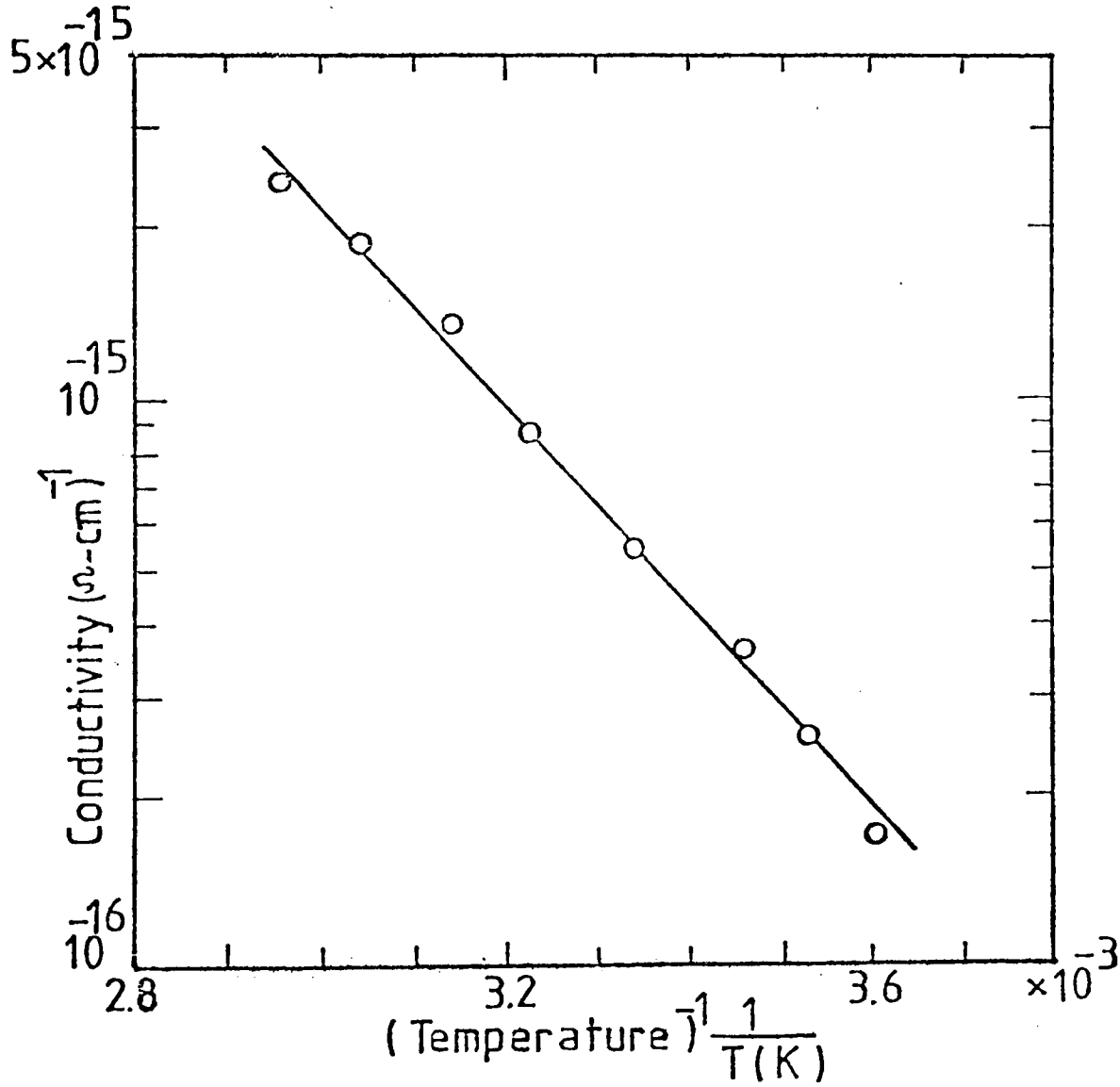

Figure 3.6 $\log\sigma$ vs $\frac{1}{T}$ for Al/PP(1800Å)/Cu samples.

under the influence of the applied electric field, into the dielectric film can also be verified by comparing the current passing through the dielectric (polypropylene)

under the same field but sandwiched between different metal electrodes. Let us consider the following table.

Table 2

Figure No.	Electrode Material Top	Base	Applied v cm^{-1} field	current A
3.5	Au	Au	2.6×10^{6}	2.5×10^{-6}
3.2	Cu	Cu	2.48×10^{6}	3.1×10^{-8}
3.2	Al	Cu	2.48×10^{6}	8.6×10^{-10}
3.3	Al	Al	2.48×10^{6}	1.3×10^{-11}

Under the same applied electric field the leakage current should be higher in the case of gold electrodes, if there is any in-diffusion of the metal from the electrode into the film. Since, $\sigma_{Au} > \sigma_{cu}$ so the current is higher when polypropylene is sandwiched between gold electrodes as compared with copper electrodes.

3.4 Electroforming

3.4.1 Introduction

The thin films of MIM samples under certain conditions undergo an electroforming process on exceeding a threshold applied voltage across the dielectric. The electroforming process is distinguished by a pronounced voltage-controlled negative resistance which appears in the I-V characteristics of the formed sample. Also, associated with the electroforming process are electroluminescence, electron emission and a memory effect. These phenomena have been reported for many

insulators including oxides[50-52,90,91], halides[54], sulphides[92] and certain polyeric materials[33,58]. Recently Hogarth and Zor[4] have shown that thermally evaporated polyethylene undergoes a similar electroforming process. The electroforming processes are affected by the electrode materials, thickness of the insulator, polarity of the bias voltage, temperature and pressure.

3.4.2 Development of electroforming

Under suitable conditions, samples of polypropylene sandwiched between copper and aluminium electrodes, having thicknesses ranging from 600Å to 1000Å showed electroforming effects followed by negative resistance and electron emission into a vacuum. It was possible to electroform the sample with either polarity. However, with negative polarity, the degree of electroforming was less. The degree of electroforming is associated with the maximum current passing through the sample, before the negative resistance region is reached. The forming voltage varied from 12 to 15V. Figure 3.7 shows the development of electroforming in a Al-PP(1000Å)-Al sample at room temperature and under a pressure of 10^{-5} torr. Curve "A" gives the voltage-current characteristics for the first run through the sample. Now the sample was left under 15V for overnight and the following day its characteristics were examined again, while the other conditions remained unchanged. The peak current was found to increase from 4.2×10^{-3}A to 2×10^{-2}A, as shown by the curve "B". For the lower values of applied voltage

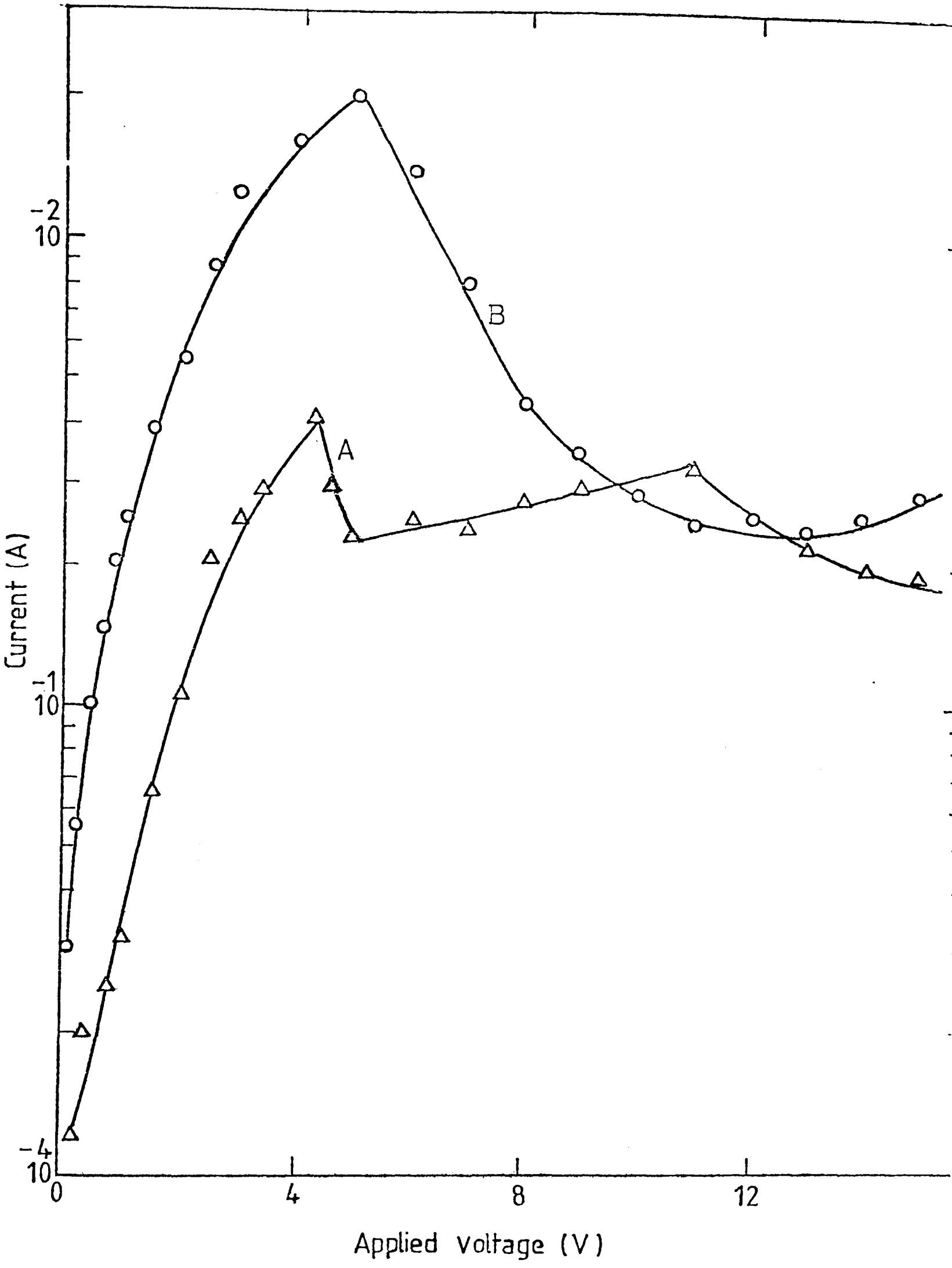

Figure 3.7 The development of electroforming in an Al-PP(1000Å)-Al sample. Curve A, I-V characteristics for the first run, curve B, I-V characteristics after the sample was being left under 15V for overnight (room temperature, ambient pressure 10^{-5} torr).

the current values are similar to those observed for the curve A, but exceeding the peak current, which is higher in this case, the current decreases sharply with increasing voltage and reflects the complete electroforming of the device. Figure 3.8 shows the voltage-current characteristics of an Al-PP(950Å)-Al sample before and after electroforming.

3.4.3 Differential negative resistance

Differential negative resistance is a characteristic of all electroformed devices. It is observed as the fast increase in circulating current with increasing voltage up to a certain point and then it starts falling to the minimum value, provided the applied voltage does not exceed the breakdown limit.

Hysteresis effects are generally observed in the voltage-current characteristics of the formed devices. Hysteresis can be either positive or negative. When the peak current for the decreasing voltage is less than that observed on increasing the voltage, the hysteresis is known as negative, while the opposite case is called positive. Negative hysteresis is shown in Figures 3.9 and 3.10. Figure 3.9 gives the voltage-current characteristics of a Cu-PP(700Å)-Cu sample with increasing and decreasing voltages at pressures less than 10^{-5} torr and at room temperature. The characteristics for the first run of increasing and decreasing voltages of a Cu-PP(600Å)-Cu sample, under the same conditions are given in the Figure 3.10. The second run with increasing and decreasing voltage appeared as positive hysteresis as shown

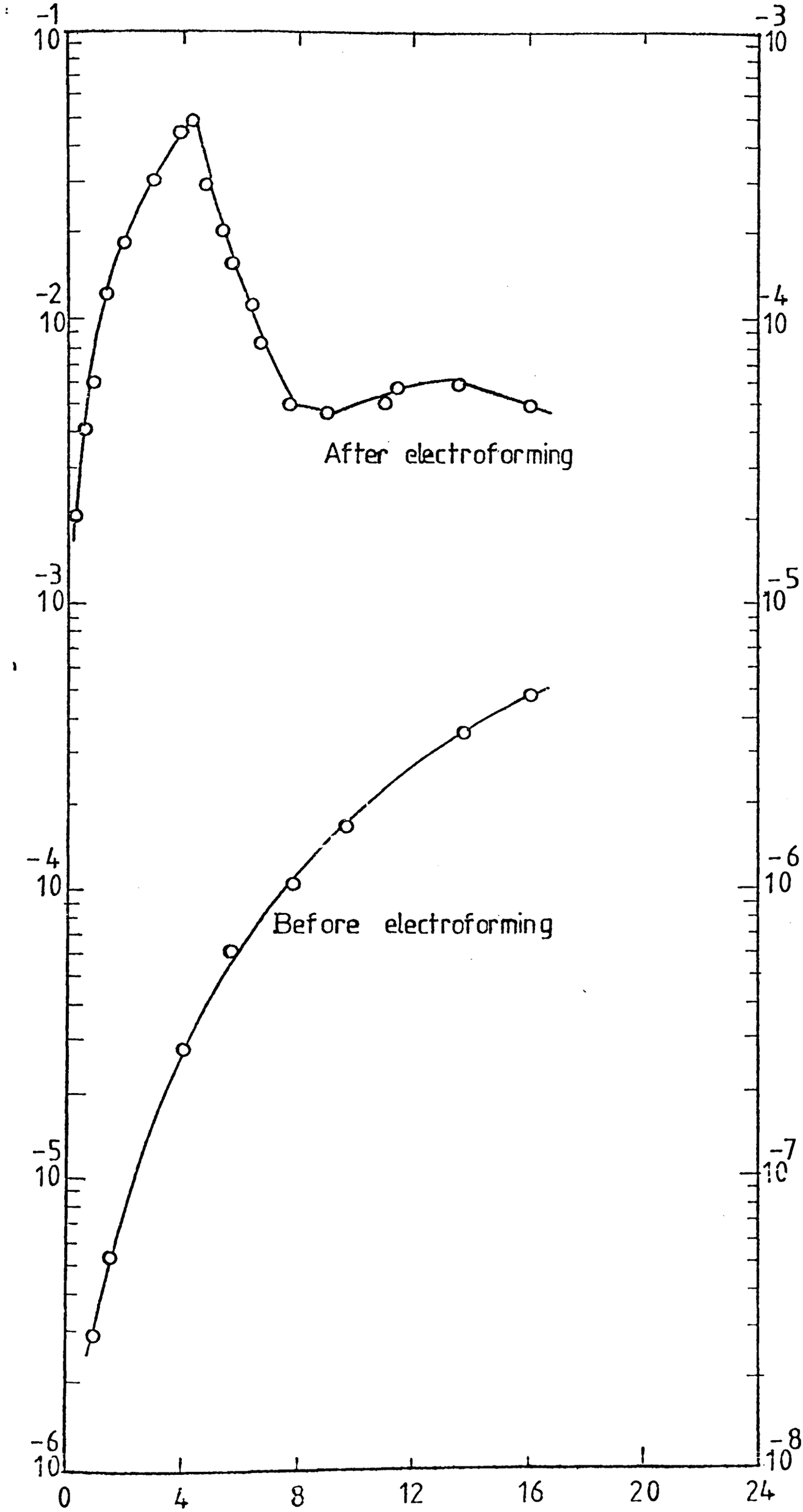

Figure 3.8 Voltage-current characteristics of an Al-PP(950Å)/Al sample before and after electroforming.
(Room temperature, ambient pressure 10^{-5} torr) (after Hogarth and Iqbal[60])

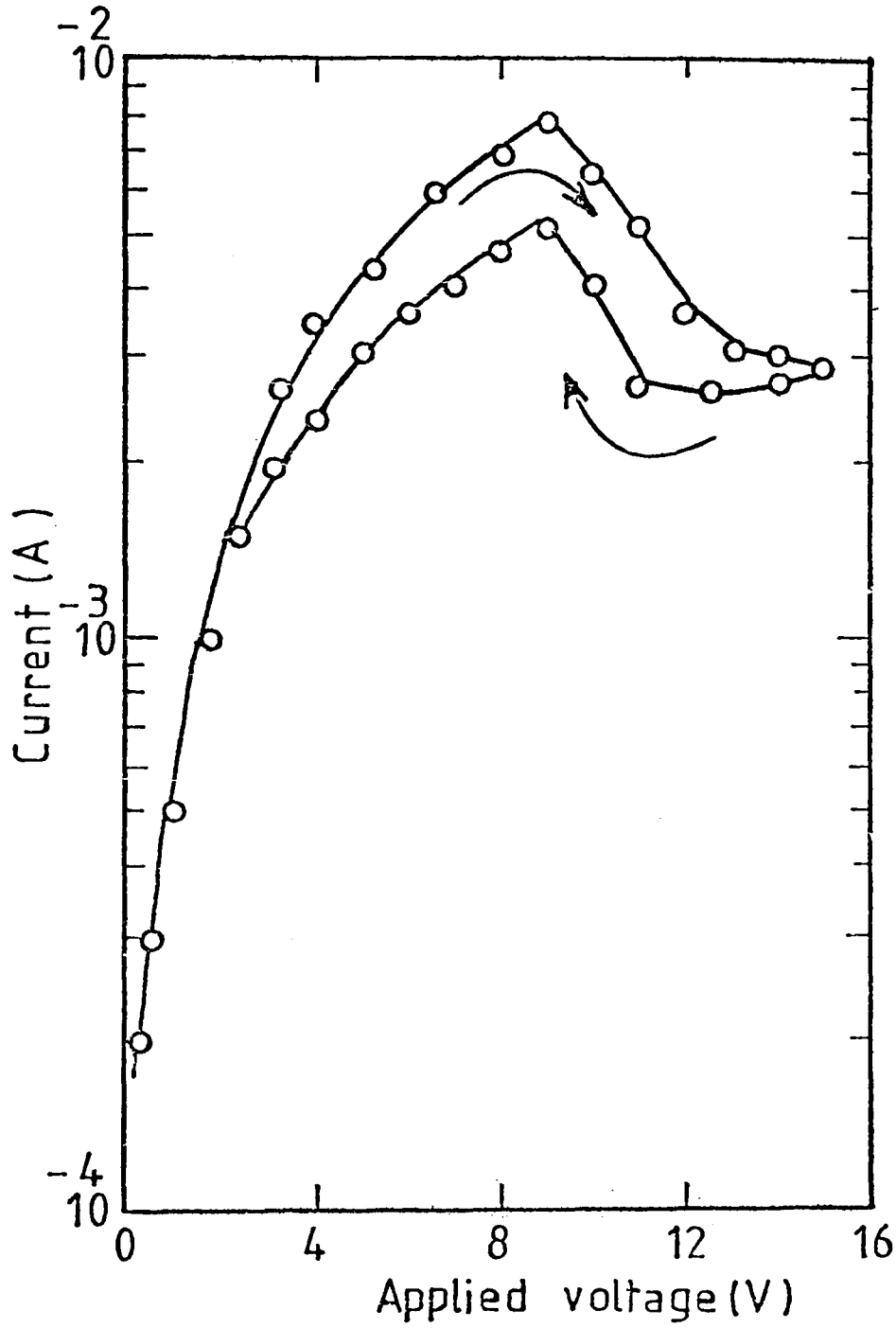

Figure 3.9 Electroforming of a Cu-PP(700Å)-Cu sample for increasing and decreasing applied voltages. (Room temperature, ambient pressure 10^{-5} torr).

in the Figure 3.11. In most cases the peak current occurred at between 5 and 7V.

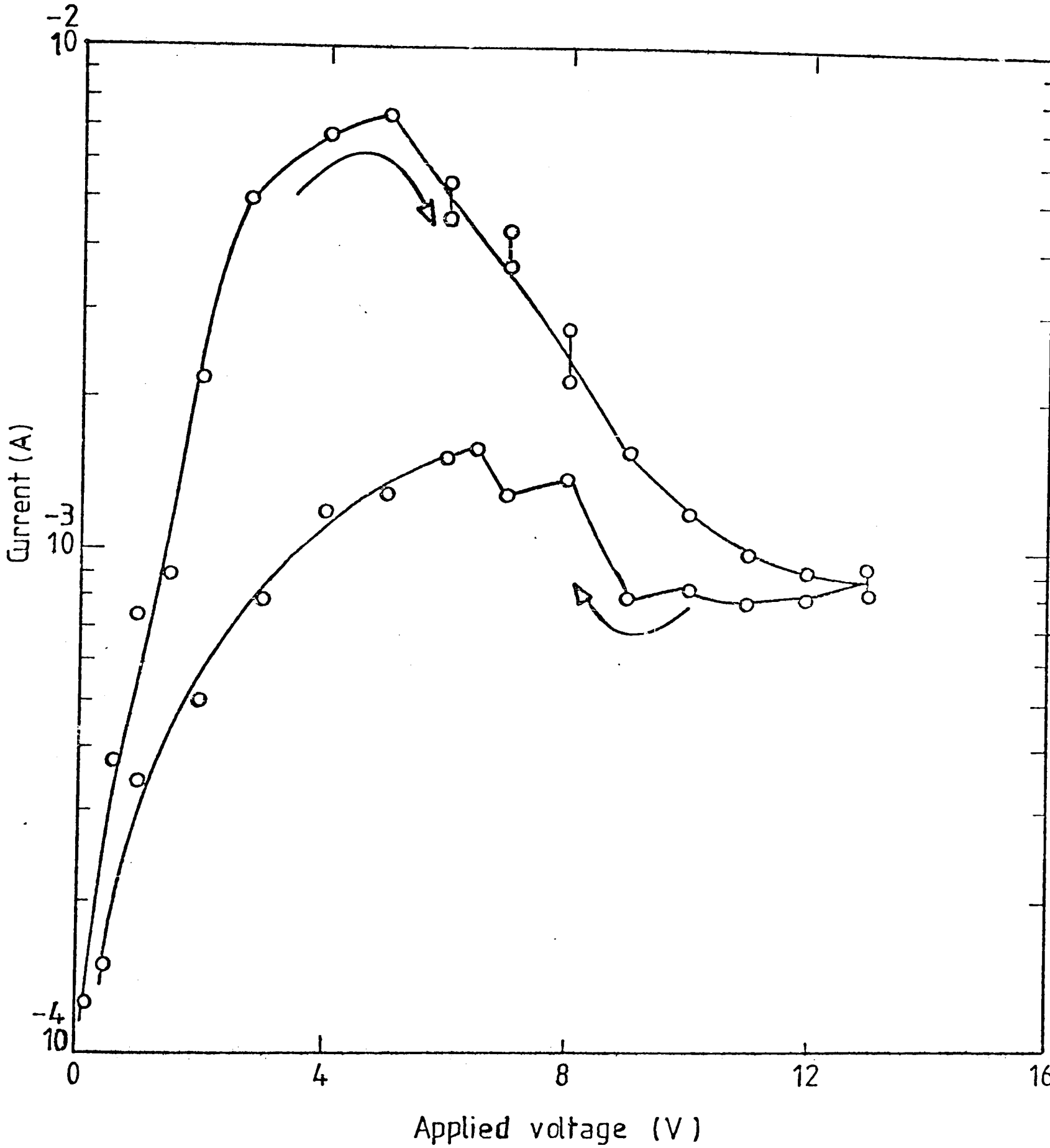

Figure 3.10 Electroforming of a Cu-PP(600Å)-Cu sample for increasing and decreasing applied voltages. (Room temperature, ambient pressure 10^{-5} torr) (after Hogarth and Iqbal[60]).

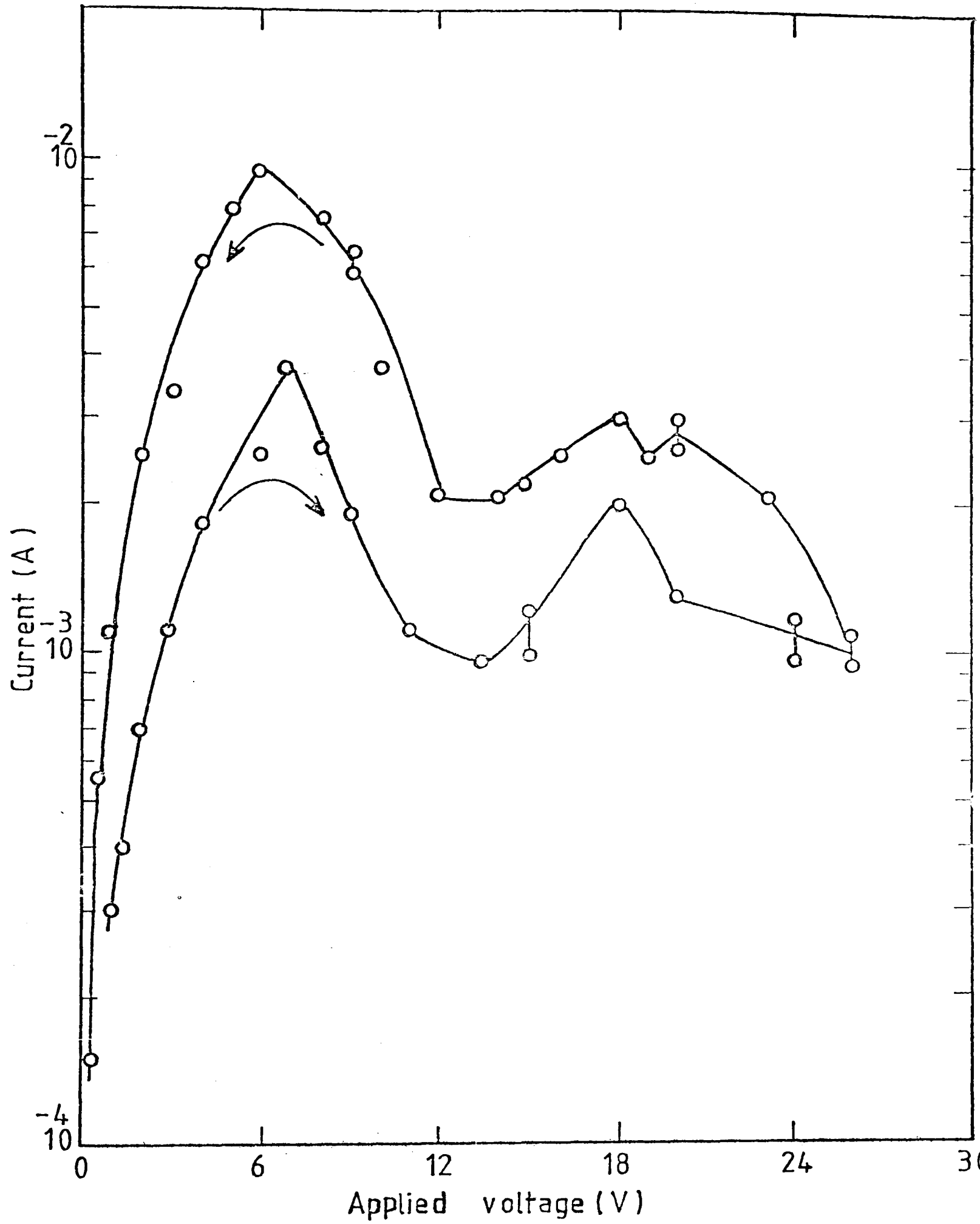

Figure 3.11 Electroforming of a Cu-PP(600Å)-Cu sample for second run of increasing and decreasing applied voltages (room temperature, ambient pressure 10^{-5} torr).

3.4.4 Effect of pressure

Pressure is an important factor in achieving electroforming . All the samples were electroformed at room temperature and under a pressure of 10^{-5} torr. It was not possible to electroform the devices at ambient air pressure. However, after electroforming in vacuum, if the pressure inside the chamber is increased to 10^{-3} torr from 10^{-5} torr by admitting some air then for the lower values of applied voltage, the current values are similar to those recorded at the lower ambient pressure, but on exceeding the peak current the decrease in current with increasing voltage shows a less rapid decrease at the higher pressure, as shown in Figure 3.12. If now some more air is admitted into the chamber and the pressure is increased up to atmospheric pressure, the voltage-current characteristics of the sample are given in the Figure 3.13. It can be seen that there is still a region of negative resistance, but the current is fluctuating due to the atmospheric disturbance. Hence, it may be concluded that electroforming leads to permanent changes in the voltage-current characteristics of the evaporated polypropylene samples sandwiched between metal electrodes.

3.4.5 Effect of temperature

Most of the measurements were carried out at room temperature and the ambient pressure of 10^{-5} torr. As mentioned before, temperature does effect the characteristics of the formed device. In order to see the effect of temperature on the electroformed polypropylene film, sandwiched between copper

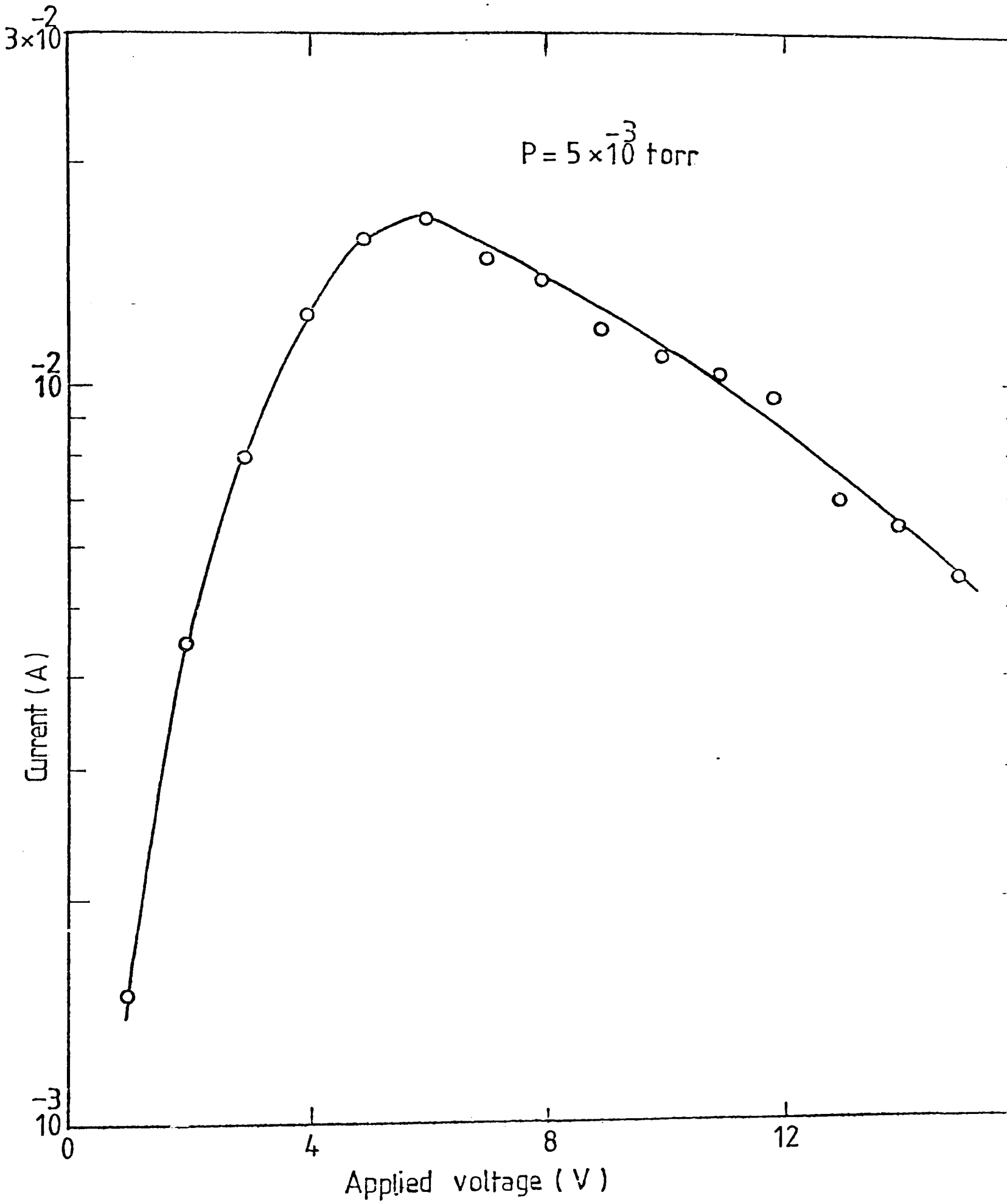

Figure 3.12 The voltage-current characteristics of a Cu-PP(600Å)-Cu sample at an ambient pressure of 10^{-3} torr (room temperature) (after Hogarth and Iqbal[60]).

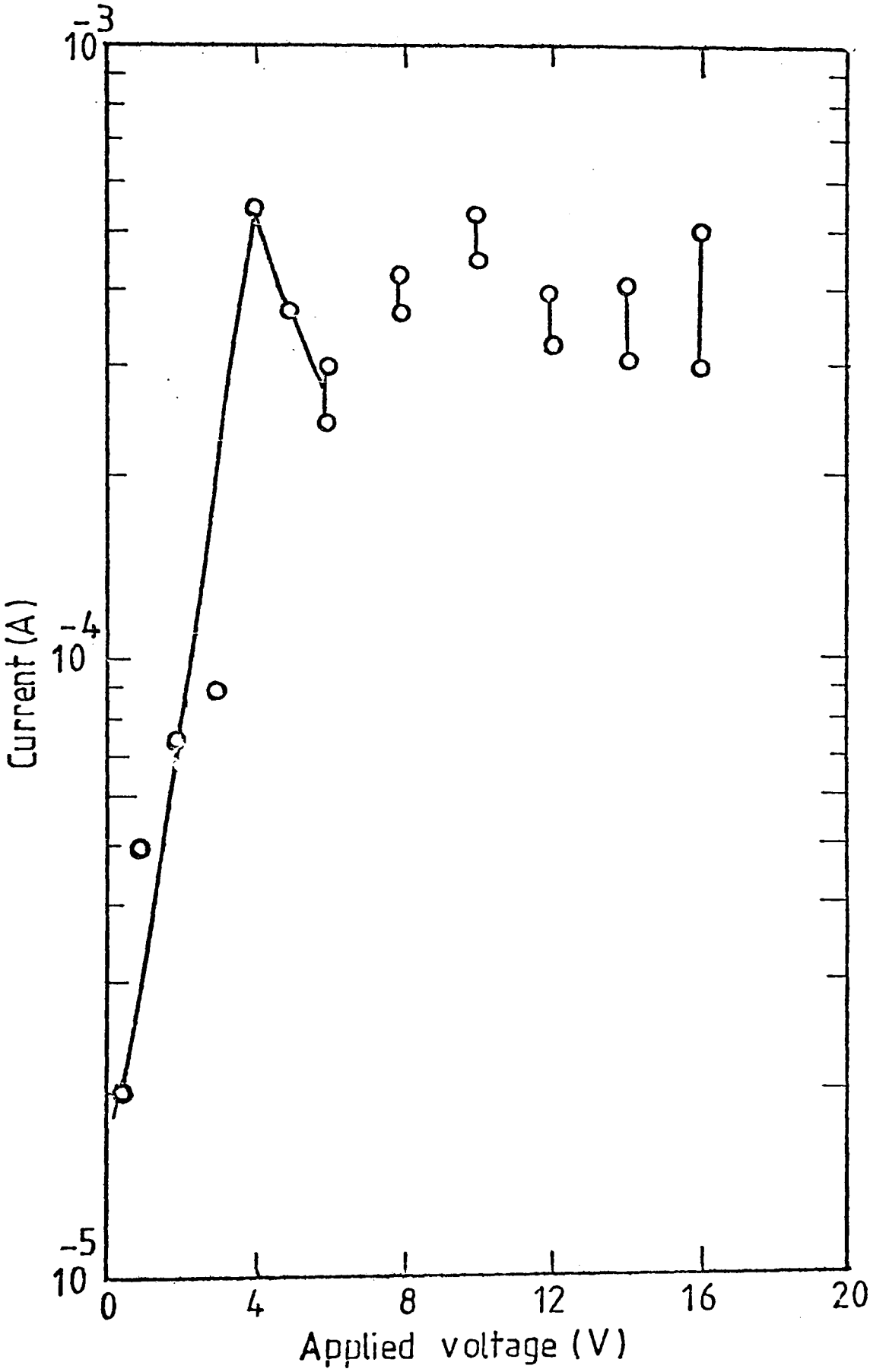

Figure 3.13 The voltage-current characteristic of a Cu-PP (600Å)-Cu sample at room temperature (atmospheric pressure).

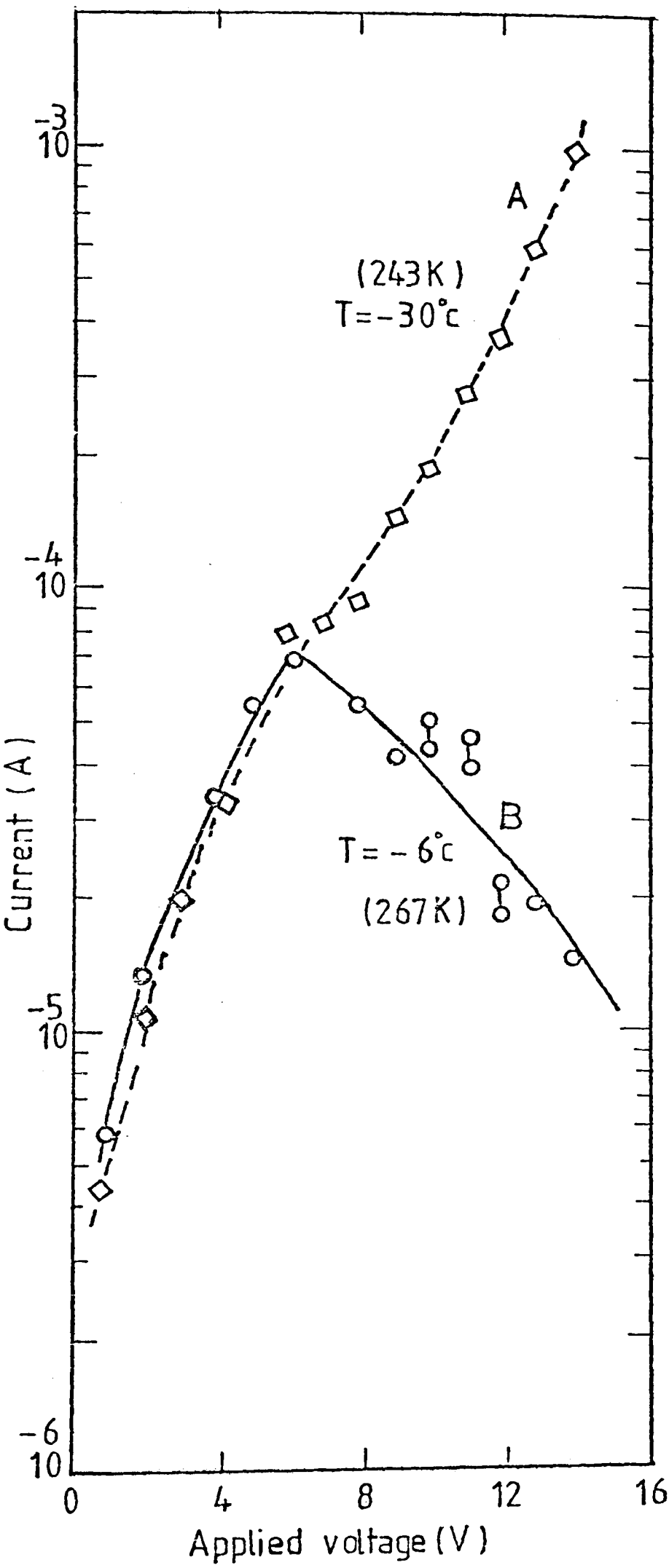

Figure 3.14 The voltage-current characteristic of a Cu-PP (600Å)-Cu sample at 243 and 267K (ambient pressure 10^{-5} torr).

electrodes, liquid nitrogen was used to cool the sample to $-30^{o}C$. The differential negative resistance region disappeared at this temperature, as shown by curve "A" in Figure 3.14. Now the sample was heated slowly and its voltage-current characteristics were examined carefully. The differential negative resistance region re-appeared at $T = -6^{o}C$, as shown in curve "B" in Figure 3.14.

3.4.6 Electron emission

Figure 3.15 shows the voltage-current characteristics of a Cu-PP(600Å)-Cu sample after electroforming at room temperature and under a pressure of 10^{-5} torr. The electron emission current collected by a subsidiary anode biased at 100V and positioned about 1.5 cm from the upper surface of the sample is also shown on this figure, while the circulating and emission currents for a Cu-PP(700Å)-Cu sample, under the same conditions are given in Figure 3.16. Unlike the behaviour of many reported MIM samples, the rapid rise of emitted electron current occurs not at a voltage corresponding to a current peak but at a voltage corresponding closely to the initial forming voltage 14.6V. An exponential increase of emission current was observed with a slow decrease in circulating current above 15 volts. Therefore the transmission coefficient, α, which is the ratio of emission current to the circulating current, also increases exponentially with bias voltages, as shown in Figure 3.17.

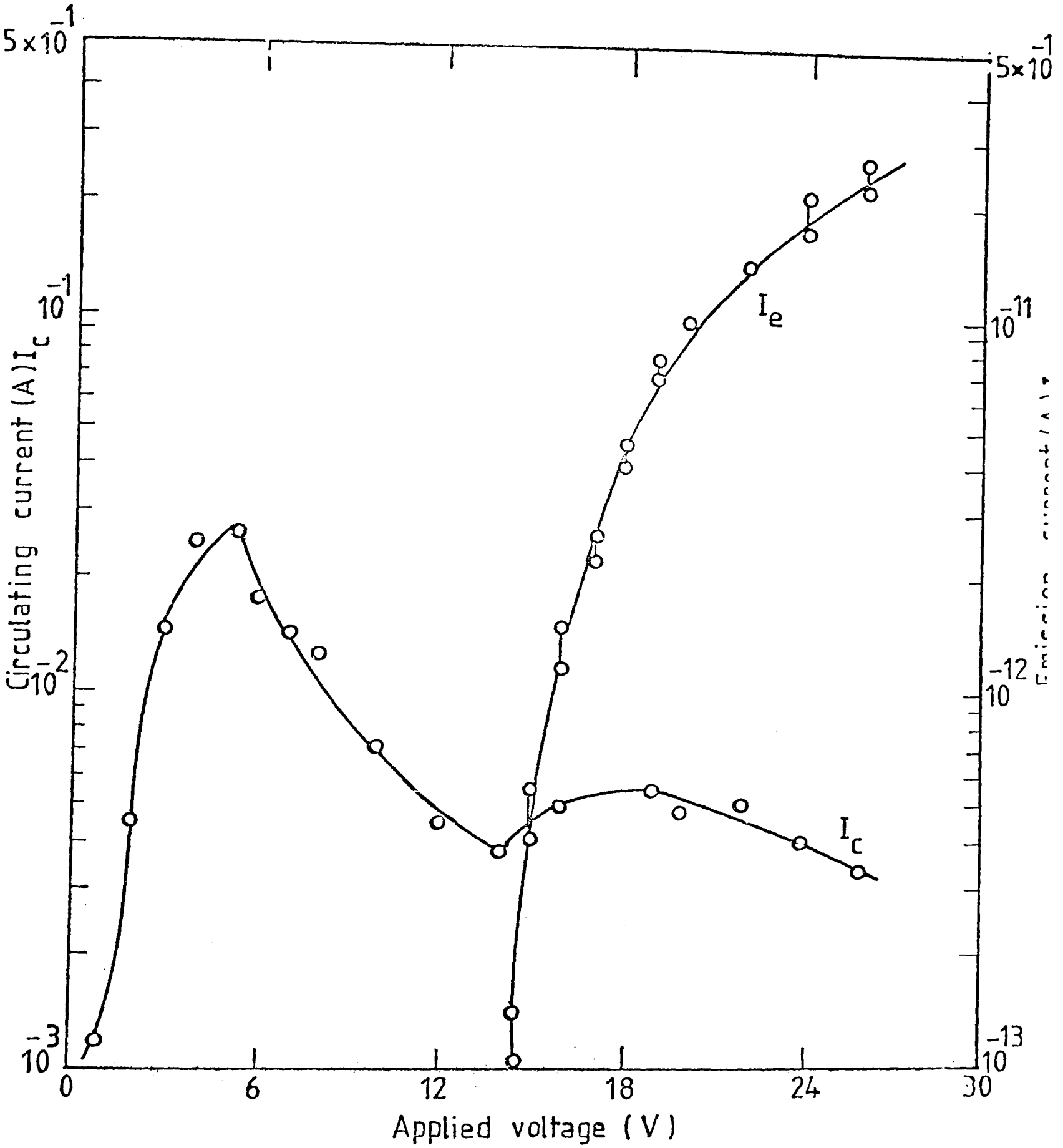

Figure 3.15 Circulating and emission current as function of applied voltage for a Cu-PP(600Å)-Cu sample. (Room temperature, ambient pressure 10^{-5} torr.) (after Hogarth and Iqbal[60]).

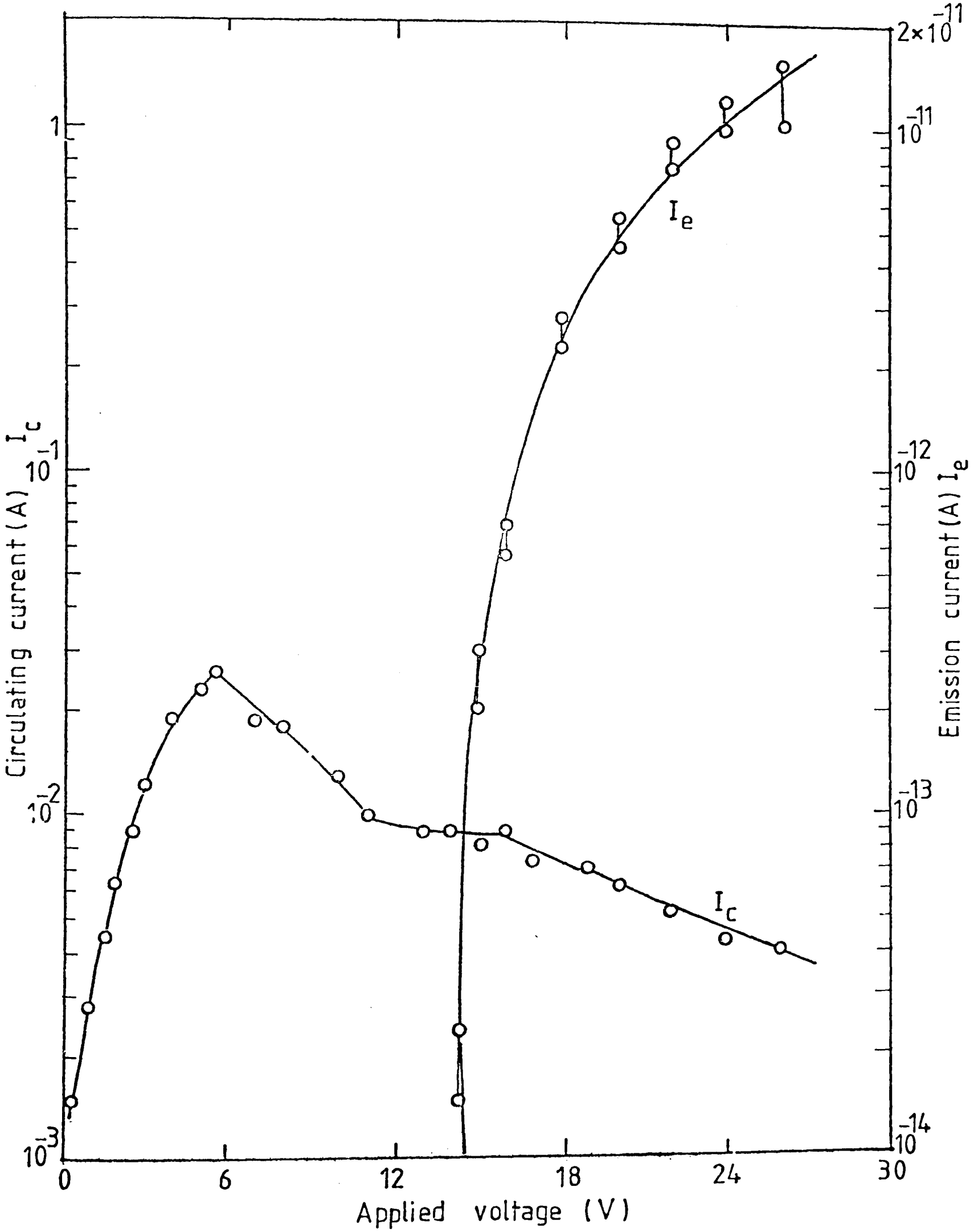

Figure 3.16 Circulating and emission current as function of applied voltage for a Cu-PP(700Å)-Cu sample. (Room temperature, ambient pressure 10^{-5} torr.)

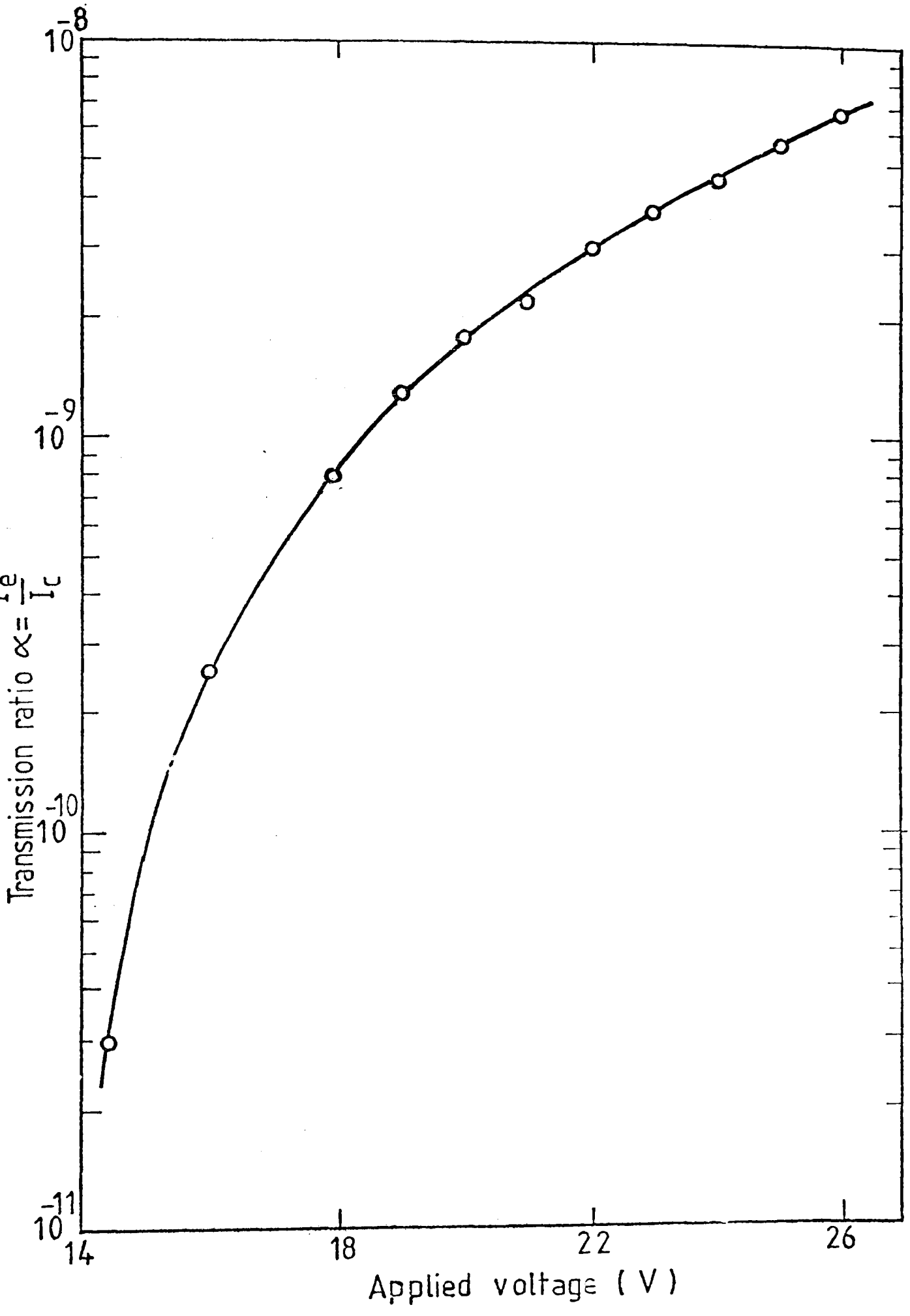

Figure 3.17 The transmission coefficient $\alpha (= \frac{I_e}{I_c})$ as function of applied voltage for a Cu-PP(600Å)-Cu sample.

3.4.7. Conclusion and discussion

A number of theories have been proposed to explain electro-forming and associated effects in insulators and these include the interaction of an impurity band and a high-field region[50,51], injection of metal ions forming broad impurity states[52,53], an electrolytic process giving rise to localized conduction paths[54,55] and the formation of filamentary metallic path[56,57]. Recent evidence suggests that a filamentary process together with some electrolysis along the filamentary regions can explain most of the experimental features associated with electro-forming and some confirmation of these ideas from electron microscopic evidence has been given by Rakhshani[120] et al and by Rakhshani[121] and Hogarth. The filamentary model[125] can be applied to explain the electro-forming phenomena in the evaporated polypropylene films. It is assumed that metal from the electrodes diffuses[5] into the dielectric under the relatively high applied forming field and forms filamentarypaths which carry the augmented current. Weak spots in the filaments may be ruptured by Joule heating and lead to the observed differential negative resistance (see Figures 3.7 to 3.11). Partial healing of the ruptured filaments may account for the lower curves of Figures 3.9 and 3.10 for decreasing voltages. The broken filaments can be healed again by gradually increasing the voltage across the sample up to 25 volts. If it is so, then on decreasing voltages, the peak current will be higher as compared with the increasing voltages. This could be used as an explanation for the higher current for decreasing voltages in Figure 3.11.

When the pressure inside the chamber containing the formed sample is increased to 10^{-3} torr from 10^{-5} torr by admitting some air, there is a less rapid decrease in the circulating current, on exceeding the peak current at higher voltages (see Figure 3.12). This can be explained by assuming that when air is admitted into the chamber the rate of rupturing of the filaments is reduced following the increased loss of heat by convection in the surrounding low pressure area which removes some of the Joule heat from the sample[60]. The electron emission may be ascribed to emission at the weak or high field regions of the filaments exciting the carriers to the hot electron condition when they are ripe for escape into the vacuum.

3.5 A.C. measurements

3.5.1 Introduction

Hung and Gliessman[126] first observed the impurity conduction in their low-temperature investigation of germanium. Since then a number of papers[127-130] haye been published on the same kind of conduction resulting from the application of steady fields. In order to explain the conduction, they all used the model based on the impurity theory of Conwell[127] and Mott[131]. According to this model, which is valid for low-temperature impurity conduction, transport occurs by electron hopping between states which are essentiall localized around acceptor or donor impurities, by exchanging energy with phonons. Conduction may also be explained in terms of tunnelling through the energy barrier from the occupied donor

to the unoccupied one. For such transport to take place, it is necessary for some of the localized states to be vacant and hence compensation of the majority impurity becomes an essential feature of impurity conduction as demonstrated by Fritzsche[132]. Pollack and Geballe[19] have presented a theory relating the hopping conductivity to the a.c. frequency. Their theory is also based upon the original model of impurity conduction.

3.5.2 Experimental techniques

The samples for the a.c. measurements were prepared in the same way as described by Hogarth and Iqbal[5]. The measurements were carried out under a pressure of 10^{-5} torr using the frequency range between 10^3 and 2×10^4 Hz at room temperature, unless stated otherwise. A Wayne Kerr audio frequency voltage generator S121 was used to apply a signal of 5V across the device, and a Wayne Kerr waveform analyser A321 along with a universal bridge B221 were used for the detector. A block diagram of the experimental set up is shown in Figure 3.18.

3.5.3 Results and discussion

Measurements of capacitance and conductance were carried out before and after the electroforming of the samples. An expected consequence of the Dearnaley filamentary model[125] used to explain the electroforming phenomena in our samples would be some significant differences in the frequency dependence of capacitance and conductance after forming

compared with the behaviour prior to forming. The hopping conduction at low and room temperatures can be identified by the a.c. conductivity measurements. Pollack and Geballe[19] have given an equation for this process

$$\sigma(\omega) = A\omega^S$$

where A is a complex constant, ω is the angular frequency, $\sigma(\omega)$ is the a.c. conductivity and $0.5 < S < 1$.

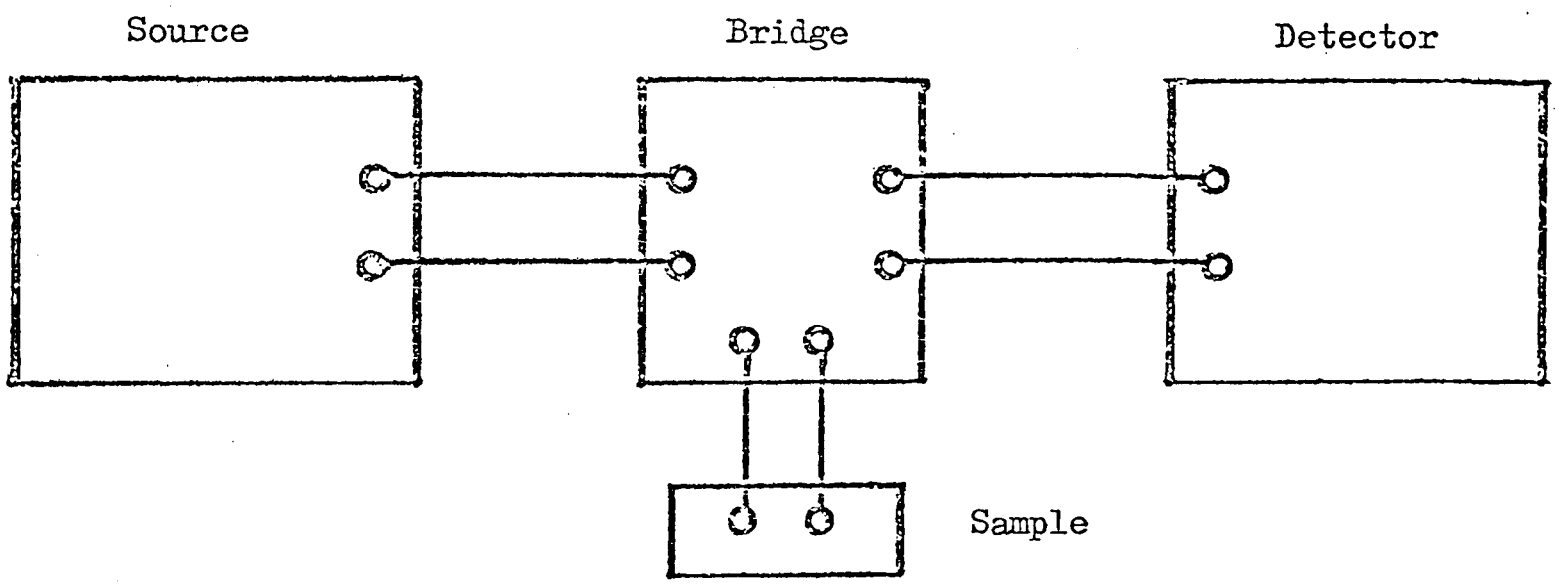

Figure 3.18 Block diagram for a.c. measurements

For hopping conduction S is generally found to be equal to 0.8. In the radio-frequency range of the applied frequency, the square-law dependence of a.c. conductivity upon frequency has been explained in terms of a two-centre hopping process[133]. Figures 3.19 and 3.20 show the plot of a.c. conductance versus frequency for evaporated polypropylene before electroforming at room temperature and at 241K respectively. The slopes of the straight lines fall within the limit $0.5 < S < 1$ and are equal to 0.85 in both cases.

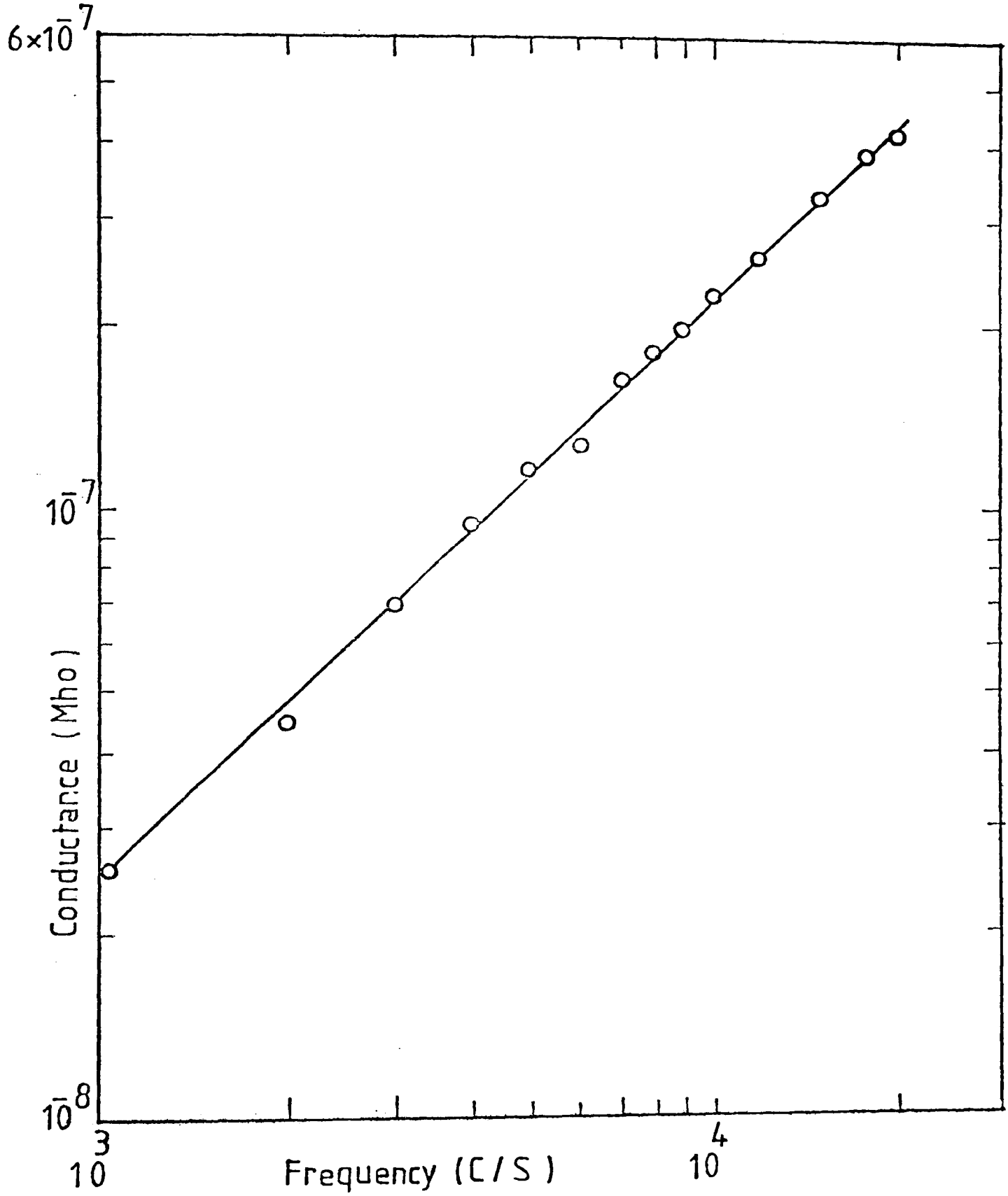

Figure 3.19 Conductance as a function of frequency for a Cu-PP(1800Å)-Cu sample. (Room temperature, ambient pressure 10^{-5} torr).

These results characterize the process of hopping conduction as a dominant process at both low and room temperatures.

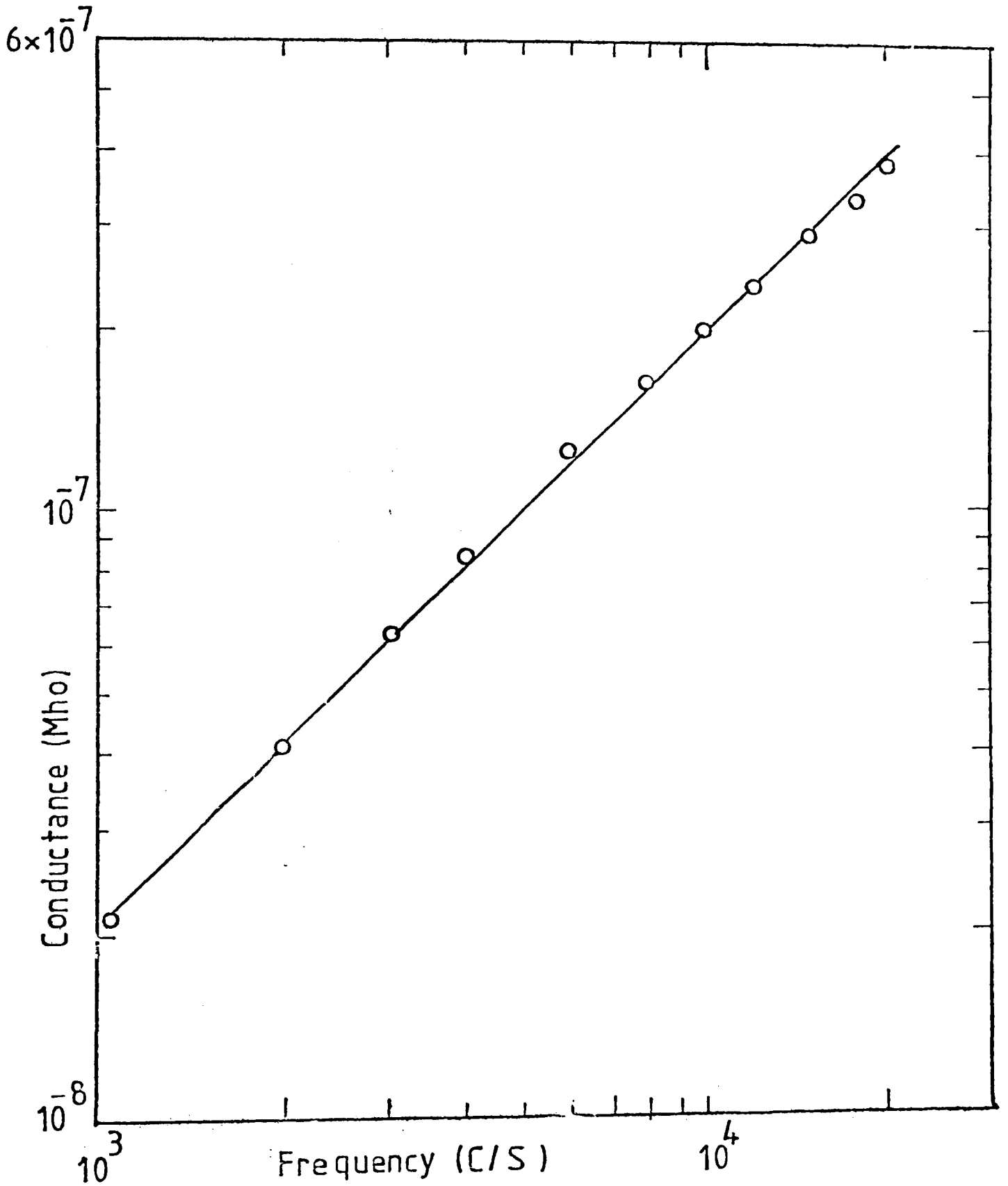

Figure 3.20 Conductance as a function of frequency for a Cu-PP(1800Å)-Cu sample at 241K (Ambient pressure 10^{-5} torr.)

Figure 3.21 shows the variation of capacitance with frequency before electroforming for a Cu-PP(1800Å)-Cu sample at an ambient pressure less than 10^{-5} torr and at room temperature.

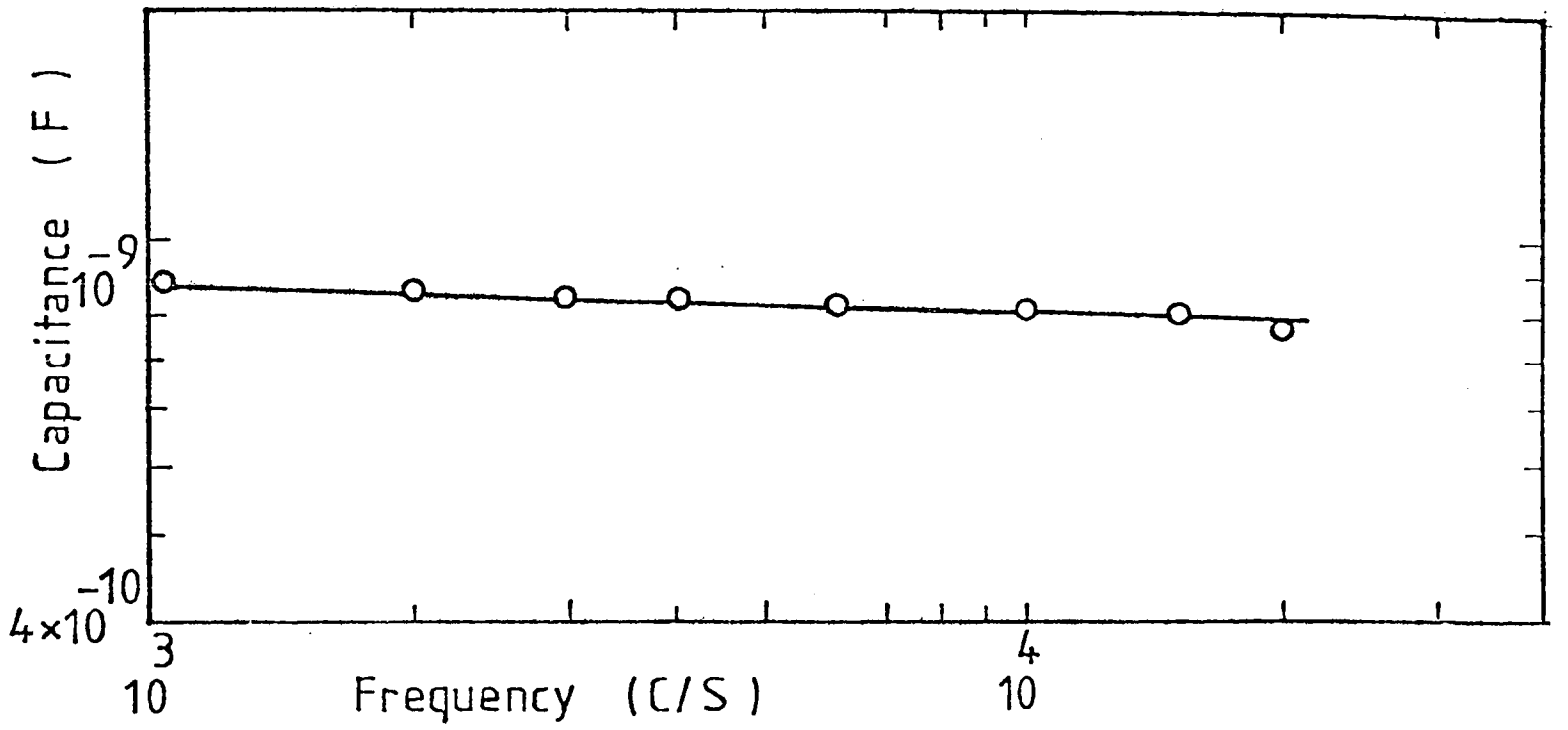

Figure 3.21 Capacitance as a function of frequency for a Cu-PP(1800Å)-Cu sample. (Room temperature, ambient pressure 10^{-5} torr.)

Figure 3.22 demonstrates the variation of capacitance with frequency at low temperature (241K) for the same sample. Before the electroforming, a linear decrease of capacitance with increasing frequency is clear from Figures 3.21 and 3.22. This could be due to the increasing leakage current with frequency and is associated with capacitance reduction. After electroforming a Cu-PP(700Å)-Cu device, an enormous increase in the conductance was noticed. Further the conductance was found to be proportional to the degree of forming and this is consistent with the Dearnaley theory

based on the generation of essentially metallic conducting filaments during the forming process. The capacitance of the sample was decreased after electroforming. It was not possible to balance the bridge and to measure the values of conductance and capacitance simultaneously after the electroforming, a result which is explained by the incidence of a high proportion of metallic conduction following the electroforming.

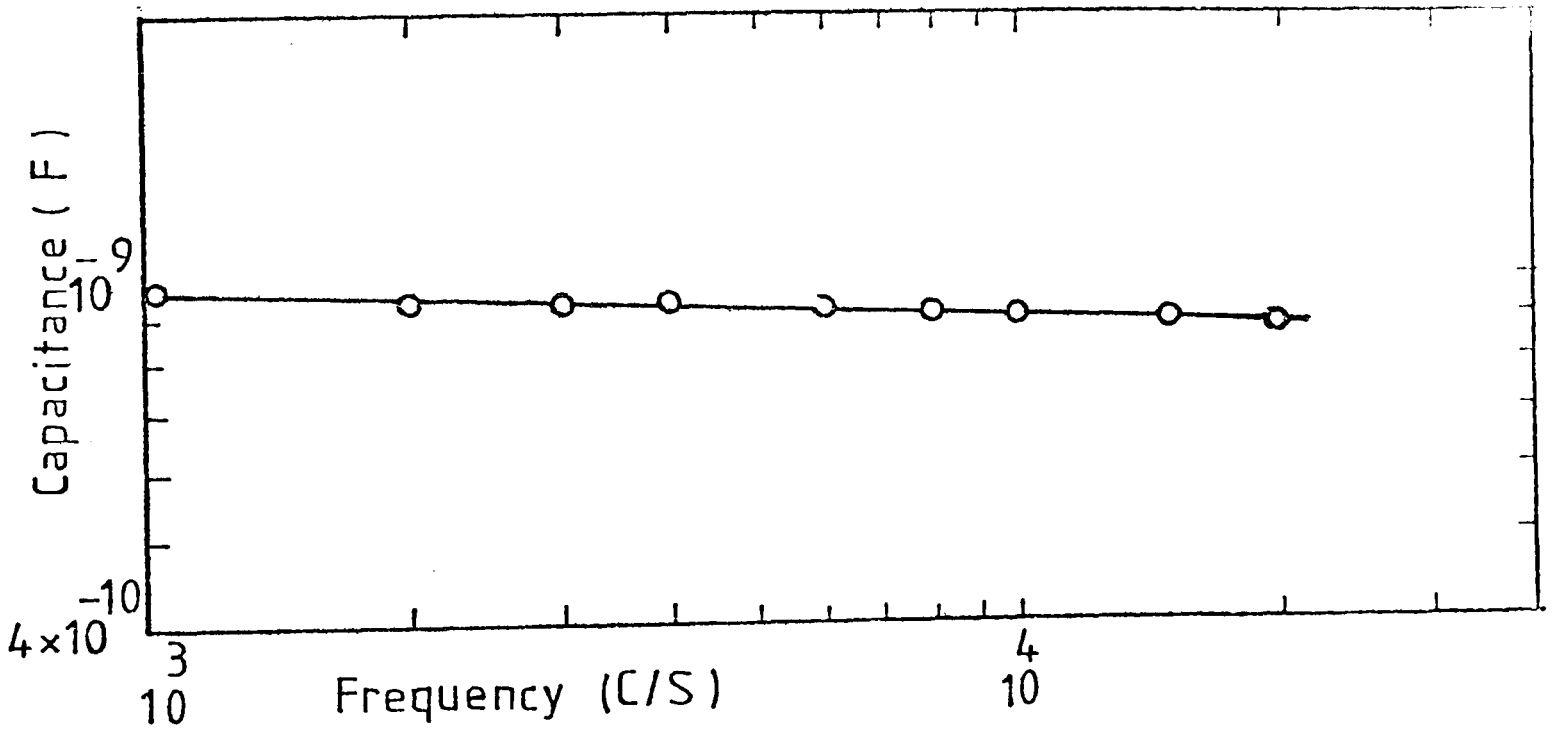

Figure 3.22 Capacitance as a function of frequency for a Cu-PP(1800Å)-Cu sample at 241K. (Ambient pressure 10^{-5} torr.)

4. CHAPTER FOUR

TSC MEASUREMENTS

4.1 Introduction

Theory and techniques of the thermally-stimulated currents have been explained in the Section 1.4. It is a useful tool to calculate the trap depth and the densities of traps in the forbidden gap of the investigated material. In polymers, charge carrier trapping may take place due to the structural disorder resulting from the un-saturated ions in chains, chain terminations, chain folding and from the amorphous/crystalline interface[14]. The study of thermally-stimulated currents in irradiated polyethylene and in teflon revealed that in teflon the $-(CF = CF_2)$, $-(CF = CF) -$ and $-CF - \underset{|}{C}F)-$ groups act as traps[134,135]. The foreign elements present in the polymers are responsible for the deeper traps while the shallow traps are due to the defects in the chain structure e.g. the presence of OH, $>CO$ groups or $-C = C-$ bonds[136].

4.2 Results and discussion

Figure 4.1 shows a series of current versus temperature curves for evaporated polypropylene at a constant heating rate but for different applied electric fields. Figure 4.2 shows a series of curves at a fixed applied field but at different heating rates. A shift in the peak temperature T_m to lower values at higher applied fields but for the same heating rate was observed; this phenomenon was similar to that found by Slowik[16] for poly-N-vinylcarbazole. Also for the same applied field but with an increase in the heating

rate, T_m shifted to higher values.

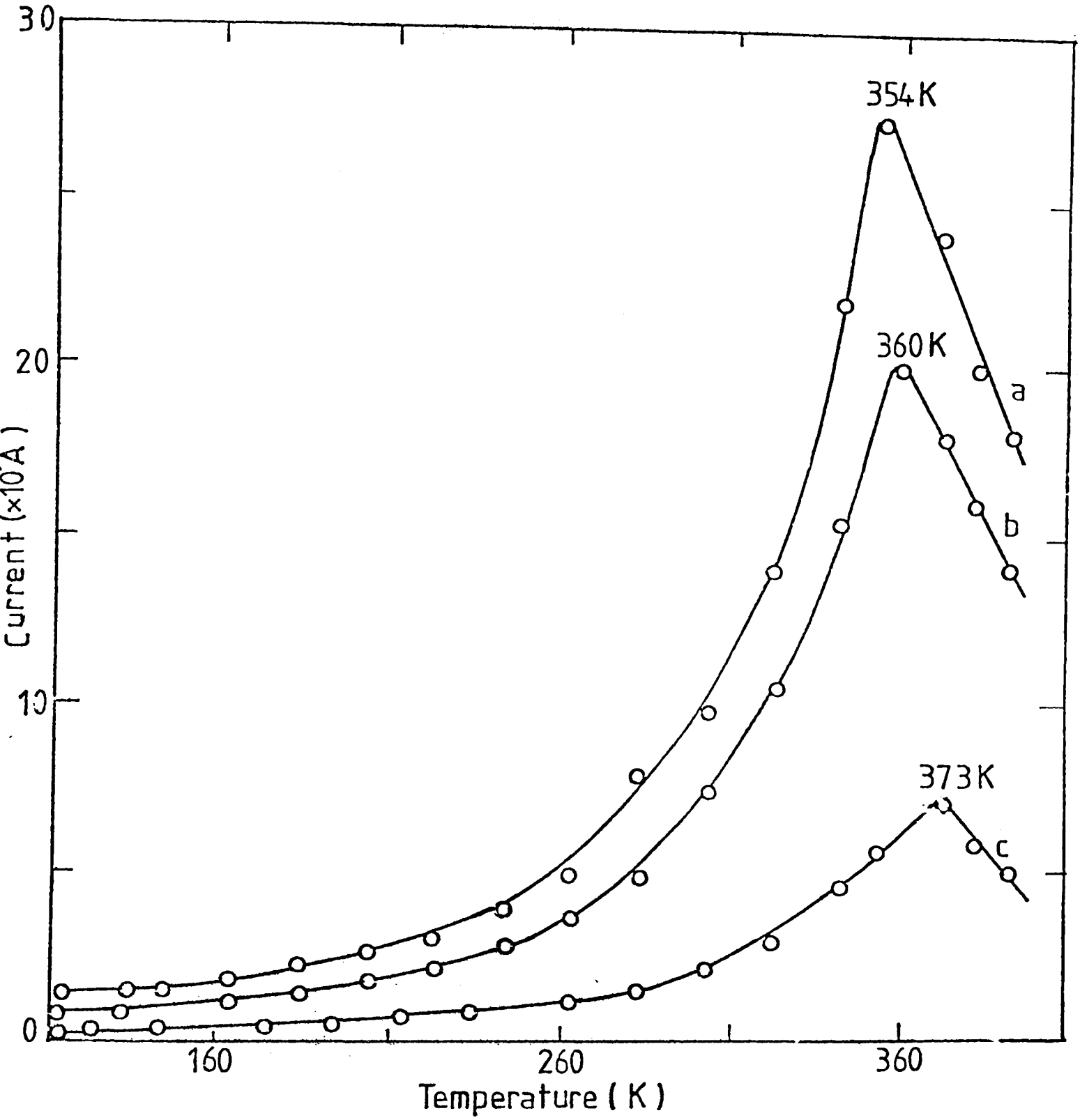

Figure 4.1 The current as a function of temperature on heating a Cu-PP(1600Å)-Cu sandwich structure at a heating rate of approximately 0.172 KS^{-1}; curve a, applied field, 3.12×10^5 V cm^{-1}, curve b, applied field 1.85×10^5 V cm^{-1}; curve c, applied field, 6.25×10^4 V cm^{-1}. (after Iqbal and Hogarth[15]).

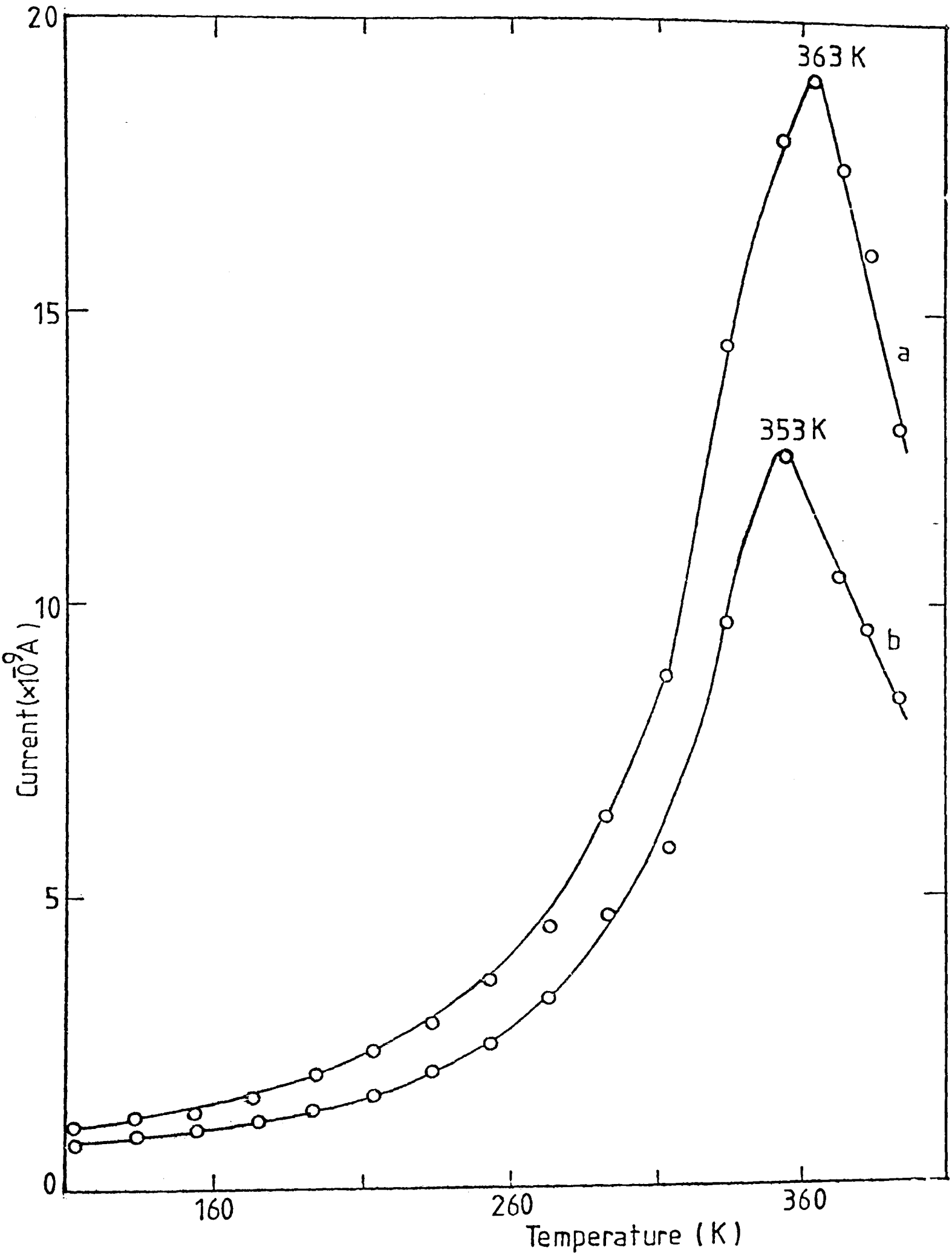

Figure 4.2 The current as a function of temperature on heating a Cu-PP(2400Å)-Cu sandwich structure at an applied field of 1.6×10^5 V cm^{-1}; curve a, heating rate, 0.217 K S^{-1}; curve b, heating rate 0.095 K S^{-1}. (after Iqbal and Hogarth[15]).

Figure 4.3 shows the dark current measured on the same sample and demonstrates the form of the TSC peak. From the results, the depth of the traps whose emptying gave rise to the current peak were calculated using an expression (1.53) given by Bube[89].

$$E_t = k T_m \ln \left(\frac{N_c e \mu}{\sigma_m} \right) \qquad (1.53)$$

Where E_t is the mean trap depth, N_c is the equivalent density of states at the bottom of the conduction band, σ_m is the peak value of electrical conductivity and μ is the carrier mobility. The values of E_t estimated for different fields and heating rates are given in Table 3.

TABLE 3

E_t for different applied fields and heating rates (after Iqbal and Hogarth[15])

Sample thickness (Å)	Applied field (V cm^{-1})	Heating rate (^{o}C S^{-1})	T_m (K)	E_t (eV)
1600	6.25 x 10^4	0.172	373	0.38
1600	1.87 x 10^5	0.172	360	0.33
1600	3.12 x 10^5	0.172	354	0.31
2400	1.61 x 10^5	0.095	353	0.32
2400	1.61 x 10^5	0.217	363	0.33

In the estimation of the trap depth the density N_c of states was taken as 1 x 10^{20} cm^{-3}. This assumption was made by Zor[43] for polyethylene and he has discussed the reason for

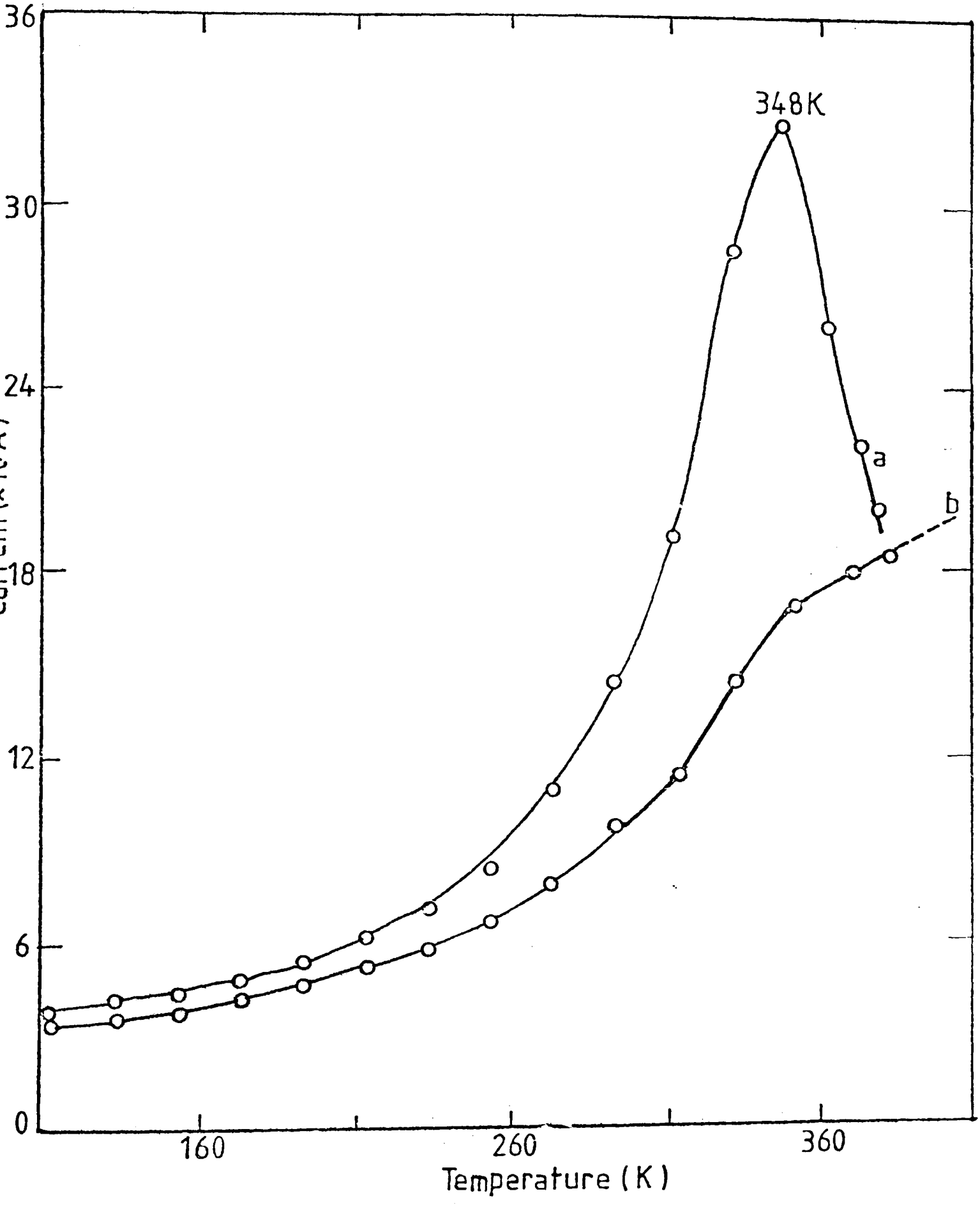

Figure 4.3 The current as a function of temperature on heating a Cu-PP(1860Å)-Cu sandwich structure; (a) after illumination at low temperature, (b) in the dark. (after Iqbal and Hogarth[15]).

assuming this value. The situation with polypropylene is expected to be broadly similar and the logarithmic function reduces the sensitivity of the value of E_t as a function of values of N_c. In order to calculate the area under the TSC curve which is taken as proportional[88] to the concentration of charge carriers released from traps, the samples were heated at two different rates but under the same applied field. The expression (1.48) given by Haine Carley-Read was used.

$$\exp\left(\frac{-E_t}{kT}\right) = \frac{n_{c_2} X - n_{c_1}}{N_c (1 - X)} \qquad (1.48)$$

We define X by the following equation.

$$X^2 = \frac{\dot{T}_1 \left(1 - {}^{n'}c_1 \, kT^2 / {}^{n}c_1 \, E_t\right)}{\dot{T}_2 \left(1 - {}^{n'}c_2 \, kT^2 / {}^{n}c_2 \, E_t\right)} \qquad (1.49)$$

$$N_t (\tau + \tau_t) = \frac{\left\{n_c + N_c \exp\left(- E_t/kT\right)\right\}^2}{\dot{T} N_c \left\{ E_t/kT^2 - {}^{n'c}/_{n_c} \right\} \exp(-E_t/kT)} \qquad (1.44)$$

In this equation n_c refers to the density of electrons in the conduction band and is given by

$$n_c = \frac{Id}{\mu eVA} \qquad (1.46)$$

The symbols are defined as follows: E_t is the trap depth, τ_t is the electron trapping time, τ is the recombination lifetime, N_t is the density of trapping centres for the particular trapping level, $\dot{T}_1$ and $\dot{T}_2$ are two different heating rates, T is the absolute temperature, k is the Boltzmann constant, n_c refers to the carrier density at heating

rate $\dot{T}_1$ and similarly for n_{c_2}, $\dot{n}_{c_1}$ is defined as dn_{c_1}/dT and similarly for $\dot{n}_{c_2}$. A is the cross-section area and d is the thickness of specimen. Equation (1.48) was solved by using an approximation.

$$-\frac{E_t}{kT} = \ln\left(\frac{n_{c_2} - n_{c_1}/X}{1/X - 1}\right) - \ln N_c$$

For the case of $X \rightarrow o$ we than have

$$-\frac{E_t}{kT} = \ln n_{c_1} - \ln N_c \qquad (4.1)$$

and for the case of $X \rightarrow \infty$ we have

$$-\frac{E_t}{kT} = \ln n_{c_2} - \ln N_c \qquad (4.2)$$

Equations (4.1) and (4.2) demonstrate the strong dependence of E_t on n_{c_1} and n_{c_2}. Substituting these values of n_{c_1} and n_{c_2} in equations (4.1) and (4.2) we obtain values of 0.32 eV and 0.31 eV, which are similar to the values obtained directly from equation (1.53). With the present data it was not possible to estimate N_t but only the quantity $N_t\ (\tau + \tau_t)$.

For $E_t = 0.31$ eV, $N_t\ (\tau + \tau_t) = 3.6 \times 10^{18}$ S cm^{-3}.

$E_t = 0.32$ eV, $N_t\ (\tau + \tau_t) = 3.3 \times 10^{18}$ S cm^{-3}.

5. CHAPTER FIVE

ANNEALING EXPERIMENTS

In the last chapters we have examined the properties of evaporated polypropylene for possible use as thin dielectric films and were able to produce standard and reproducible results of electrical measurements[5]. In this section we look at the effect of vacuum heat treatment on the structure and on the relevant electrical properties of these films

5.1 Introduction

There is always the possibility of producing structural defects during the deposition of the films, unless a great deal of special care is taken, some of these defects may be annealed out of the film by heat treatment. As a general rule the resistivity of evaporated films particularly metallic films decreases with annealing but for some materials, heat treatment may lead to an increase in film resistivity. This increase may be due to the effects of oxidation and/or agglomeration[137]. In some cases the resistance changes are caused by a recombination of the interstitial atoms and lattice vacancies as a result of the heat treatment[138]. Agglomeration is associated with the reverting of a continuous structure of a very thin film to an island structure when subjected to a vacuum heat treatment. This process is detected by the large increase in the resistance of the film. Kane et al[139] have reported three-stage agglomeration due to vacuum annealing for a gold film deposited on a zinc sulphide substrate. Initially small holes are formed in the film, then they are enlarged and

finally the continuous film separates into islands. Any change in the resistance of the film occurs during the second and the third stages. They also mentioned the migration of gold atoms, which is necessary for agglomeration, as it is a thermally-activated process. Skofronick and Phillips[140] studied the additional agglomeration in the films which were discontinuous when first deposited. Initially on annealing a slight decrease in the resistance of the film was observed but then it increased irreversibly by several orders of magnitude. They explained their results by suggesting that the heat treatment caused islands, which then coalesced with the large ones and the mean spacing between them increased. This explains the high value of the resistance. Thin films when heated in air can also undergo an increase in resistance because of oxidation[141].

5.2 Experimental techniques

Polypropylene was evaporated in a vacuum of about 10^{-5} torr from a stainless steel boat onto electron microscope specimen support grids (see Figure 5.1). Other specimens prepared at the same time were deposited on slides with copper electrodes as described previously[5]. Annealing treatments were carried out in a subsidiary vacuum system. The electrical measurements were of the kind described in sec.3.1. Structural measurements were made using a JEM7 electron microscope both for microscopy and for electron diffraction.

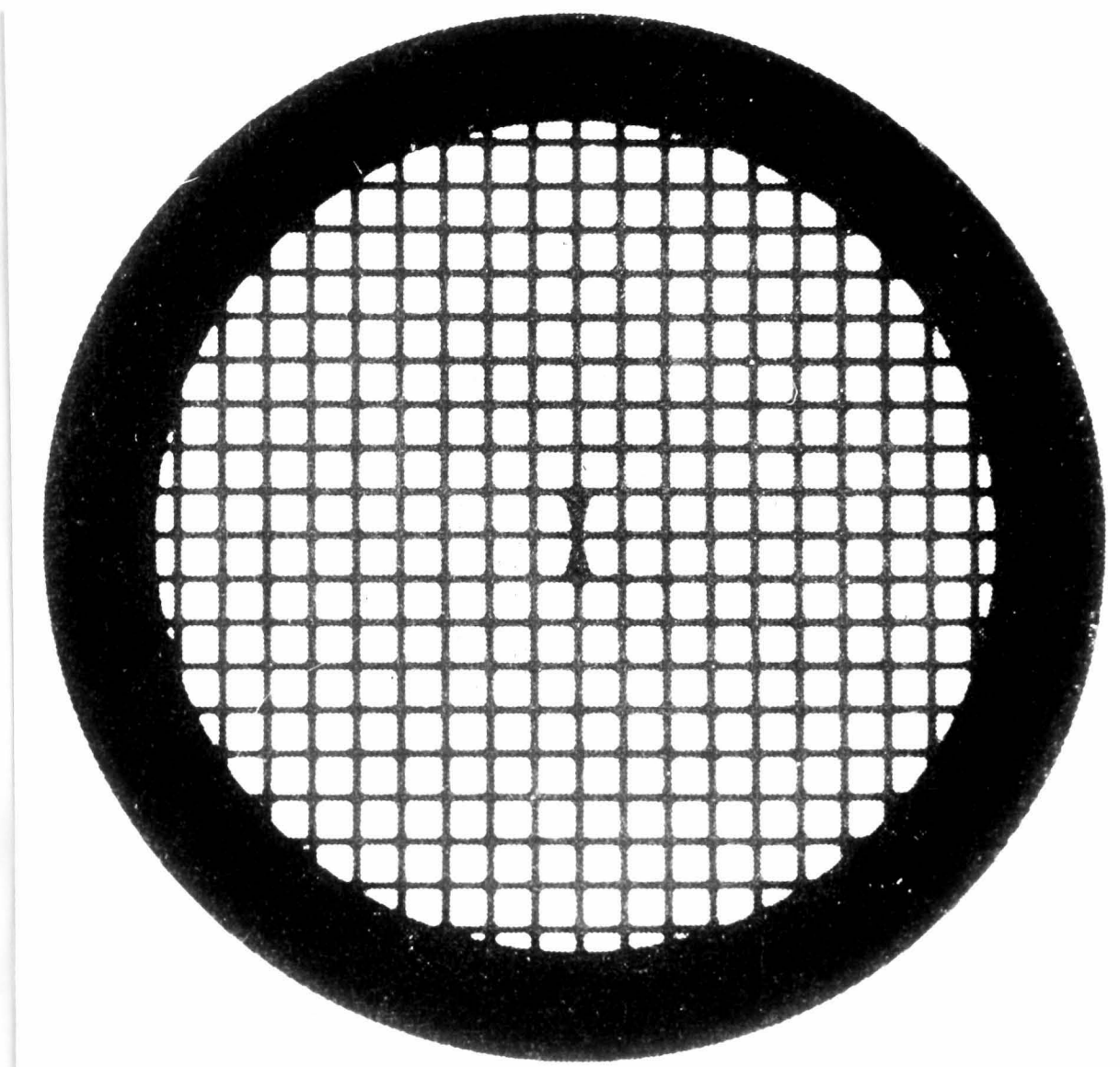

Figure 5.1 Electron microscope grid.

5.3 Results and discussion

5.3.1 Electrical

The current-voltage characteristic of a freshly-deposited Cu-PP(900Å)-Cu sample at a pressure of less than 10^{-5} torr and at room temperature is shown in curve B of Figure 5.2. After a vacuum heat treatment at 110°C for about 30 minutes and allowing the specimen to cool to room temperature, the characteristic was again measured as shown in curve A. The sample resistivity was found to increase from 3.4×10^{12} ohm-cm. to 1.2×10^{13} ohm cm. Such changes are typical of all the specimens examined. Figure 5.3 also shows the current-voltage characteristics of a Cu-PP(2029Å)-Cu sample before (curve B) and after (curve A) the heat treatment. The resistivity of the sample also increased due to the heat treatment. As mentioned above such an increase in the film resistivity is believed to be due to agglomeration.

5.3.2 Microscopy

The resistance measurements can be correlated with electron micrographs to establish the correspondence between agglomeration and resistance increase. A series of evaporated layers of polypropylene from 150Å to 1600Å thick were examined in the electron microscope before and after a vacuum heat treatment. By considering the micrographs in Figures 5.4(a) and (b) there are two main effects of the heat treatment, an increase of particle size and an increase in the distance between particles. These effects occur as a result of particle migration and agglomeration.

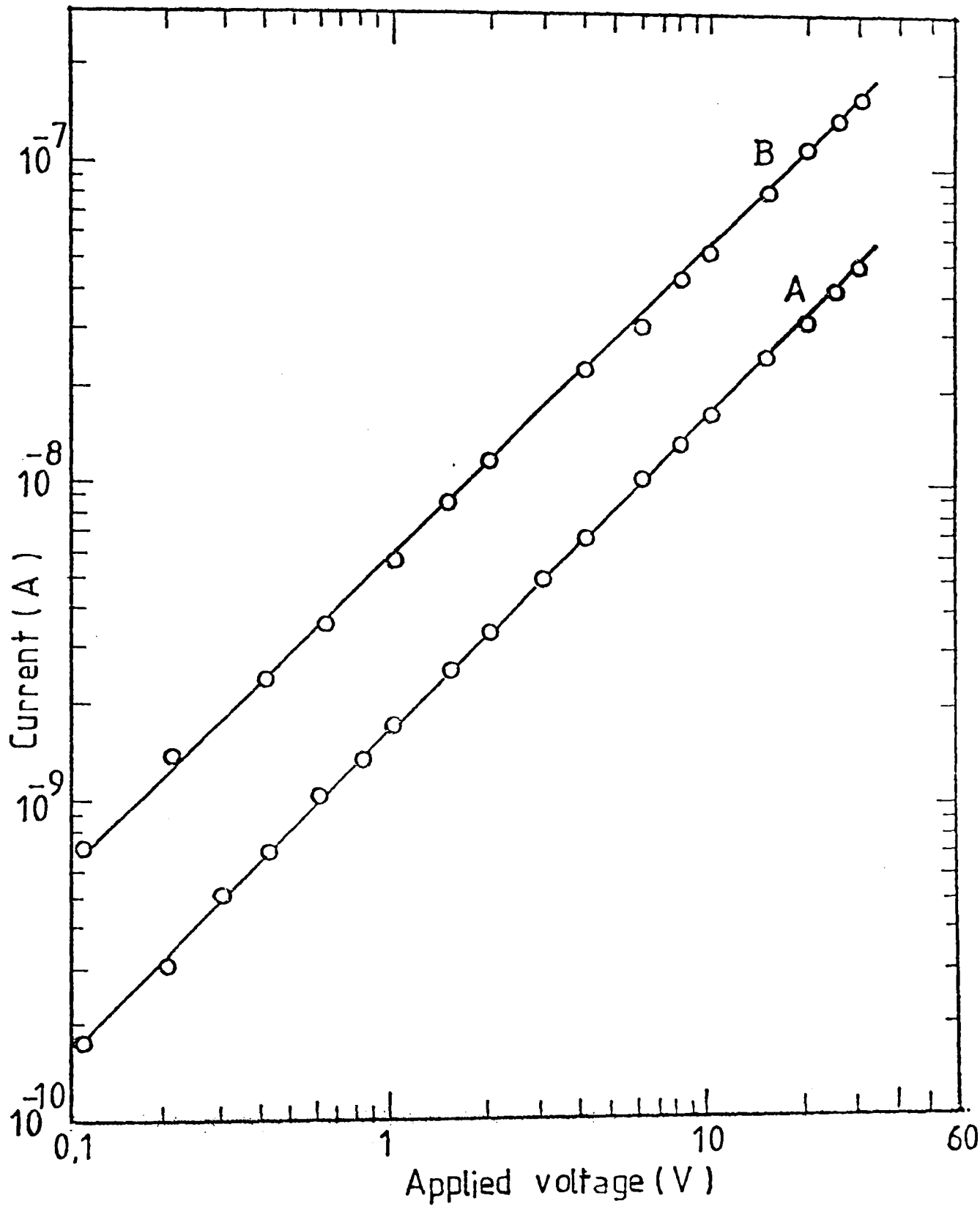

Figure 5.2 Voltage-current characteristic of a freshly-deposited Cu-PP(900Å)-Cu sample; curve A, after heat treatment curve B, before heat treatment. (Room temperature, ambient pressure 10^{-5} torr.)

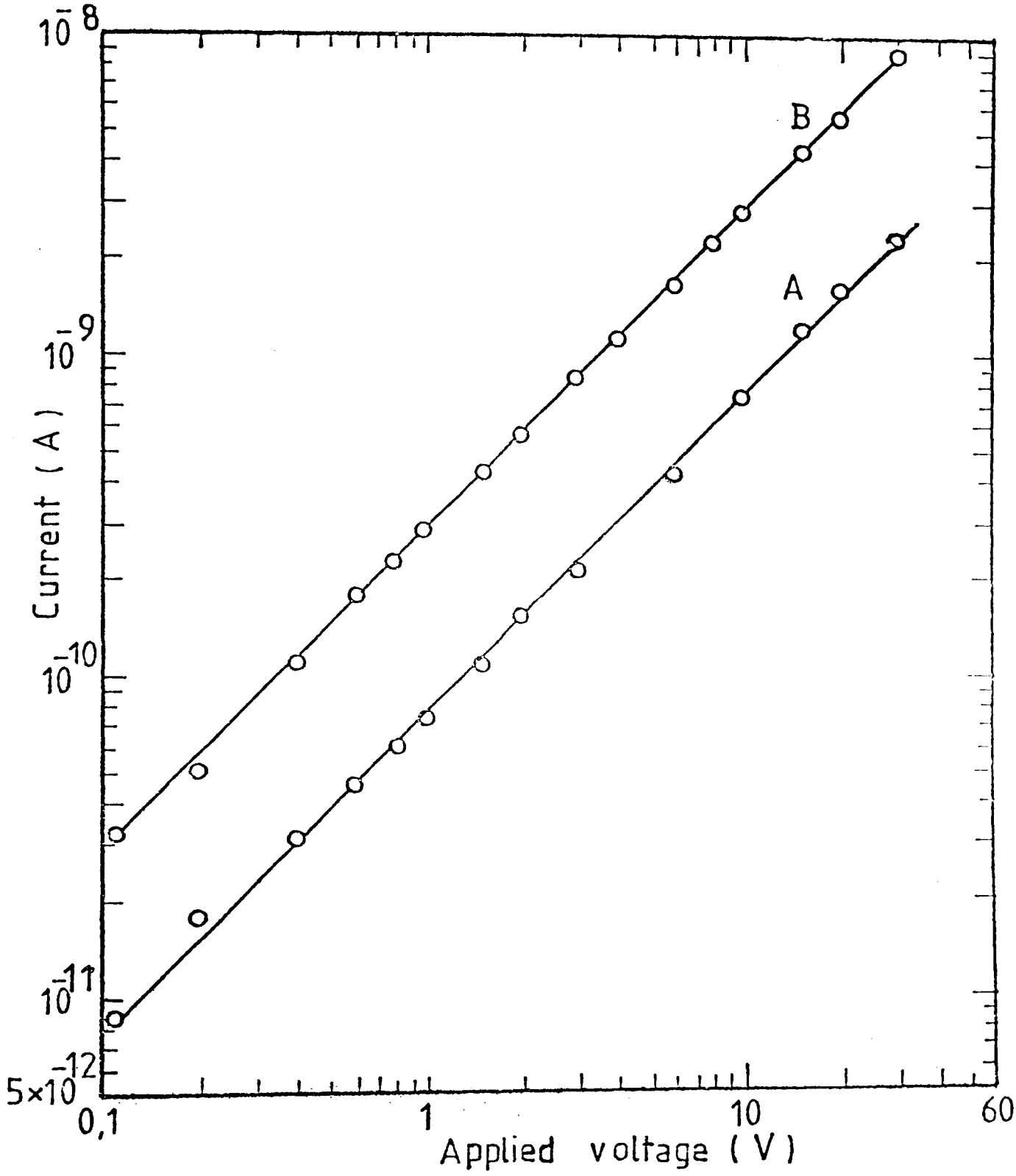

Figure 5.3 Voltage-current characteristic of a freshly-deposited Cu-PP(2029Å)-Cu sample curve A, after heat treatment, curve B, before heat treatment. (Room temperature, ambient pressure 10^{-5} torr).

If electrical conduction occurs by electron hopping between particles then an increased spacing would lead to a reduced electrical conductivity[140]. The original chain structure of the polymer is also broken during the heat treatment and the atomic clusters are re-arranged. Similar changes were found in layers having thicknesses of 600Å, 1000Å and 1600Å. Many links between small aggregated particles form during the deposition of the film as may be seen in Figures 5.5(a), 5.6(a) and 5.7(a). These may provide diffusion paths for the copper introduced from the electrodes under the influence of the applied field as suggested by Hogarth and Iqbal[5]. After heat treatments the micrographs 5.5(b), 5.6(b) and 5.7(b) show that the links are reduced in number so that a further reason for the increase in resistivity is given. Table 4 lists the main features of the micrographic examination of these polypropylene films.

5.3.3 Structures

Apart from the change in resistivity, heat treatment may also bring some micro-structural changes in thin films. Koshy[142] has studied the effect of heat treatment on the structure of thin rhodium films in vacuum and in air at different temperatures. The transmission electron diffraction patterns of evaporated polypropylene shown in Figures 5.8, 5.9, 5.10 and 5.11 indicate that the samples are essentially amorphous although the diffuse patterns could be in part due to the presence of micro-crystallites. Although the full structural investigation would require very elaborate

TABLE 4

PP Thickness Å	Magnification or Electron Diffraction Photographs	Figure No.	Condition
150	10,000	5.4(a)	B
150	10,000	5.4(b)	A
600	2,200	5.5(a)	B
600	2,200	5.5(b)	A
1000	2,200	5.6(a)	B
1000	2,200	5.6(b)	A
1600	2,200	5.7(a)	B
1600	2,200	5.7(b)	A
150	E.D.P.	5.8(b)	B
150	E.D.P.	5.8(b)	A
600	E.D.P.	5.9(a)	B
600	E.D.P.	5.9(b)	A
1000	E.D.P.	5.10(a)	B
1000	E.D.P.	5.10(b)	A
1600	E.D.P.	5.11(a)	B
1600	E.D.P.	5.11(b)	A

B - before heating

A - after heating

instrumentation in order to determine the radial distribution, nevertheless some estimate of changes in the crystalline character of the layers can be made by a microphotometer examination of the diffraction patterns before and after the heat treatment. A narrowing of line-width indicates an increase in the crystallite size and all the diffraction patterns show this feature as a result of the heat treatment. Figures 5.12(a), 5.13(a) and 5.14(a) show the microphotometer traces of non-annealed films and Figures 5.12(b), 5.13(b) and 5.14(b) indicate the microphotometer traces for the same rings after the samples had been annealed. Table 5 gives the main features of the microphotometer traces. These results are entirely consistent with the results of the micrographic examination and of the electrical measurement.

TABLE 5

Thickness Å	Line width cm.	Figure no.	Condition	Remarks
150	5.0	5.12(a)	B	--
150	3.9	5.12(b)	A	More crystalline
1000	5.6	5.13(a)	B	--
1000	4.4	5.13(b)	A	More crystalline
1600	4.3	5.14(a)	B	--
1600	2.5	5.14(b)	A	More crystalline

B - before heat treatment

A - after heat treatment

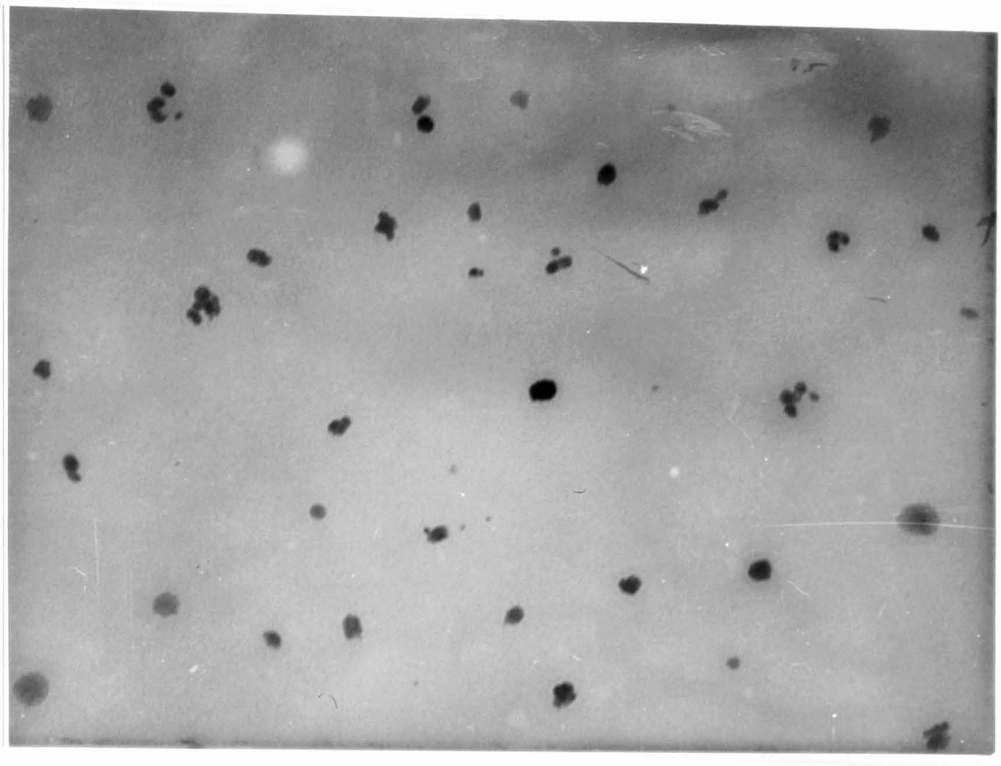

(a)

Figure 5.4 Electron micrographs of an evaporated layer of polypropylene (150Å) (a) before heating (b) after heating.

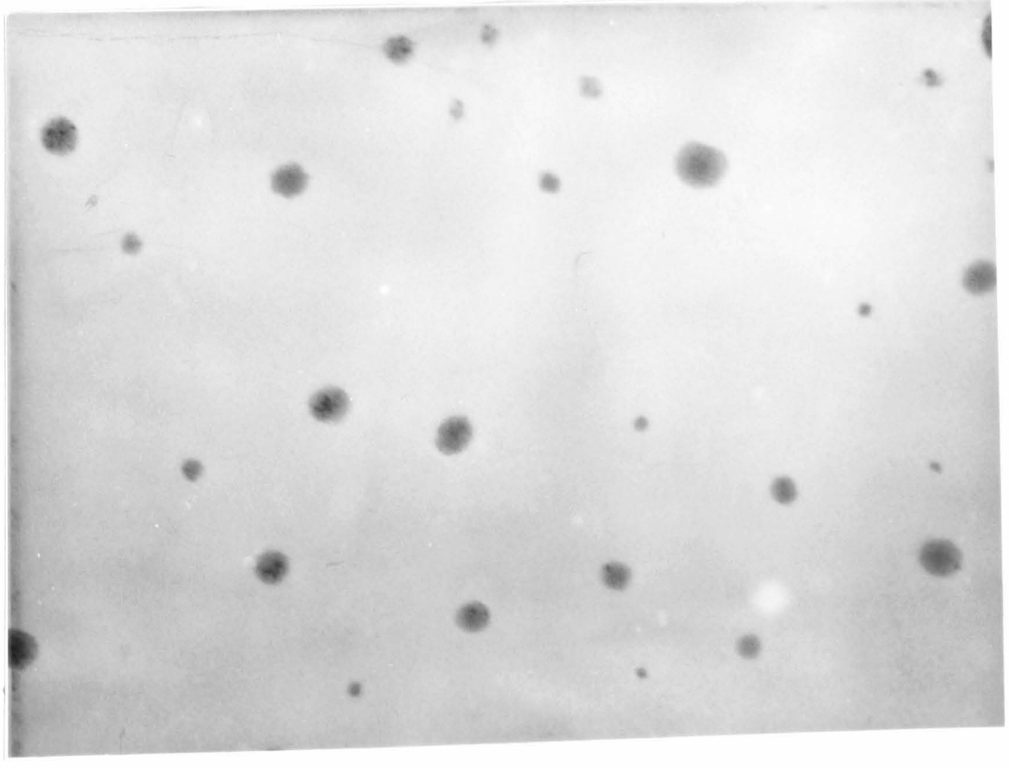

(b)

(a)

Figure 5.5 Electron micrographs of an evaporated layer of polypropylene (600Å) (a) before heating (b) after heating.

(b)

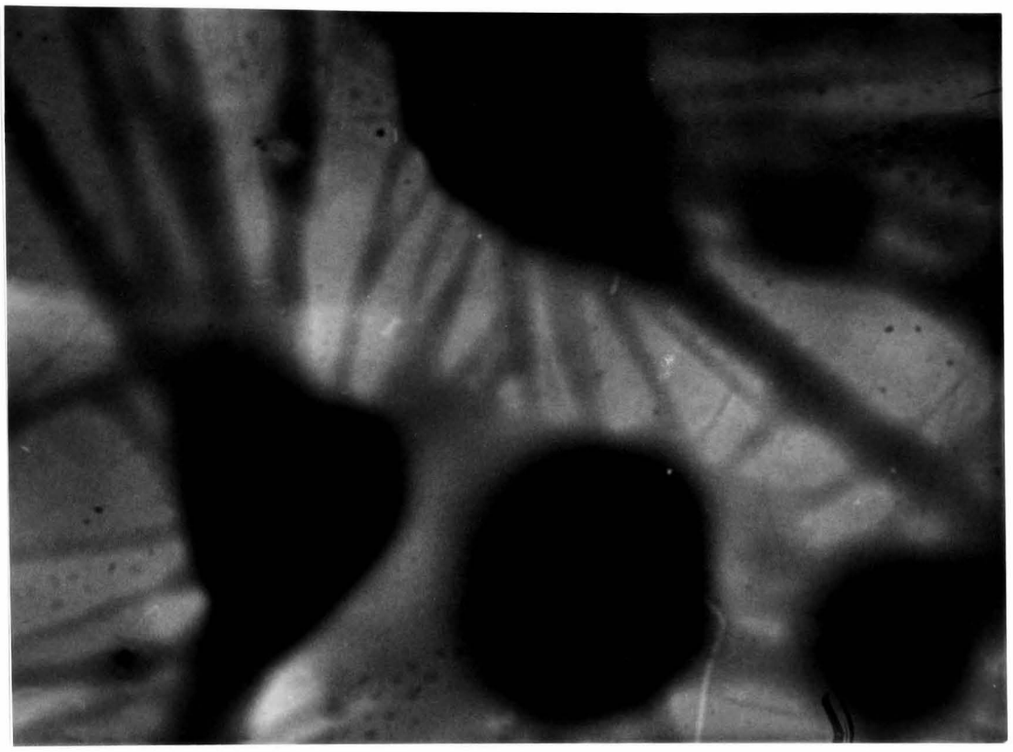

(a)

Figure 5.6 Electron micrographs of an evaporated layer of polypropylene (1000Å) (a) before heating (b) after heating.

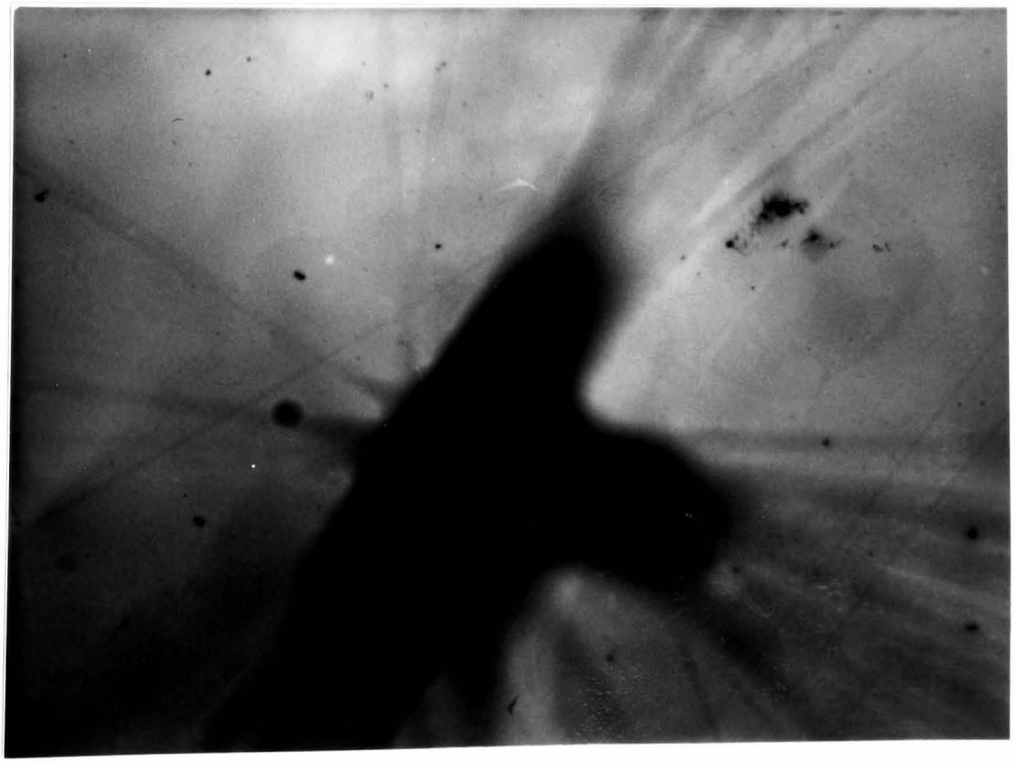

(b)

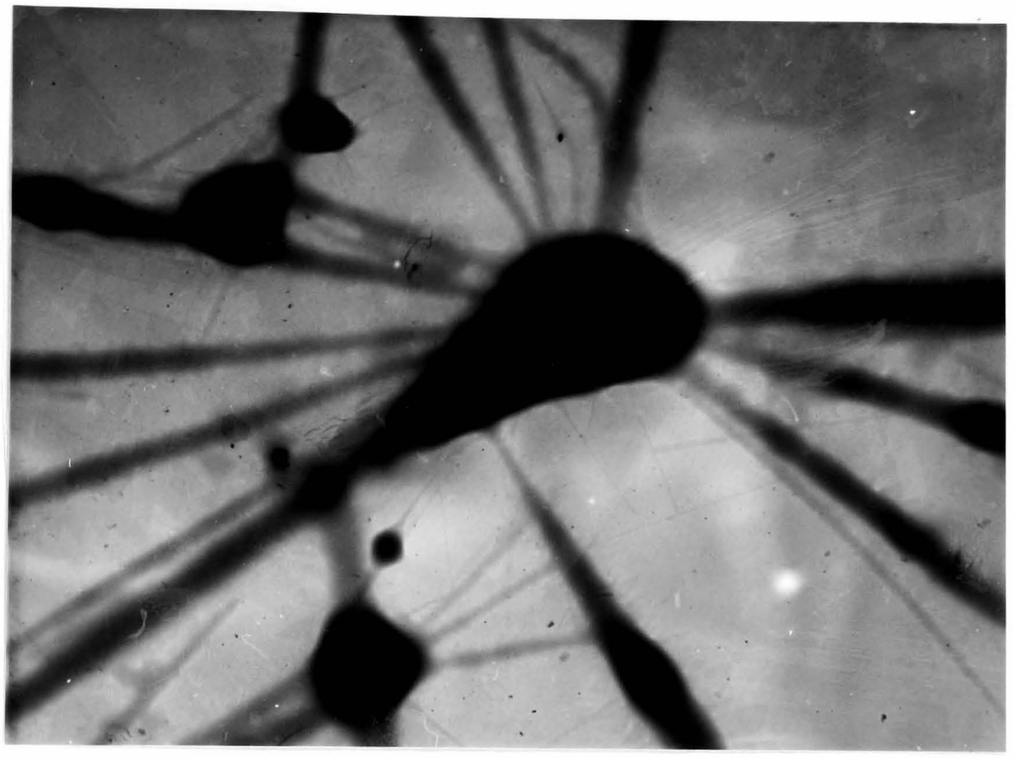

(a)

Figure 5.7 Electron micrographs of an evaporated layer of polypropylene (1600Å) (a) before heating (b) after heating.

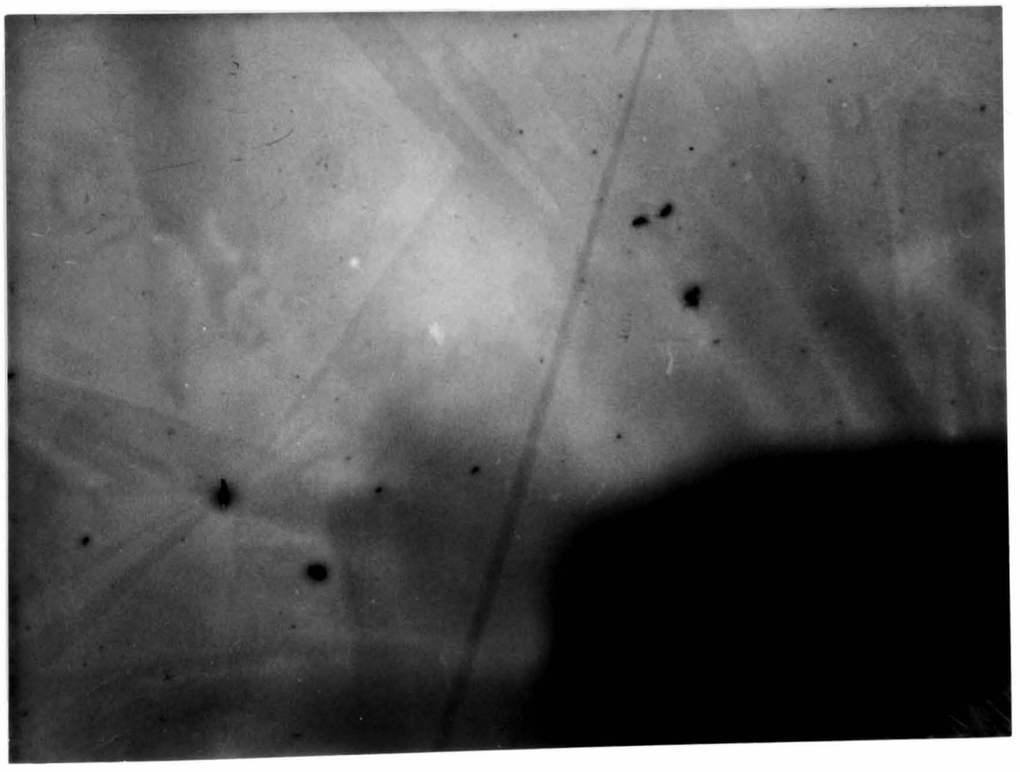

(b)

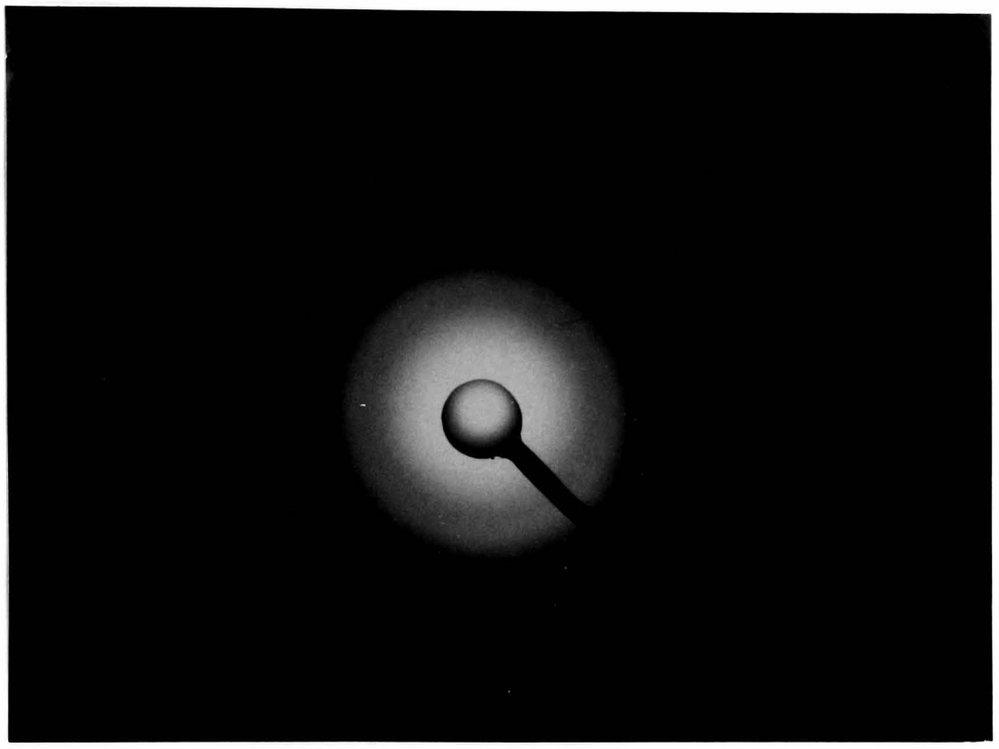

(a)

Figure 5.8 Electron diffraction patterns of an evaporated layer of polypropylene (150Å) (a) before heating (b) after heating.

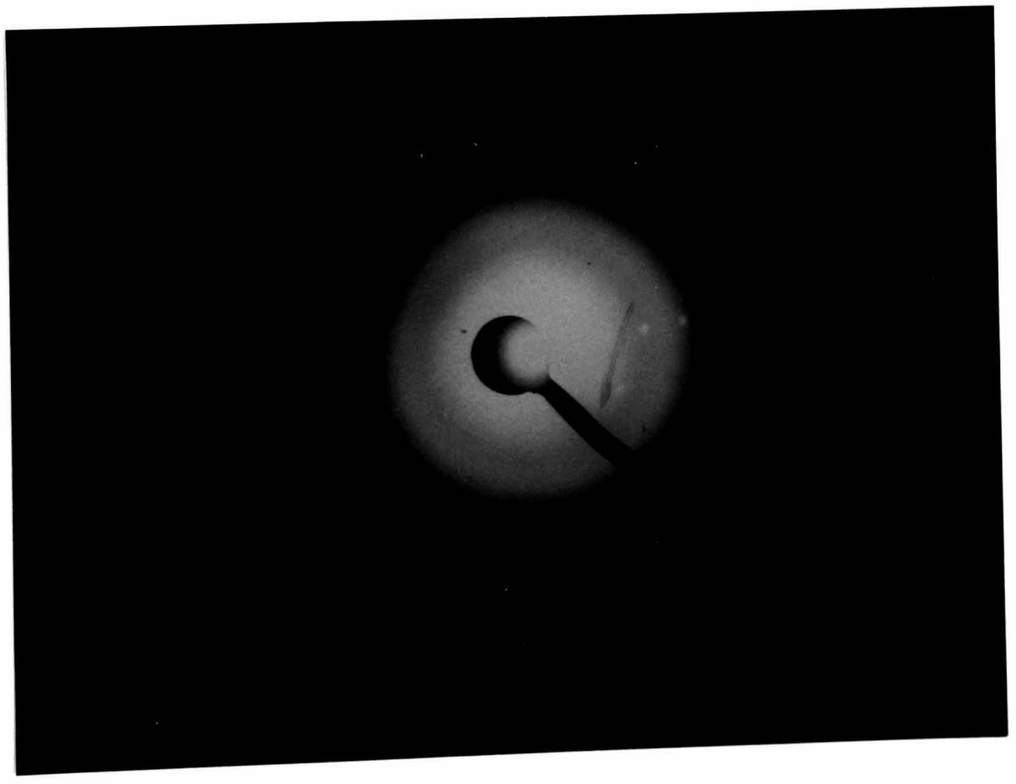

(b)

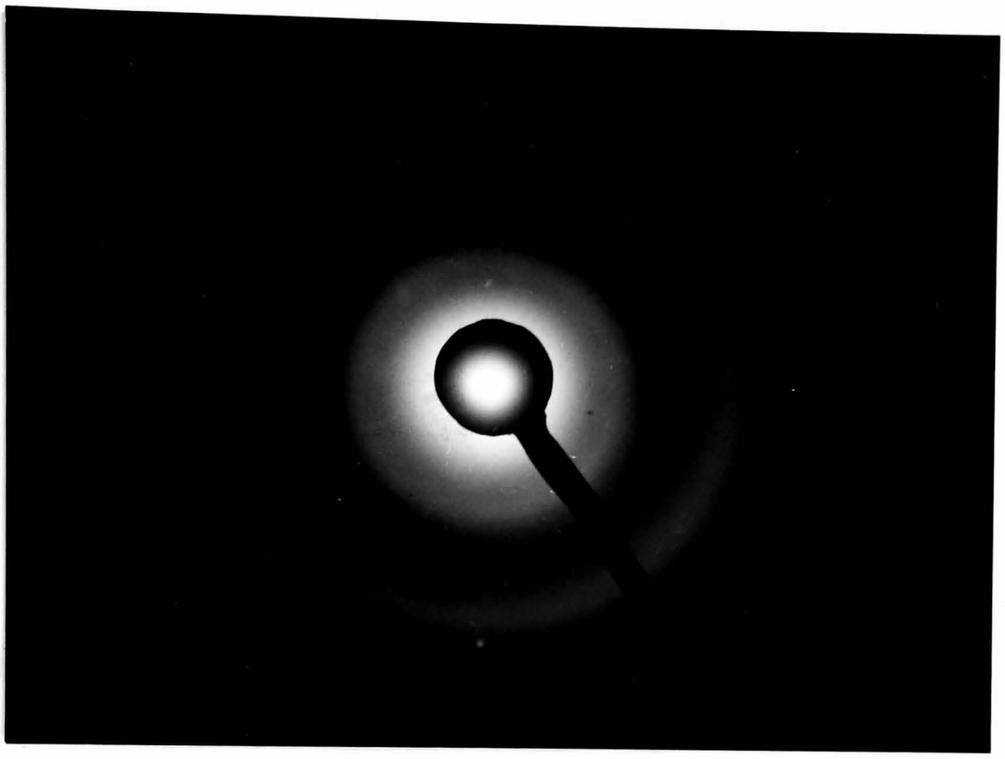

(a)

Figure 5.9 Electron diffraction patterns of an evaporated layer of polypropylene (600Å) (a) before heating (b) after heating.

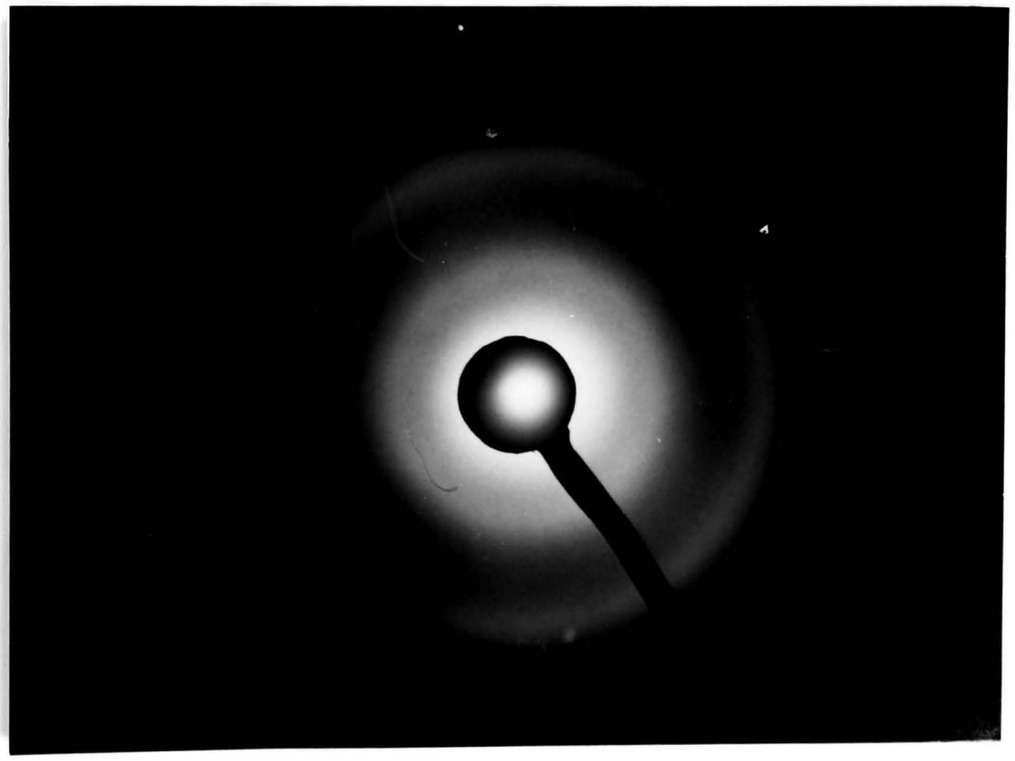

(b)

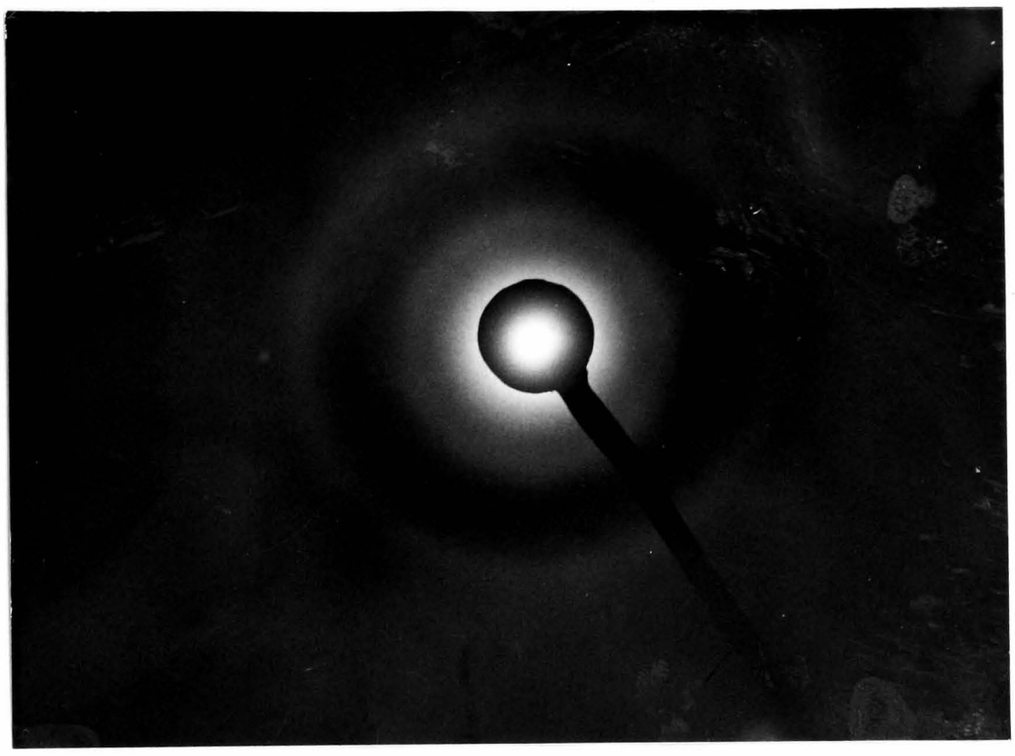

(a)

Figure 5.10 Electron diffraction patterns of an evaporated layer of polypropylene (1000Å) (a) before heating (b) after heating.

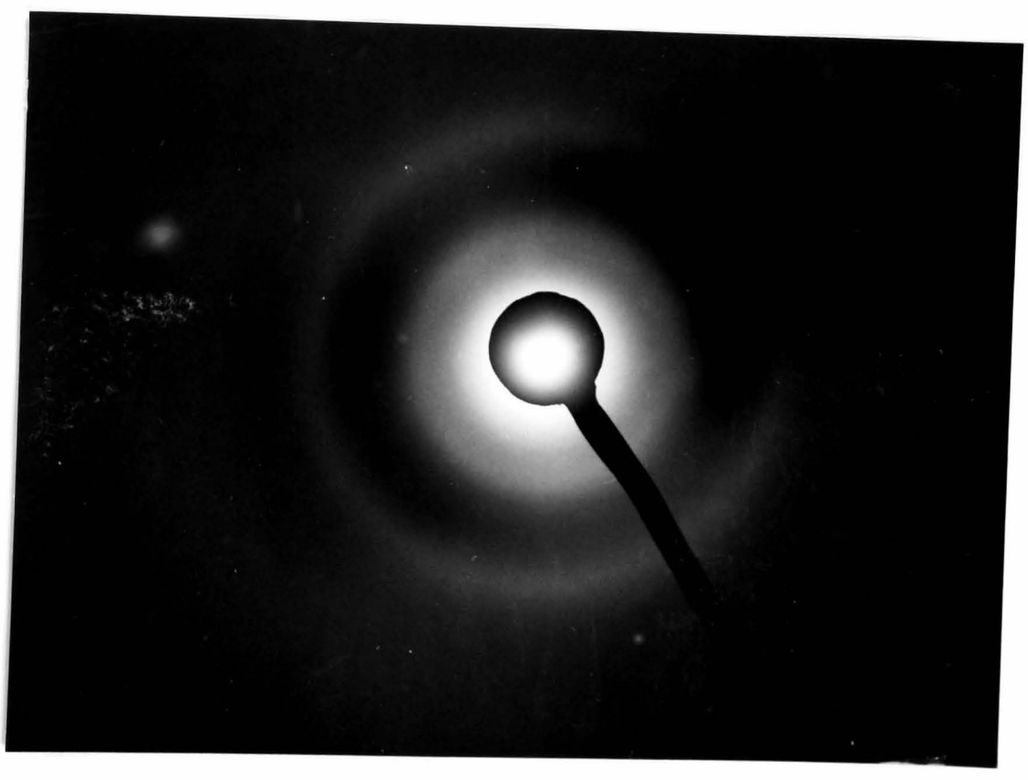

(b)

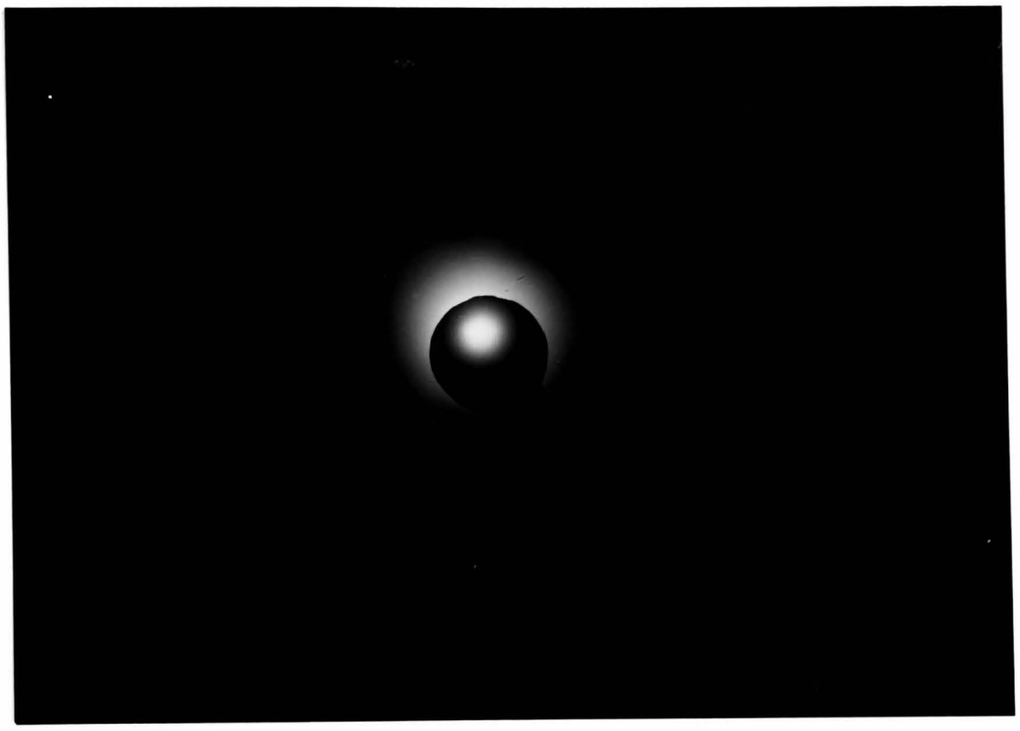

(a)

Figure 5.11 Electron diffraction patterns of an evaporated layer of polypropylene (1600Å) (a) before heating (b) after heating.

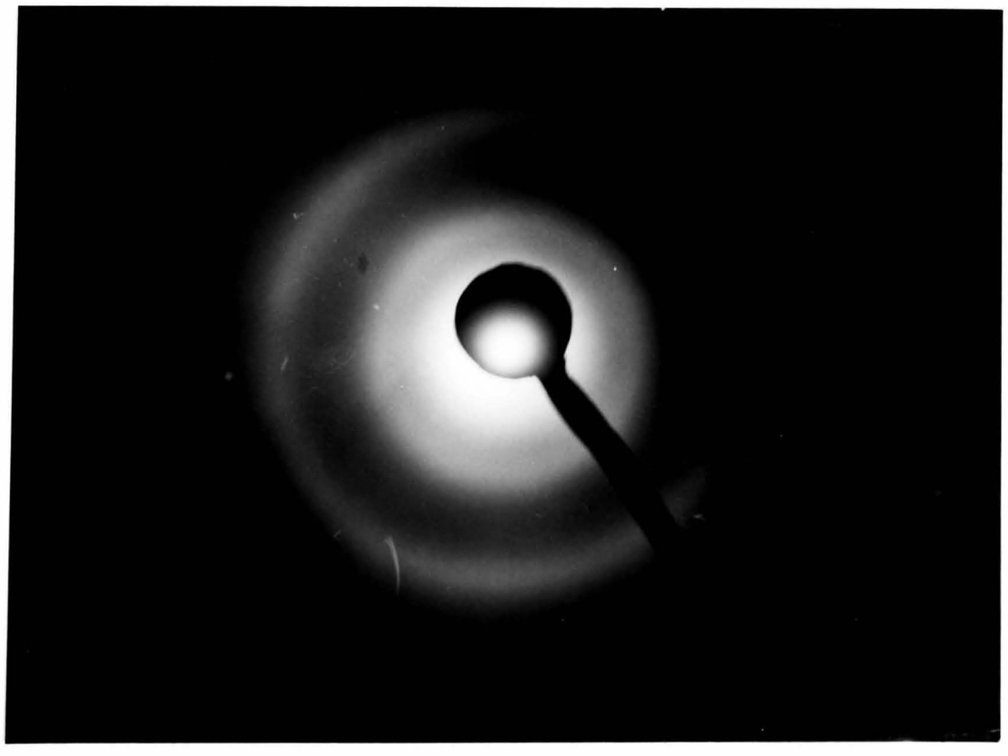

(b)

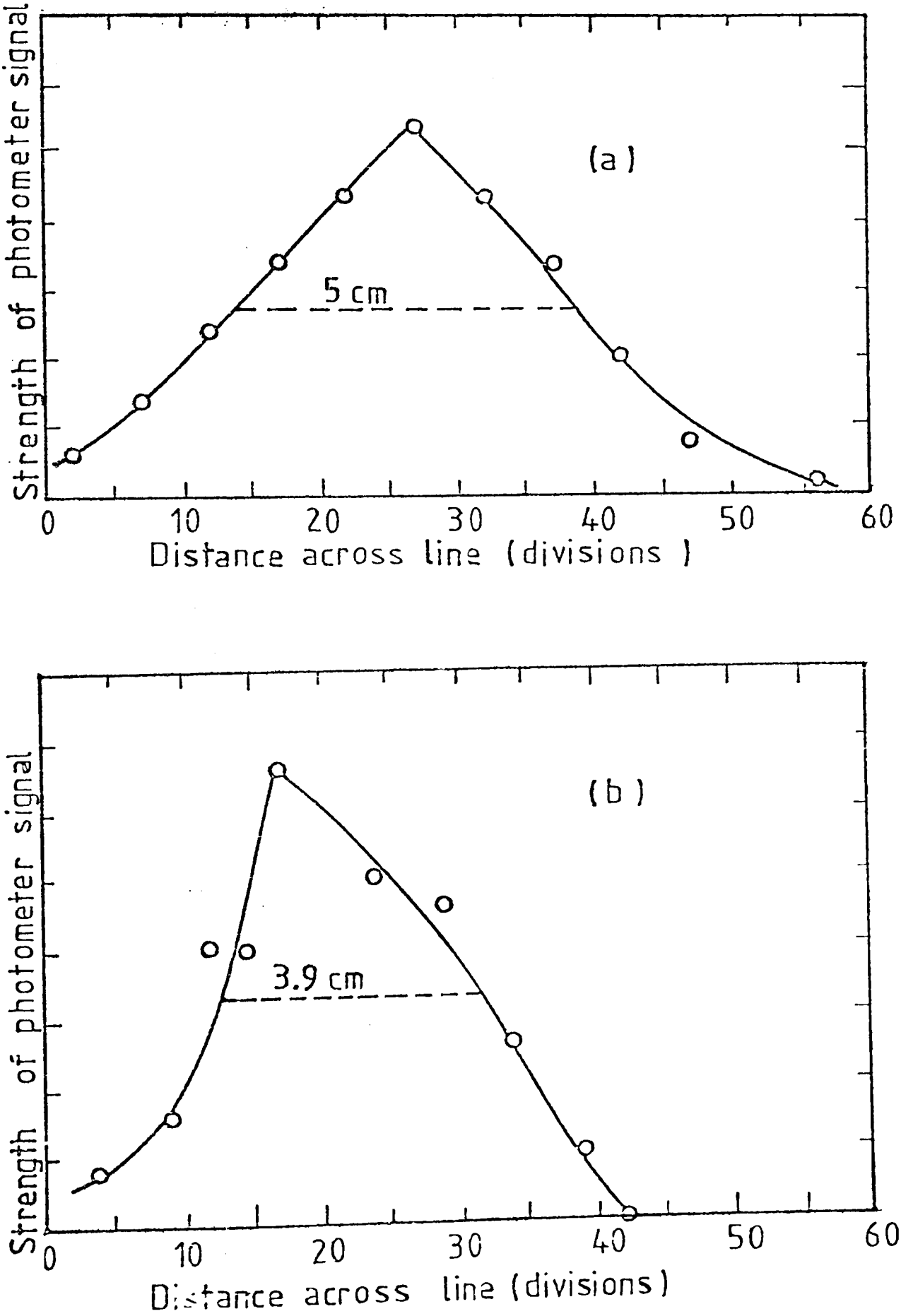

Figure 5.12 Microphotometer curves of a diffraction line width (a) before annealing (b) after annealing (PP = 150 Å)

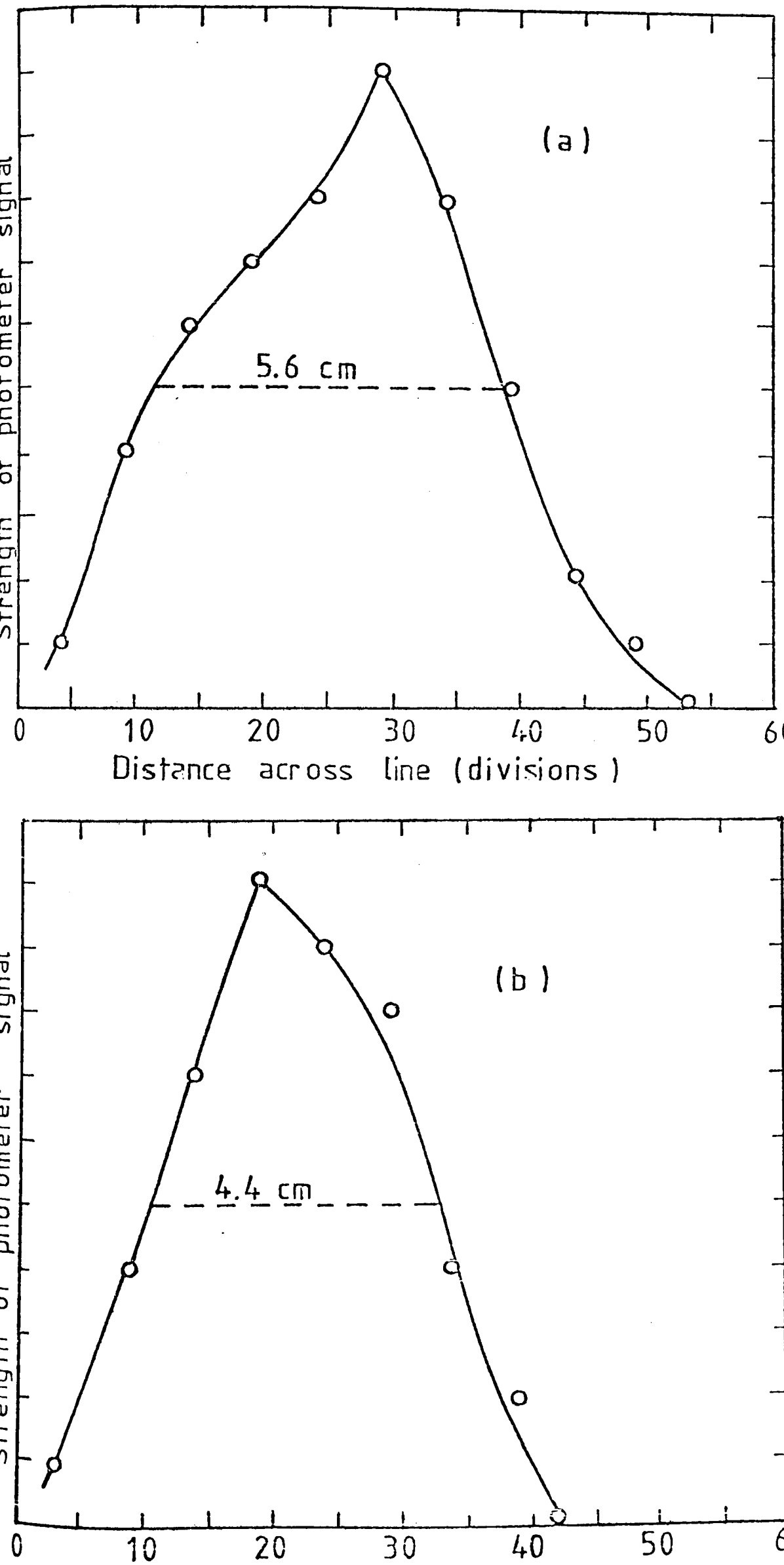

Figure 5.13 Micro-photometer curves of a diffraction line width (a) before annealing

(b) after annealing (PP = 1000Å)

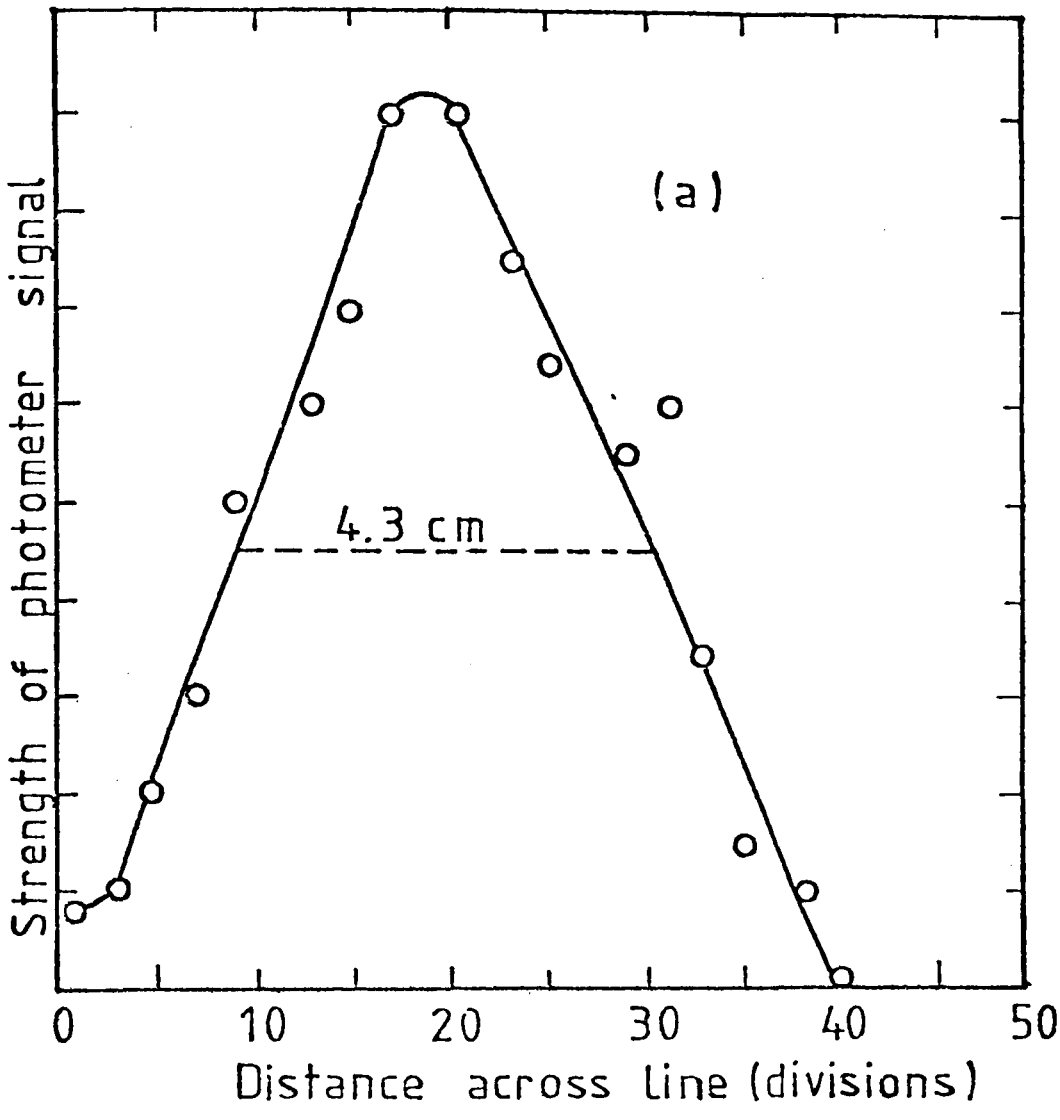

Figure 5.14 Micro-photometer curves of a diffraction line width

(a) before annealing

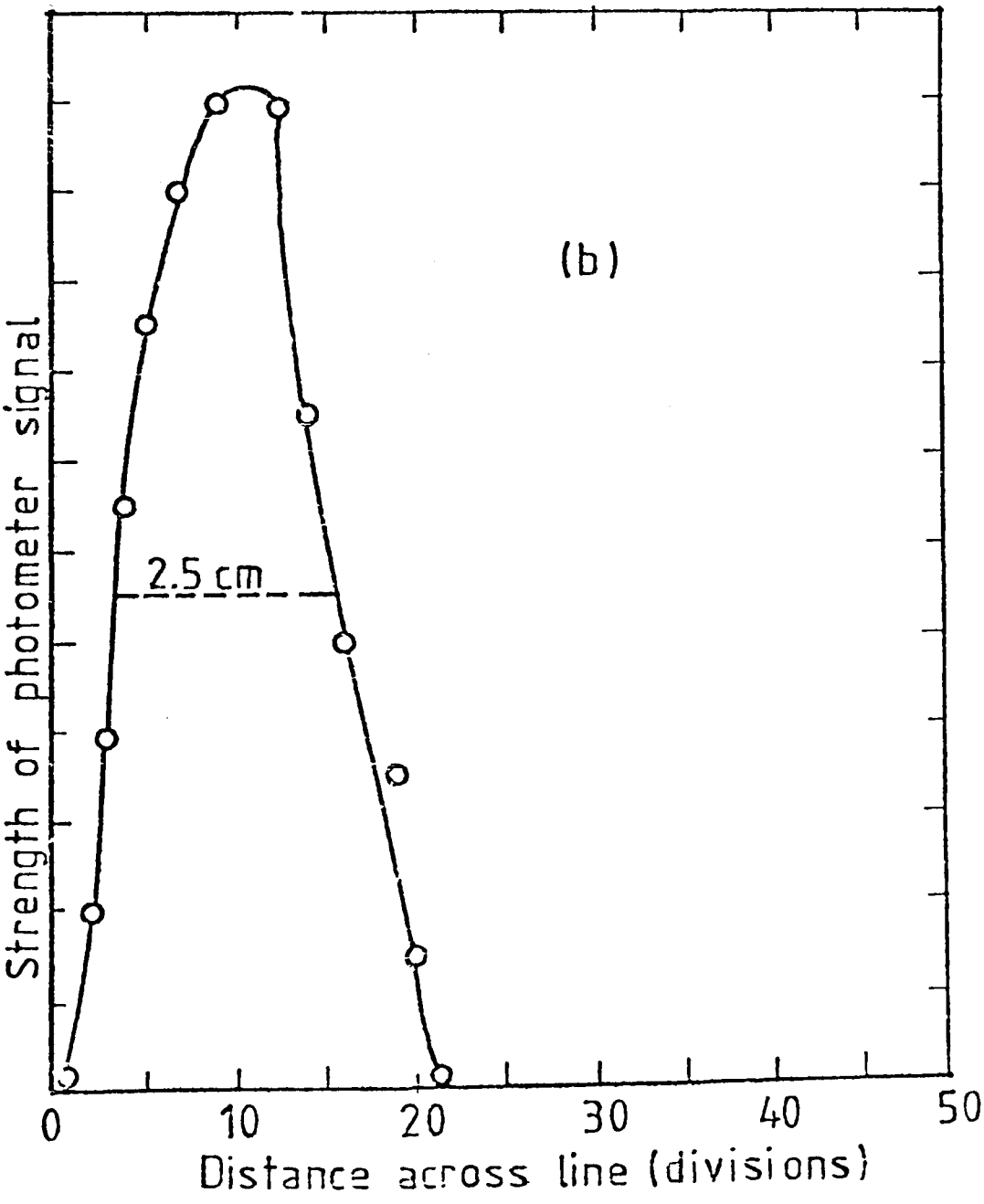

(b) after annealing

(PP =1600Å)

6. CHAPTER SIX

DISCUSSION AND CONCLUSIONS

Thin dielectric layers have become very important during the last few years. They may be used for insulating layers in capacitors, thin film transistors and also as protective coatings. For such applications the electrical properties of films must be examined thoroughly and a lot of research is in progress on different materials in many universities and research organisations. Due to low production costs and their excellent electrical and mechanical properties, the polymers have many industrial applications. There are several methods of forming a metal-insulator interface. The methods include chemical decomposition, thermal evaporation, electron-gun bombardment, sputtering of metal onto chemically etched, mechanically polished, vacuum-cleaved or ion bombarded insulator surfaces. The ability of an insulator to resist the passage of direct current is not necessarily the same as its ability to resist alternating currents. In the former case the resistivity of the material plays an important role, while, in the latter, the power factor and permittivity are more relevant for determining the power loss occurring in alternating fields. The power factor is a measure of that fraction of the electrical energy applied to the material which is dissipated as heat and is irrecoverable. The permittivity is an important characteristic of particular dielectric materials at particular frequencies. Most common polymer materials can be divided into two groups: (i) polymers

having high resistivity, low permittivity and negligible power factor and usually known as non-polar polymers and (ii) polymers with low resistivity and higher permittivity and power factor. They are generally referred to as polar polymers. Polypropylene belongs to the former group. It has a high value of electrical bulk resistivity of order 10^{17} Ω -cm and a low value of permittivity of 2.13. Polypropylene was recognised by Reddish[143] as being a superior insulator to low density polyethylene, probably due to the method of polymerization which enabled it to be purified more effectively. The power factor of polypropylene is very low, so the power losses in large capacitors with polypropylene as dielectric are much smaller than in many other dielectrics. The breakdown fields of polypropylene are very high, (up to 700V/μm).

From a study of previously published work it is clear that some vacuum-evaporated polymers have characteristics similar to those of the original bulk material. As an example of this proposition we may consider the work of White[26] who obtained thin films of polyethylene by vacuum evaporation onto glass microscope slides. For the electrical measurements Al-PE-Al sandwiches were prepared and Schottky emission was found to be the dominant conduction mechanism. Capacitance measurement led to the value of permittivity equal to 2.02, while for bulk polyethylene it is equal to 2.25. So, we can say that the deposited material on the surface of the glass slide is very similar to the material in the evaporation boat. This result confirms the idea that the vacuum evaporation of

polymers results in the breaking of certain chemical bonds within their molecules, thus leading to the formation of active fragments, and these fragments when they reach the substrate, react with one another to form a polymer coating on the surface[13]. The electrical conductivity (and its reciprocal resistivity) is a volume property of a polymer and is directly related to the structure and to the nature of the conduction process[144,145]. Scott[146] pointed out that changes in the composition or in the conduction process are usually reflected by changes in the resistivity before other properties exhibit significant changes. The exact relationship between the observed resistivity parameters and the structural parameters of the polymer, which determine the magnitude of the resistivity parameters are not fully known. Once these relations are understood, these measurements will become more significant.

We have examined the current-voltage characteristics of polypropylene films, sandwiched between different metal electrodes and formed by vacuum evaporation. The film thicknesses were between 750Å and 2400Å. It was not possible to explain the conduction by the standard mechanisms, e.g. tunnelling, Schottky emission, Poole-Frenkel effect or the space-charge conduction, due to the ohmic behaviour of the films with all the electrodes. There seems to be no considerable effect of the applied electric field because of the high resistivity of the film, which was of the order of 10^{14} Ω-cm. An ohmic contact does not sufficiently change the equilibrium carrier densities within the insulator to affect the sample characteristics and it has a linear and symmetrical

current-voltage characteristic. Also, it has no obvious potential barrier at the metal-insulator interface. In the case of semiconductors there is most likely to be an ohmic contact, when the metallic electrode is deposited on a semiconductor which is heavily doped. Correspondingly, in polymers the large quantity of impurities increases the chance of finding an ohmic contact at the metal-insulator interface. In the current-voltage characteristics of polypropylene films, there was evidence of electron trapping [5] and the trap depth was estimated by using the thermally-stimulated current technique and was found equal to 0.33 eV[15]. Thin films of evaporated polypropylene also showed electro-forming and electron emission under suitable conditions[60]. The results were found consistent with a theory based on the generation of conducting filaments during the high field forming process. The increase in the a.c. conductivity of the sample after electroforming also indicated the presence of filaments in the formed device. Also, the a.c. conductivity measurements could be used to identify the hopping conduction at low and room temperatures.

Pollack and Geballe[19] have given an equation for the process which is $\sigma(\omega) = A\omega^{s}$, where A is a complex constant, ω is the angular frequency, $\sigma(\omega)$ is the conductance and $0.5 < S < 1$. For hopping conduction S, is found to be 0.8 In the case of polypropylene films S was equal to 0.85, both at room and low temperatures, which is consistent with the process of hopping conduction. A linear decrease in the capacitance of the device with increasing frequency was observed before electroforming. This could be due to the

increasing leakage current with frequency and is associated with capacitance reduction.

Annealing of polypropylene films produced some very interesting results. Experiments were carried out with polypropylene layers formed by vacuum evaporation and having thicknesses between 900Å and 2600Å. A vacuum heat treatment of the sample at 110°C for about 30 minutes and followed by its gradual cooling to room temperature increased its resistivity as compared with its value before annealing. In case of a sample of typical thickness of 900Å, the resistivity was found to increase from $3.4 \times 10^{12}\Omega$-cm to $1.2 \times 10^{13}\Omega$-cm. This behaviour was found to be common for all samples examined. The increase in resistivity is associated with agglomeration, which is the reverting of a continuous structure of a thin film to an island structure when subjected to the vacuum heat treatment. By examining a series of layers from 150Å to 1600Å thick in the electron microscope we were able to say that during the deposition of the film many links are formed within the film. As suggested previously[5], the electrode material is introduced into the film under the influence of the electric field. The in-diffusion of the metal electrodes into the film can also be varified by comparing the current passing through the films under the influence of the same electric field, but sandwiched between different electrodes. As a result of this, it was found that the current was higher when the film was sandwiched between gold electrodes as compared with copper. Since the electrical conductivity of gold is greater than that of copper, this explains the

higher current in the case of gold electrodes. The links (of polypropylene) formed during the deposition of the film provided diffusion paths for the electrode material. After the heat treatment these links are reduced in numner, so this is consistent with the increase in resistivity.

The permittivity of the film can be calculated from the following relation.

$$\varepsilon = \frac{cd}{A\varepsilon_o} \qquad (6.1)$$

Where ε is the permittivity or dielectric constant of the material, C is the capacitance and A is the area of the sample and ε_o is the permittivity of the free space. $(8.85 \times 10^{-12} Fm^{-1})$. A polypropylene film sandwiched between copper electrodes and having a thickness of 1800Å, gave the capacitance value equal to 0.9 nF (at 20 kHz), using $A = 0.1 \times 10^{-4}\ m^2$, we get $\varepsilon = 1.83$. While for the bulk polypropylene $\epsilon = 2.13$. This shows that the permittivity of the evaporated film is very close to the permittivity of the bulk polypropylene. Therefore we can say that the films formed by the vacuum evaporation are similar to the starting material. Thin films of polyethylene formed by vacuum evaporation have been studied extensively and it was reported[23] that the vacuum-evaporated films are amorphous before annealing and became polycrystalline after annealing. Also, a large amount of trapped gas and other gaseous hydrocarbons are expelled from the film during annealing, thus leading to a reduction in its volume. Annealing in vacuum increased the resistivity of the polypropylene film so it seems to be important to measure the

permittivity of the sample after annealing. The capacitance of an evaporated layer of polypropylene (2589Å thick) was found to increase slightly from 0.59 nF to 0.62 nF after annealing. An increase in the capacitance of evaporated polyethylene after annealing has also been reported. If all the factors remain constant in equation 6.1, the capacitance is inversely proportional to the thickness of the device. As mentioned, during annealing, the polyethylene films release some gaseous hydrocarbons trapped within the film. This causes a decrease in the thickness of the film; therefore the capacitance increases after annealing. The same thing is believed to be happening in case of polypropylene. Although there is evidence of rearrangement of the atomic clusters after annealing in the evaporated polypropylene films, nevertheless the permittivity remains almost the same. For example the permittivity values of a sample (2589Å) were 1.75 and 1.81 before and after annealing respectively. So the annealing does not markedly change the nature of the material. The only apparent effect it has is to break the links between the particles, so that the average distance between them is increased. As is clear from the a.c. measurement, the electrical conduction takes place due to the electron hopping between the particles and an increased spacing would lead to a reduced electrical conductivity. In polymers the similar structure of the monomers, which are closely packed in the chains may provide some partly ordered crystalline regions (crystallites) but due to the long chains, the polymer molecules become entangled with one another.

The existence of these entanglements prevents the complete crystallization, therefore there must exist disordered or amorphous regions between the crystallites.

The structural results do provide for the first time evidence of the microscopic nature of the evaporated polypropylene films. The transmission electron diffraction patterns of the several evaporated layers of polypropylene, having different thicknesses certainly indicated the amorphous structure of these films, but after annealing there was evidence of some micro-crystallites. However as a whole the structure remained essentially non-crystalline. Nevertheless some estimate of change in the crystalline character of the layers was made by the photomicrometric examination of the diffraction patterns before and after the heat-treatment. By comparing the half-width of the micro-photometer traces of non-annealed films with those of annealed films, the half-width was found to decrease after annealing. This indicates the increase in crystallite size, i.e. the evaporated polypropylene films become more crystalline after annealing.

The structural results which relate to the earlier results in the thesis on electrical and electronic trapping phenomena are believed to be novel for evaporated polymers and it may be that the form of behaviour observed with evaporated polypropylene is typical of what occurs with many evaporated polymer films.

REFERENCES

1. R.W. Christy, J.Appl.Phys., 31, (1960) 1680.
2. R.W. Christy, J.Appl.Phys., 35, (1964) 2179.
3. J.R. Hanscomb and Y.Kaahwa, J.Phys.D.Appl.Phys., 12, (1979) 579.
4. C.A. Hogarth and M. Zor, Thin Solid Films, 27, (1975) L5.
5. C.A. Hogarth and T. Iqbal, Thin Solid Films, 51, (1978) L45.
6. A.M. Mearns, Thin Solid Films, 3, (1969) 201.
7. M. White, Thin Solid Films, 18, (1973) 157.
8. A.C. Rostogi and K.L. Chopra, Thin Solid Films, 18, (1973) 187.
9. S.L. Madorsky, Thermal Degradation of Organic Polymers, Krieger (1975).
10. A.G. Cooper, A.B. Keller and J.R. Waring, J.Polym.Sci., 11, (1953) 215.
11. M.Suzuki, Y. Tanakan and S.Ito, Japan. J.Appl.Phys.10 (1971) 817.
12. G.L. Slominskii, V.A. Belyi and A.M. Krasnovskii, High-Molecular Compounds, Part B, No.4 (1968), P.427.
13. I.L. Rock, D.M. Rafalovick and V.G. Zadorazhnyi, Instrum.Exp. Tech. (USSR), 19, (1976) 1215.
14. A.K. Jonscher, "International Meeting of Electrostatic Charging", Frankfurt (1973) 29.
15. T. Iqbal and C.A. Hogarth, Thin Solid Films, 61, (1979) 23.
16. John H. Slowik, J.Appl.Phys., 47, (1976) 2982.
17. Inan Chen, J.Appl.Phys., 47, (1976) 2988.
18. J. Kevorkian, M.M. Labes, D.C. Larson and D.C. Wu, Disc. Faraday Soc., 51, (1971) 139.
19. M. Pollack and T.H. Geballe, Phys.Rev., 122, (1961) 1742.
20. S.L. Madorsky, S. Strauss, D. Thompson and L. Williamson, J.Polymer Science, 4, (1949) 639.

21. S.L. Madorsky, J.Polymer Science, 9, (1952) 133.

22. N. Grassie, Polymer Science Vol.2 (By A.K. Jenkins) P-1443.

23. P.P. Luff and M. White, Thin Solid Films, 6, (1970) 175.

24. A.V. Amelin, O.F. Pozdnyakov, V.R. Regel and T.R. Sanfirana, Soviet Phys-Solid State, 12,(1970) 2034.

25. J.A. Lane, Brighton College of Tech., Project Report No.156, (1967).

26. M. White, Vacuum, 15, (1965) 449.

27. N. Grassie and H.W. Melville, Pro.Roy.Soc., 199A, (1949) 14.

28. J.F. Kinstle, Polymer Letter Ed., 15, (1977) 467.

29. V.D. Moiseev, M.B. Neman and A.N. Kryukova, Vysokomole Kulyarnye Soedineniya, 1, (1956) 1352.

30. D. Rysovy and L. Balaban, Pol.Sci., USSR., 3, (1962) 147.

31. L.V. Gregor, Thin Solid Films, 2, (1968) 235.

32. P.R. Emtage and W. Tantraporn, Phys.Rev.Lett., 8, (1962) 267.

33. H.T. Mann, J.Appl.Phys., 35, (1964) 2173.

34. L.V. Gregor and L.H. Kaplan, Thin Solid Films, 2, (1968) 95.

35. J. Tyezkowski, M. Zielinski and M. Kryzsewski, Thin Solid Films, 55, (1978) 253.

36. G. Lengyel, J.Appl.Phys., 37, (1966) 807.

37. A.C. Lilly and J.R. Mcdowell, J.Appl.Phys., 39, (1968) 141.

38. A.C. Lilly and D.A. Lowitz, J.Appl.Phys., 39, (1968) 4360.

39. O. Dwyer, J.Appl.Phys., 37, (1966) 599.

40. Koichi Kamisako, S. Akiyama and Kenichi Shinohora, Jap. J.Appl.Phys., 13, (1974) 1780.

41. E. Staryga and J. Swiatek, Thin Solid Films, 56 (1979) 311.

42. M. Kryszewski and J. Swiatek, Acta.Phys.Pol., A45, (1974) 119.

43. M. Zor, Ph.D. Thesis, Brunel University, 1977.

44. Y. Miyoshi and K. Chino, Jap.J.Appl.Phys., 6, (1967) 181.

45. A.V. Rogger, Phys.Rev.Lett., 9, (1962) 368.

46. D.K. Gupta and M.K. Barbarez, J.Phys.D., Appl.Phys., 6, (1973) 867.

47. Masakuni, Suzuki, Kiyohide Takahashi and Shinichiro Mintani, Jap.J.Appl.Phys., 14, (1976) 741.

48. Shireesh D. Phadke, K. Sathianandan and N. Karekar, Thin Solid Films, 51, (1978) L9.

49. J. Chutia and K. Barua, Thin Solid Films, 55, (1978) 387.

50. T.W. Hickmott, J.Appl.Phys., 33, (1962) 2669.

51. T.W. Hickmott, J.Appl.Phys., 34, (1963) 1569.

52. J.G. Simmons and R.R. Verderber, Proc.R.Soc., A301, (1967) 77.

53. R.R. Verderber, J.G. Simmons and B. Eales, Phil.Mag., 16, (1967) 1049.

54. P.D. Greene, E.L. Bush and I.R. Rawlings, Proceedings of the Symposium on Deposited Thin Film Dielectric Materials, edited by F. Vratny (New York, The Electrochemical Society) (1968) 167.

55. C. Barriac, P. Pinard and F. Davoine, Phys.Stat.Sol., 34, (1969) 621.

56. G. Dearnley, D.V. Morgan and A.M. Stoneham, J.Non-Crystalline Solids, 4, (1970) 593.

57. J.E. Ralph and J.W. Woodcock, J.Non-Crystalline Solids, 7, (1972) 236.

58. K.H. Gundlach and J. Kadlec, Phys.Stat.Sol., (a)10, (1972) 371.

59. J. Gazso, Thin Solid Films, 21, (1974) 43.

60. C.A. Hogarth and T. Iqbal, Int.J.Electronics, 47, (1979) 349.

61. N.F. Mott and E.A. Davis, "Electronic Process in Non-Crystalline Materials", Oxford University Press 1971.

62. N.F. Mott and R.W. Gurney, "Electronic Process in Ionic Crystals", Oxford University Press, 1940.

63. A. Rose, Phys.Rev., 97, (1955) 1538.

64. M.A. Lampert, Phys.Rev., 103, (1956) 1648.

65. M.A. Lampert, A. Rose and R.W. Smith, J.Appl.Chem. Solids, 8, (1959) 484.

66. P. Mark and W. Helfrich, J.Appl.Phys., 33, (1962) 205.

67. M.A. Lampert and P. Mark, "Current injection in Solid", (New York, Academic Press) 1970.

68. W. Schottky, Z. Physik, 15, (1914) 872.

69. K.L. Chopra, "Thin Film Phenomena", (McGraw-Hill Book Company) New York, 1969.

70. J. Frenkel, Phys.Rev., 54, (1938) 647.

71. C.A. Mead, Phys.Rev., 128, (1962) 2088.

72. J.G. Simmons, Phys.Rev., 155, (1967) 657.

73. J.G. Simmons, Phys.Rev., 106, (1968) 912.

74. J. Frenkel, Z. Physik., 35, (1926) 652.

75. W. Schottky and C. Wagner, Z. Physik.Chem., B11, (1930) 163.

76. C. Wagner, Z.Physik.Chem., B22, (1933) 181.

77. R.J. Friauf, J.Chem.Phys., 22, (1954) 1329.

78. P.H. Sutter and A.S. Nowick, J.Appl.Phys., 34, (1963) 734.

79. C.P. Beans, J.C. Fisher and D.A. Vermilyea, Phys.Rev., 101, (1956) 551.

80. D.R. Lamb "Electrical Conduction Mechanism in Thin Insulating Films". Spottiswoode Ballantyne & Co., 1967 (London).

81. R.H. Fowler and L.W. Nordheim, Proc.Roy.Soc., A119, (1928) 173.

82. J. Frenkel, Phys.Rev., 36, (1930) 1604.

83. R. Holm, J.Appl.Phys., 22, (1951) 569.

84. J.G. Simmons, J.Appl.Phys., 35, (1964) 2655.

85. J.G. Simmons, Phys.Rev.Lett., 23, (1969) 297.

86. J. Bardeen, Phys.Rev., 71, (1947) 717.

87. D.M. Pai, J.Chem.Phys., 52, (1970) 2285.

88. M.E. Haine and R.E. Carley-Read, Brit.J.Appl.Phys., (J.Phys.D) 1, (1968) 1257.

89. R.H. Bube "Photo-Conductivity of Solids" (Wily, U.S.A. 1960)

90. R.A. Collins and R.D. Gould, Solid St.Elec., 14, (1972) 805.

91. R.D. Gould and C.A. Hogarth, Int.J.Elec., 37, (1974) 157.

92. R.R. Sutherlands, J.Phys.D., 4 (1971) 468.

93. T.H. Mann, J.Appl.Phys., 35 (1964) 2173.

94. C. Barriac, F. Graud-Heraud, P. Pinard and F. Davoine, C.R. Acad.Sci. Paris. 262, (1966) 900.

95. H. Kanter and W.A. Feibelman J.Appl.Phys., 33, (1962) 3580.

96. G.S. Kreynina, L.N. Selivanov and T.I. Shumskaia Ratio Eng.Elec.Phys., 5, (1960) 219.

97. G.S. Kreynina, Radio Eng.Elec.Phys., 7, (1962) 166.

98. G.S. Kreynina, Radio Eng.Elec.Phys., 7, (1962) 1949.

99. S.R. Pollack, W.O. Freitag and C.E. Morris, Electro Chem. Tech., 1, (1963) 96.

100. S.R. Pollack, J.Appl.Phys., 34, (1963) 877.

101. T.W. Hickmott, J.Appl.Phys., 35, (1964) 2118.

102. T.W. Hickmott, J.Appl.Phys., 35, (1964) 2679.

103. G.A. Filarertav, V.I. Stafeyeu, G.A. Cherkashim, M.S. Luric Yu.Z. Bubnov and Z.H.S. Asnina, Rad.Eng.Elec.Phys., 11, (1966) 246.

104. R.A. Collins, G. Brown and R.R. Sutherland, J.Phys. D4, (1971) L49.

105. R.D. Gould and C.A. Hogarth, Phy.Stat.Sol(a), 23, (1974) 531.

106. R.W. Lomax and J.G. Simmons, Radio Elect.Eng., 35, (1968) 265.

107. T.W. Hickmott, Thin Solid Films, 9, (1972) 431.

108. T.W. Hickmott, J.Appl.Phys., 36, (1965) 1885.

109. R.R. Verderber and J.G. Simmons, Rad.Elect.Eng., 33, (1967) 347.

110. J.G. Simmons, R.R. Verderber, J. Lytollis and R. Lomax, Phy.Rev.Letters, 17, (1966) 675.

111. L. Eekertova, Czech, J.Phys., B75, (1965) 111.

112. W.A. Thornton, Phys.Rev., 116, (1959) 893.

113. R.C. Jaklevic, D.K. Donald, J. Lamble and W.C. Vassel, Appl.Phys.Letters, 2, (1963) 7.

114. M. Aven and D.A. Cisusand, J.Appl.Phys., 35, (1964) 606.

115. J.M. Woodcock and J.E. Ralph, J.Non-Cryst.Solids, 11, (1972) 83.

116. C. Barriac, P. Pinard and F. Davoine, C.R.Acd.Sci., Paris 226, (1968) 243.

117. G. Dearnaley, Phys. Letters, 25A, (1967) 760.

118. N.F. Mott, Phill.Mag., 17, (1968) 1257.

119. P.W. Anderson, Phys.Rev., 109, (1958) 1492.

120. A.E. Rakshani, C.A. Hogarth and A.A. Abidi, J.Non.Cryst. Solids, 20, (1976) 25.

121. A.E. Rakshani and C.A. Hogarth, J.Non.Cryst.Solids, 21, (1976) 147.

122. F.D. Green, E.L. Bush and I.R. Rowling, Proc.Symp. on Deposited Thin Film Dielectric Materials, Montreal Ed.F. Vratny (New York, The Electro Chemical Soc., 1969) P-167.

123. J. Stuke, J.Non.Cryst.Solids, 4, (1970) 1.

124. E.A. Davis and N.F. Mott, Phil.Mag., 22, (1970) 903.

125. G. Dearnaley, Thin Solid Films, 3, (1969) 161.

126. C.S. Hung and J.R. Gleissman, Phys.Rev., 79, (1950) 726.

127. E.M. Conwell, Phys.Rev., 103, (1956) 51.

128. S.H. Koeing and G. Gunther Mohr, J.Phys.Chem.Solids, 2, (1957) 268.

129. A. Miller and E. Abrahams, Phy.Rev., 120, (1960) 745.

130. K.R. Atkins, R. Donovand and R.H. Walmsley, Phy.Rev., 118, (1960) 411.

131. N.F. Mott, Can.J.Phys., 34, (1956) 1356.

132. H. Fritzsche, J.Chem.Phys.Solids, 6, (1958) 69.

133. F. Argall and A.K. Jonscher, Thin Solid Films, 2, (1968) 185.

134. M.M. Perlman and S. Unger. In Charge Starge and Transport in Dielectric.

135. M.M. Perlman, Ed.Electrochemical Soc. Inc. Pincetron, N.J., (1973) 105.

136. M. Kryszewski, J.Polymer Sci.Symp., 50, (1975) 359.

137. L.I. Massel, Handbook of Thin Film Tech. (McGraw-Hill - 1970) P13-26.

138. V. Vand, Proc.Phys.Soc., London, 55, (1943) 222.

139. W.M. Kane, J.P. Spratt and L.W. Hershinger, J.Appl.Phys. 37, (1966) 2085.

140. J.E. Shofronick and W.B. Phillips, Proc.Inten.Symp., (1966) 591.

141. H. Basseches, J.Electrochem.Soc., 109, (1962) 475.

142. J. Koshy, Thin Solid Films, 51, (1978) L17.

143. K.A. Buckingham and W. Reddish, W.Proc.I.E.E., 144, (1967) 1810.

144. R.W. Warfield and M.C. Petree, SPE Trans., 1, (1961) 80.

145. R.W. Warfield and M.C. Petree, Makromal.Chem., 58, (1962) 139.

146. A.H. Scott, SPE.J., 18, (1962) 1375.